DEPARTMENT OF THE AIR FORCE
AIR UNIVERSITY

AIR FORCE INSTITUTE OF TECHNOLOGY

Wright-Patterson Air Force Base, Ohio

AFIT/GE/ENG/ENP/88D-1

THE RESPONSE OF SINGLE ELEMENT HgCdTe AND InSb SOLID STATE INFRARED DETECTORS TO MILLIMETER WAVE ELECTROMAGNETIC ENERGY

THESIS

Thomas D. Moore
Captain, USAF

AFIT/GE/ENG/ENP/88D-1

Approved for public release; distribution unlimited

AFIT/GE/ENG/ENP/88D-1

THE RESPONSE OF SINGLE ELEMENT HgCdTe AND InSb SOLID STATE INFRARED DETECTORS TO MILLIMETER WAVE ELECTROMAGNETIC ENERGY

THESIS

Presented to the Faculty of the School of Engineering
of the Air Force Institute of Technology
Air University
In Partial Fulfillment of the
Requirements for the Degree of
Master of Science in Electrical Engineering

Thomas D. Moore, B.S.E.E.
Captain, USAF

December 1988

Preface

The purpose of this thesis was to measure the response of solid state infrared detectors to millimeter wave electromagnetic energy. Captains Arley Huggins and Dave Reddy of the Air Force Electronic Warfare Center at Kelly AFB, Texas proposed this topic.

Two types of detectors were tested: Indium Antimonide (InSb) and Mercury Cadmium Teluride (HgCdTe). The individual detectors were not tested as separate entities, but as part of the dewar and preamplifier system in which they were encompassed. However, the tests were able to differentiate which part of the system generated a response to incident millimeter wave energy.

I'd like to extend my deep appreciation to the Air Force Wright Aeronautical Laboratories at Wright-Patterson Air Force Base for their support. Several AFWAL branches were instrumental in providing hardware and facilities to support the thesis effort. Dan Murray and his staff at AFWAL/AAWP-2 provided extensive technical support along with the use of their facilities and microwave equipment. A special note of thanks is extended to Joe Karnish and Angelo Lombardo who frequently interrupted their schedules to assist me in setting up and locating test equipment and hardware. Dr. Paul Schriber of AFWAL/AADO-3 and George Vogel of AFWAL/AAW provided the loan of the infrared

detectors which were tested during the thesis experiment.

I'd also like to express my gratitude to my thesis advisor, Major Stone, for his technical guidance and personal encouragement throughout the thesis. Additionally, the patience and support given to me by my wife and children, Becky, Ashley and Suzanne was deeply appreciated.

Thomas D. Moore

Abstract

An experimental determination of the millimeter wave (MMW) response of single element InSb and HgCdTe infrared (IR) detectors is made. The detectors were mounted in standard metal dewars and cooled to 77K. Bias and amplification for the detectors were provided by external preamplifiers. The detectors were irradiated with amplitude modulated (AM) electromagnetic energy in the Ka and E microwave bands. MMW transmitter power levels were limited to values of less than 10 mW. Tests were accomplished in the near-field of standard gain pyramidal horns. Response measurements were made on a spectrum analyzer by monitoring the level of the MMW AM rate spectral component. The detector MMW responses were measured for linearity, RF, AM rate, and polarization dependence. The effect of simultaneous IR and MMW sources in the detector field-of-view were also examined. Of the detectors tested, only the HgCdTe detector exhibited a MMW response. The measured HgCdTe MMW response was square law in behavior and displayed dependence on the RF, AM rate, and polarization of the incident MMW. The MMW response was not effected by the presence of IR sources.

Table of Contents

List of Figures

Figure Page

List of Tables

THE RESPONSE OF SINGLE ELEMENT HgCdTe AND InSb SOLID STATE INFRARED DETECTORS TO MILLIMETER WAVE ELECTROMAGNETIC ENERGY

I. Introduction

Background

Infrared (IR) tracking sensors and missile seekers have developed both in number and sophistication since their original employment by the military. The advances have made the IR systems less susceptible to traditional IR countermeasures. As a result, new countermeasures are required. Developments in millimeter wave (MMW) technology have led to increased interest in fielding MMW sensors and dual MMW/IR sensors. Some of the technical problems experienced in implementing the dual sensors suggest a susceptibility of IR sensors to MMW energy. This in turn suggests that high power MMW energy may be used to upset IR systems.

Infrared missile systems are used by militaries throughout the world. Taylor documents over 26 different IR guidance and control missile systems known to be in use by more than ten countries worldwide (Taylor, 1980). Infrared systems have also evolved technically. Early systems such as the Sidewinder 1A used a "center null" tracking system

with limited accuracy. Improved tracking was obtained with a conical-scan tracking technique used in the Falcon and Redeye systems (May and Van Zee, 1983). Image scanning techniques, detector arrays, improved detector materials, cooling methods, pattern recognition schemes and microprocessors have all combined to better IR tracking and sensing capabilities. The increase in IR capabilities has in turn led to a decrease in vulnerability to traditional IR countermeasures. For example, May and Van Zee discussed the use of flares as traditional IR countermeasures used against comparatively large field-of-view (FOV) systems such as the conical scan, center null, and checkerboard reticle systems. These systems must have a FOV large enough to acquire the target which leaves the sensor susceptible to flares imaged in the FOV (May and Van Zee, 1983). The flare may be defeated by using pattern recognition techniques in conjunction with image scanning methodologies and focal plane arrays. An image scanner uses a small instantaneous FOV which is scanned throughout a larger field-of-view. The focal plane array uses an array of detectors which can sample the entire scene instantaneously. In this manner, the position of a flare or hot spot may be tracked and/or differentiated from another target. By monitoring the movement and relative position of the flare, pattern recognition schemes can differentiate between the flare and target (May and Van Zee, 1983). Another development

involves the simultaneous operation of two or more sensors in different IR wavelength windows. By using multiple wavelength windows, it is possible to accurately identify the pulse resulting from IR radiation received from target aircraft, background, and countermeasures simultaneously (May and Van Zee, 1983).

Millimeter wave systems have a distinct advantage over IR systems in that MMW energy can propagate through dust, smoke, and battlefield obscurants virtually unattenuated (Reedy, 1981:42). Battlefield obscurants tested include hexachloroethane, white and red phosphorus wick, fog, oil, plasticized white phosphorus, white and red phosphorus wedges, and dust resulting from high explosives (Bhartia and Bahl, 1984: 175). The primary disadvantage for MMW systems are that they are weather limited. The principle causes of MMW attenuation in the atmosphere are due to the absorption, scattering, and depolarization of the MMW due to water vapor and oxygen molecules. The degree of attenuation is dependent upon the ambient pressure, temperature, and water vapor concentration. For example, water vapor has a higher dielectric constant than ice. Because of this, raindrops both absorb and scatter MMW to a greater degree than ice crystals or hail (Bhartia and Bahl, 1984:154-164). Within the MMW band of 30 - 300 GHz are four "windows" in which atmospheric attenuation of MMW energy is minimum. These windows have center frequencies of 35, 94, 120, and 220 GHz

with bandwidths of 16, 23, 26, and 70 GHz respectively. The windows and large bandwidths provide frequency diversity, high information rates, very high range resolution, and wide-band spread spectrum capabilities to MMW systems (Bhartia and Bahl, 1984: 3-4).

There is a growing interest within the defense community to field dual common aperture MMW and IR sensors. A dual-mode common aperture system which permits simultaneous operation as an infrared and millimeter wave system has been designed and built as a prototype by Honeywell, Inc. Various coatings and materials were used to separate the MMW energy from the IR sensor due to a concern that millimeter radiation emitted from the MMW feedhorn would cause interference with the IR detector preamplifiers and signal conditioning electronics. However, if any interference was caused by the MMW energy during the tests performed by Honeywell, no data is presented quantifying the disruption (Benser, et al., 1987).

The possibility of MMW interference with IR sensors may be used as an advantage as a possible countermeasure technique against IR systems. While older IR missile seekers are still employed by many defense forces throughout the world, the need for new countermeasures is made evident by advances in IR technology, processing schemes, and computer capabilities.

Problem

The desire to field dual mode MMW/IR sensors and the possibility of using MMW energy to upset or counter IR systems require knowing the response of IR detectors to MMW energy. Presently, the effect of MMW energy on state-of-the-art IR detectors is not very well known. The purpose of this thesis is to experimentally measure the response of HgCdTe and InSb IR detectors to MMW energy in the Ka and E microwave bands.

Current Knowledge

The infrared region is generally defined as the wavelength band from 0.75 to 1000 μm (Kruse, et al., 1962:2). Solid state IR detectors are usually characterized by their response to incident IR radiation with wavelengths greater than 2 μm (Emmons, et al., 1985). However, within this region, the operating range is still more restricted. Boyd lists the cutoff wavelengths for a number of common pure semiconductors at room temperature as ranging from 0.39 to 5.4 μm. Boyd states that the cutoff wavelength can be extended somewhat for semiconductors operated in the intrinsic photoconductive mode by mixing solid solutions of two different semiconductors. However, Boyd explains that it is difficult to produce materials which extend the cutoff wavelength to more than 30 μm (Boyd, 1983:160). Emmons and others tabulated cutoff wavelengths ranging from 9 to 125 μm

for several extrinsic photoconductive detectors. (Emmons, et al., 1985). Although IR detectors are usually characterized by their response to incident radiation within the wavelength ranges described above, the response of IR detectors to longer wavelengths such as millimeter waves may become more important in the future.

In a study by Weber and Kulpa, semiconductor crystals exhibited sensitivity to electromagnetic radiation in the 100 to 1000 GHz frequency region. The sensitivity was observed when the semiconductors were operated in the hot-electron photoconductive mode. In the article, hot-electron photoconductivity is described as the result of free electrons in the conduction band of the semiconductors absorbing incident radiation. Weber and Kulpa explain the mode in the following way:

> At low temperatures (approximately 4 K), the coupling of the electrons to the lattice is much weaker than at room temperature. Thus the electron temperature, which is the same as that of the lattice at room temperature, can be very much different from that of the lattice at low temperatures. This means that radiation absorbed by the electrons can raise the electron temperature above that of the lattice. This increase in electron temperature is observable by a change in the electron mobility and thus the photoconductivity. The process does not have a long wavelength threshold [Weber and Kulpa, 1980:373].

Furthermore, their results show that the absorption process becomes constant for wavelengths in excess of the characteristic electron-electron interaction length. The article differentiates between the various modes in which

the semiconductor may operate. The intrinsic mode in which the HgCdTe detector tested operates, responded within the 8 to 12 micron wavelength region. The intrinsic photoconductive mode is the result of electronic transitions between the valence and conduction states of the semiconductor. The long wavelength cutoff is due to the energy gap of the material (Weber and Kulpa, 1980:373).

Another mode of operation is called impurity or extrinsic photoionization in which impurities are ionized to increase the concentration of electrons or holes. This occurs at longer wavelengths than that of intrinsic operation (Weber and Kulpa, 1980:373).

A fourth type of photoconductivity described by Weber and Kulpa is called hopping. This effect is due to electronic tunneling transitions between impurity states. Weber and Kulpa elaborate:

> This long wavelength effect is only observed at very low temperatures where freeze-out of free electrons from the conduction band onto impurity sites occurs, thus diminishing the free-electron absorption contribution. Under these conditions, a hopping movement of electrons from donor site to donor site characterizes the observed photoconductivity [Weber and Kulpa, 1980:373].

Of the two long wavelength modes, the hot-electron mode was observed to dominate in the near millimeter wave region. (Weber and Kulpa, 1980:372-373)

The experiments performed by Weber and Kulpa were performed with [Hg,Cd]Te crystals. Success in operating the

crystals in the hot-electron photoconductive mode was experienced with several samples of the crystals. The experiments were performed with the detector placed in a liquid helium cryostat at the end of a 10 mm diameter 100 cm long, gold-coated waveguide with the detector cooled to 77 k. Radiation of wavelengths less than 100 μm were prevented from irradiating the crystal through the use of a filter. Various sources of radiation were then allowed to irradiate the crystal: 1.2 mm, 2.5 mm, and 4.3 mm. Power losses were monitored and incident power on the detector was determined. Sensitivity was obtained for wavelengths longer than 1 mm for incident source power averaging about 200 μW. The peak responsivity observed was about 2.5 V/W for wavelengths greater than 1 mm. Detector responsivity was also measured for various pulse times between 0.1 and 10 μs at a wavelength of 2.5 mm. Some rolloff of the response is observable in the reported data for pulses shorter than about 1 x 10 μs. The authors also report sensitivity in the near millimeter wave range for samples of InSb. Noise equivalent power (NEP) measurements made by Weber and Kulpa with optimum parameters indicated a NEP of 200 $\mu W/(Hz)^{1/2}$ for [Hg,Cd]Te and 100 $\mu W/(Hz)^{1/2}$ for a sample of InSb tested in the same experimental setup (Weber and Kulpa, 1980: 373-380).

Protecting a system from unwanted energy which might couple into a system was investigated by Sega and Norgard in an experiment in which they used conductive mesh to shield infrared detectors from microwave radiation. Sega and Norgard discussed the techniques with which a conductive mesh that is opaque to microwave but transparent to IR energy could be placed around an IR scanner to prevent microwave energy from penetrating into the IR system. One of the main concerns was the heating of the detector by the microwave energy. Shielding effectiveness was determined by placing the mesh between two standard gain horns and comparing the power transfer between the two horns with that which occurred when the horns were separated only by free space (Sega and Norgard, 1987:214).

Related studies describing the coupling of electromagnetic radiation through apertures in structures were found. In one study, Adams and others provided method of moments treatments on coupling through apertures in a plane screen, long slots in a plane screen, apertures in a body-of-revolution, and coupling to wires beyond the aperture. The specific results were dependent on the wavelength and relative size and orientation of the structure and aperture (Adams, et al., 1975:366-367). A report produced for the Air Force Weapons Laboratory at Kirtland AFB, New Mexico, described nuclear electromagnetic pulse (EMP) interaction with complex systems; one of the

byproducts of a nuclear explosion are electromagnetic fields (EMP Interaction, 1980: 2). In the study, electromagnetic interaction problems were approached by applying the appropriate boundary value conditions for the aperture geometry and material composition and then solving Maxwell's equations. The structural dimensions and resulting solutions provided within the report are usually stated relative to the incident radiation wavelength. The report details electromagnetic interaction with round, slotted, and elliptical apertures, apertures in curved surfaces and other modifications, cables, imperfect conductors, screens, composites and other geometries (EMP Interaction, 1980). Another study analyzing the propagation of electromagnetic energy through apertures was accomplished by Graves, et al.. Again, aperture sizes, shapes, and structural relationships are described relative to the incident radiation wavelength. This generalizes the results and allows the application of the solution to diverse electromagnetic scattering and coupling problems. Graves, et al. noted that it is difficult to determine the effectiveness of electromagnetic shielding in the presence of an aperture. However, some general relationships provided by Graves, et al. can be used in qualitatively assessing propagation of energy through apertures. First, the degree of coupling through the aperture increases with frequency. Second, coupling or penetration should be maximum at resonance or when the

aperture is a half wavelength in diameter (Graves, et al., 1975). With wavelengths within the millimeter range, the aperture sizes required for coupling are not very large. For example, at 35 GHz (near the low frequency end of the millimeter range) a half wavelength corresponds to 0.43 cm. At a frequency of 94 GHz, a half wavelength is only 0.16 cm long. In the electromagnetic coupling studies mentioned above, the results tend to be generic in nature. Structural sizes are stated as being electrically small, large, or intermediate. Because of the general nature in which the problems are approached, the results are applicable to various electromagnetic problems and can be extended to the millimeter wave region.

Scope

The IR detector response to MMW energy will be determined experimentally within the Ka and E microwave bands. The physical mechanisms within the detector which might allow the response such as "hopping" or "tunnelling" will not be determined. Rather, empiricle results are sought.

The emphasis of the experiments will be twofold. First, determine if the detector is responding to the incident MMW energy. Second, characterize the detector output response for the incident MMW power and frequency.

Criteria

The appropriate voltage or current output of the IR detectors will be monitored on a display device such as an oscilloscope or spectrum analyzer. A change in the IR detector output signal when MMW energy is applied to the detector will be signified as a response.

Approach

The IR detectors tested will be irradiated with MMW energy in the range from 26.5 - 40 and 60 - 90 GHz. All of the tests will be conducted using free space as the medium. The IR detectors tested will be mounted within dewar assemblies. Dewars are double walled vacuum enclosures designed to maintain a coolant within a internal central wall to allow cooling of the detector (Kruse, et al., 1962: 394).

Initially, the detector will be placed on a laboratory bench and irradiated with MMW energy of a known frequency and field strength. If a response is noted, efforts will be made to isolate the response to the detector. Once a detector is found to have a response, MMW RFs will be swept to determine the frequency response. The MMW source will then be amplitude modulated at various rates to check for any rate dependence. Additional tests to characterize the detector response will include power level variations, detector operating temperature, and polarization.

Propagation of the MMW energy will be accomplished using pyramidal horn antennas. Ideally, only the detector should be irradiated. It may be possible for MMW energy to couple to external leads and mounting hardware. As any resulting response would not be a true "detector" response, all efforts will be made to eliminate or isolate such effects. Before detector testing is initiated, the power and field patterns of the horns will be characterized by a combination of theoretical calculations and experimental measurements to allow determination of incident power levels on the IR detectors; MMW source power levels will be limited to less than 100 mW.

Materials and Equipment

The MMW equipment, support, and laboratory space required for the experiment were donated by AFWAL/AAWP.

Several infrared detectors have been located and are available for testing. Two indium antimonide and one mercury cadmium telluride detector/dewar assemblies and preamplifiers have been obtained from AFWAL.

Sequence of Presentation

Chapter II will describe and list the equipment used during the experiment. Experimental procedures will be covered in Chapter III. Results will be presented next in Chapter IV. Conclusions and recommendations will be presented in Chapter V.

II. Equipment Layout and Description

Introduction

Special equipment was not required for the experiment. Standard items were used throughout. A general description of the experimental apparatus will be provided in the main text. The signal sources and hardware necessary to generate them will be described first. The IR test devices will be depicted next. The test equipment used will be covered last. The equipment specifications and inventory will be attached as Appendices A and B.

The general layout of the experimental setup is illustrated by block diagram in Figure 1. A microwave source and antenna are elevated on an adjustable platform. The device under test is mounted on another adjustable platform which is placed on a movable sled. The arrangement allows for height, azimuth, and range adjustment on a repeatable basis.

Sources

The heart of the experimental apparatus are the sources used to irradiate the test devices. Both millimeter wave and infrared signal sources were necessary. The MMW sources provided the energy required to bring about the hypothesized response in the IR detectors. Infrared sources were needed to verify detector operation and to set up operating

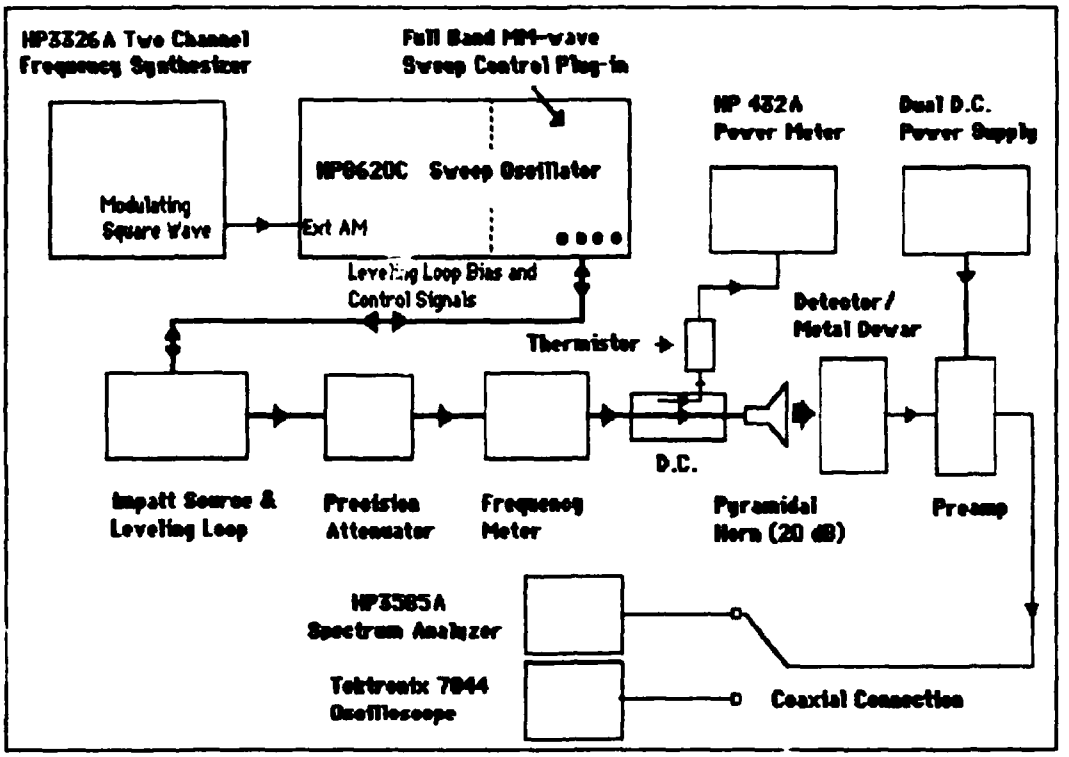

Figure 1. Experimental Equipment Block Diagram.

conditions in several parts of the experiment. The millimeter wave energy was generated using microwave transmitters, hardware, and pyramidal horn antennas. A variable temperature blackbody was used to generate the desired infrared signals.

MMW Sources. Millimeter wave sources were available from 26.5 GHz to 90 GHz. Unfortunately, antennas were only available for two bands within this range. As a result, only the Ka and E MMW bands covering 26.5-40 GHz and 60-90 GHz were utilized. The generation of millimeter wave energy in the Ka and E bands was provided by an HP8620C Sweep

Oscillator, MMW Sweep Control Plug-in, Sweep Source, Leveling Loop, and associated hardware.

The HP8620C Sweep Oscillator provides full RF sweep capability across each band. The sweep is separated into three smaller RF sub-bands. The Ka band is split into three sub-bands: 26.5-30 GHz, 30-35 GHz, and 35-40 GHz. The E band is divided into: 60-70 GHz, 70-80 GHz, and 80-90 GHz. The sweep oscillator generates the voltage waveforms which control the RF frequency sweep. The sweep modes available are : full, partial, and continuous wave (CW). The sweep control can be automatic, manual, or external. In the manual mode, the sweep can be varied in a continuous manner across a sub-band or stopped at a individual CW RFs. Only the CW mode was used in the experiment. Frequency changes were accomplished by manually tuning the front panel frequency vernier. The sweep voltage waveforms generated by the sweep oscillator drive the sweep control plug-in. The sweep control plug-in accepts the sweep voltage waveforms and generates the bias currents required to drive the sweep source. The plug-in also provides the current to drive the RF modulator which provides amplitude leveling and modulation.

The sweep source is made up of three IMPATT diodes each mounted on a frequency tuned cavity. Each IMPATT diode corresponds to one of three sub-bands selectable on the front panel of the HP8620C Sweep Oscillator. The proper

diode is selected by a solenoid actuated four-port rotary switch. The switch may be manually or automatically operated by the sweep control plug-in. The IMPATT diode RF output is fed to the Leveling Loop.

The Leveling Loop contains a Faraday type ferrite core rotation device (modulator), 10 dB directional coupler, and Schottky-barrier broadband detector diode. The output of the detector is fed to the sweep control plug-in to close the feedback loop and generate leveling control.

The modulator provides the leveling action. The modulator attenuates the MMW energy by rotating the E-fields as they propagate through its ferrite core. The amount of rotation and thus insertion loss is controlled by an external bias current which is provided by the sweep control plug-in. The modulator allows leveling of the output signal and amplitude modulation of the RF. Amplitude modulation may be provided by a 1 kHz squarewave internal to the sweep oscillator or by an external modulating waveform connected to a rear panel input. The output of the modulator is sent to a 10 dB directional coupler.

The coupled port of the 10 dB directional coupler is connected to a Schottky-barrier broadband detector. The detector output is returned to the sweep control plug-in for RF leveling. The through port of the directional coupler is sent to a Hughes Millimeter-Wave Direct Reading Frequency Meter.

The frequency meter is connected directly into the waveguide line. The outside of the meter is a drum calibrated to read frequency directly in units of GHz. The meter provides a quick and accurate way to determine the frequency of the CW RF being transmitted. The RF output of the frequency meter is coupled to a Hughes Millimeter-Wave Direct Reading Attenuator.

The attenuator is connected directly into the waveguide. The degree of attenuation (0-50 dB) is manually controlled by rotating the drum outside of the meter. Attenuation is read directly from the expanded helical drum calibration marks. The attenuator output feeds a 20 dB directional coupler. The directional coupler throughput is sent to a 20 dB pyramidal horn. The coupled output is sent to a device for the purpose of monitoring the level of the transmitted RF.

In the Ka band, power measurement of the output MMW signal is accomplished by sensing the coupled output of the 20 dB directional coupler with a thermistor. The output current from the thermistor is then measured using an HP432A power meter. The power delivered to the transmitting antenna is determined by adding the 20 dB coupling factor plus a thermistor correction factor to the power reading (dBm) taken from the meter. The thermistor correction factors are provided on the thermistor mount by the manufacturer and are listed in Table 1.

Table 1. Thermistor Correction Factors (Ka Band)

Frequency (GHz)	Correction Factor
26.5	+0.15
28.0	+0.45
31.0	+0.30
34.5	+0.35
37.0	+0.10
40.0	+0.10

During the initial testing of the microwave equipment, the E band thermistor was determined to be defective and was returned to the manufacturer for repair. Monitoring of the output signal was then accomplished by connecting a broadband detector to the coupled port of the 20 dB directional coupler and measuring the detector output voltage on an oscilloscope.

The broadband detectors used are Schottky-barrier diodes. The detector outputs have a sensitivity flatness (when connected into a megohm load) of ± 1.5 dB across the band when operated at power levels in the square law region. Typical detector sensitivities of 550 mV/mW and 250 mV/mW are listed for the Ka and E bands respectively (Millimeter Products, 1985: 91). Appendix A lists sensitivity and flatness specification values for the diodes as documented in the equipment data sheets.

The final component in the RF transmission process was the pyramidal horn antenna. Standard 20 dB gain horns were used in both bands. The measured horn dimensions are listed in Table 2. Figure 2 illustrates the horn dimension definitions used.

Table 2. Pyramidal Horn Dimensions

Band	A (mm)	B (mm)	Re (mm)
Ka	40	32	53
E	18	13.5	40

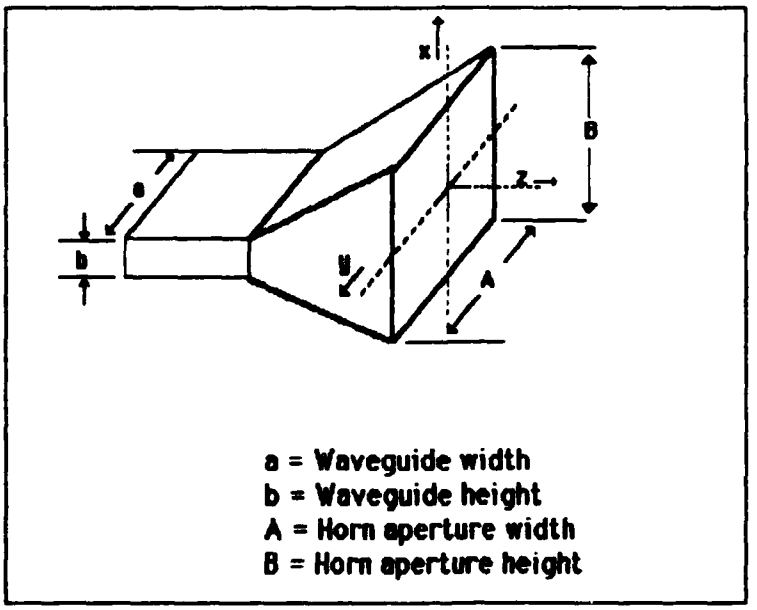

Figure 2. Pyramidal Horn Dimensions.

IR Source. An infrared source was required to verify IR detector operation and to test the detector response with an in-band and MMW signal simultaneously in the detector FOV. The IR source was generated by a standard variable temperature IR blackbody source. The blackbody output was chopped at a 673.9 Hz rate and redirected using a beam steering instrument.

The beam steering instrument is essentially two high grade optical mirrors which provide a 90° change in direction to a beam incident upon either of the two mirror's surface. Each mirror is adjustable in azimuth and elevation. Gross adjustment is obtained by repositioning the retaining collars which secure each mirror to the vertical post of the steering instrument. The top mirror has additional controls for coarse and fine adjustment of rotation and tilt. Figure 3 illustrates placement of the blackbody, chopper, and the beam steering instrument.

Test Objects

Three IR detectors, each mounted in metal dewar containers, were tested. All were manufactured by Judson Infrared, Inc. Two of the detectors were InSb and one used HgCdTe as the active element. Specific data on the detectors was not provided. However, some information was obtained from the manufacturer based on original delivery orders (Justice, 13 July 1988). Confirmation of the data

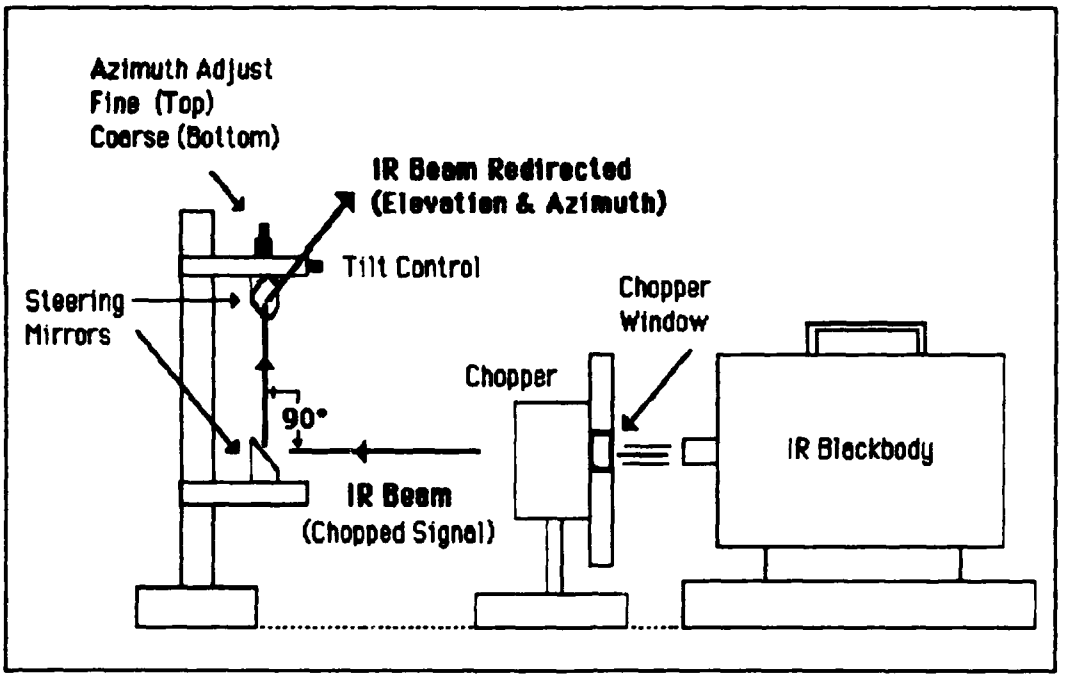

Figure 3. Redirection of the IR Blackbody Output.

could not be obtained. Individual test device item specifications, both typical and those provided by the manufacturer, are included in Appendix A.

Each IR detector was mounted in a Judson M204 Metal Sideview Dewar. Figure 4 illustrates the physical dimensions of the M204 dewar. The metal dewar allows for the cryogenic cooling of a detector to 77K. The detector is centered and mounted directly behind the dewar window. The dewars have an average hold time of 8 hours for the liquid nitrogen and can be repumped if the dewar vacuum is lost.

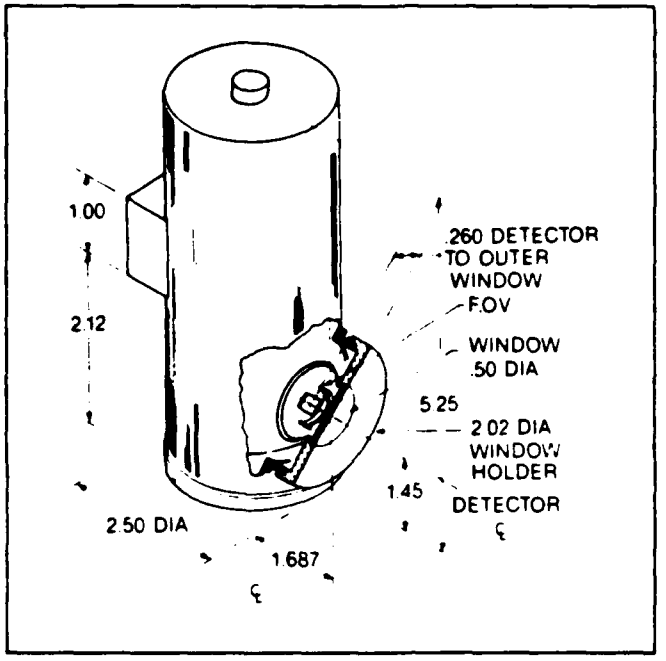

Figure 4. Style M204 Metal Sideview Dewar (Judson : 14). Note: Dimensions in inches.

Data sheets for the particular InSb detectors tested were not available. At the time of the original sale, the detectors were delivered with sapphire windows in the dewar (Justice, 13 July 1987). It is probable that the window materials were still sapphire at the time of this experiment. The window material was clear when observed with the eye. No coloration was apparent. Although this does not confirm sapphire as the window material, it does rule out some of the possible materials which are visibly opaque.

The InSb detector element sizes were also unknown. The dewar containers were sealed units. However, it was apparent that one InSb detector (SN 8568) had a larger detector element than the other. Comparing the size with that of the HgCdTe detector (which was known), it is likely that the larger detector (SN 8568) was 4 mm square in size. The other InSb detector (SN 8752) appeared to about the same size as the HgCdTe detector or 2 mm square.

The InSb detectors operate in the photovoltaic mode. The preamplifiers provided (Model 700 and PA700) convert the output from current to voltage while maintaining the detector at zero volt bias (Judson: 2,16). The preamplifiers have a frequency bandwidth from DC to 50 kHz. Typical specifications for the J10 Series of InSb detectors and the Model 700 amplifier are included in Appendix A.

The data provided by the manufacturer for the HgCdTe detector indicated that the window material was ZnS. The window appeared to be clear and colorless when viewed with the eye. This seems to cast some doubt as to the validity of the window material being ZnS. A lens known to be constructed of ZnS was observed. It was clear and had a yellowish tint when viewed with the eye. Because of this, the window material was treated as unknown.

Test Equipment

Test measurement equipment used during the experiment consisted of a HP3326A Spectrum Analyzer, an HP432A power meter, measuring tape, plastic ruler, and oscilloscope.

The outputs of the IR detector and preamplifier were measured on either a spectrum analyzer or oscilloscope. Because of the small signal levels, most of the response measurements were performed in the frequency domain using the spectrum analyzer. The HP3585A 20 Hz to 40 MHz Spectrum Analyzer used featured an 80 dB dynamic range, ±0.4 dB amplitude accuracy, digital storage, and a resolution variable bandwidth down to 3 Hz. This spectrum analyzer provided an excellent low level signal measurement capability. The oscilloscope was used infrequently to make voltage measurements of the IR detector preamplifier output. At some RFs and close ranges, the detected RF output could be observed in the time domain on the oscilloscope. The oscilloscope was used exclusively in measuring the relatively strong signal output from the RF broadband detectors.

Microwave power level measurements (Ka band) were accomplished using an HP432A power meter in conjunction with a thermistor mounted on the coupled port of the output microwave directional coupler (reference Figure 1). Distance and separation measurements were accomplished using a steel tape measure and plastic metric ruler.

III. Experimental Procedures

Introduction

The purpose of the experiment was to empirically measure the response of infrared detectors to incident MMW radiation in the Ka (26.5-35 GHz) and E (60-90 GHz) microwave bands. Several aspects of a MMW response from the IR detectors were investigated. First, the detectors were tested to observe if any response to MMW energy was present. If a response was observed, additional tests including linearity, polarization dependence, detector temperature, and RF response were performed to characterize the response.

The experiment was conducted in three phases. The first phase of the tests examined the power radiated by the transmitter. Both the magnitude of the on-axis fields and antenna pattern of the transmitting horn were measured. In order to obtain MMW power densities which produced a measurable IR detector response, measurements were conducted in the near-field of the transmitting antennas. Phase I measurements were conducted primarily in the Ka band. The results were combined with analytical predictions to obtain information for the E band.

The next phase of tests determined if each specific IR detector responded to the available MMW microwave power. If the detector responded, further tests were performed to

discover the manner in which the MMW coupled to the detector. Response linearity, polarization dependence, and the effect of placing multiple sources within the detector field of view were some of the aspects tested. The final test phase measured the IR detector response versus RF and amplitude modulation rates.

A description of each experimental phase and associated tests will be provided in the text. Some items are common to the tests used throughout the experiment: amplitude modulated continuous wave (CW) RF irradiation, modulating waveform, detector response measurement, and for the most part the orientation of the transmitting horn and IR detector/dewar. A photograph of the experimental setup is shown in Figure 5. The RF was provided by one of three IMPATT diodes driven by a HP8620C Sweep Oscillator with a Full Band MM-Wave Sweep Control Plug-in. The RF was routed from the IMPATT diodes through the waveguide and associated microwave devices (described in Chapter II) to the pyramidal horn to free space. Only the continuous wave RF mode of the HP8620C Sweep Oscillator was used for the tests. RF changes were accomplished manually via a front panel control. The RF was amplitude modulated via an external source (HP3326A). In all of the IR detector tests, the modulating waveform was a squarewave (50% dutycycle). During antenna measurements, the CW RF was unmodulated.

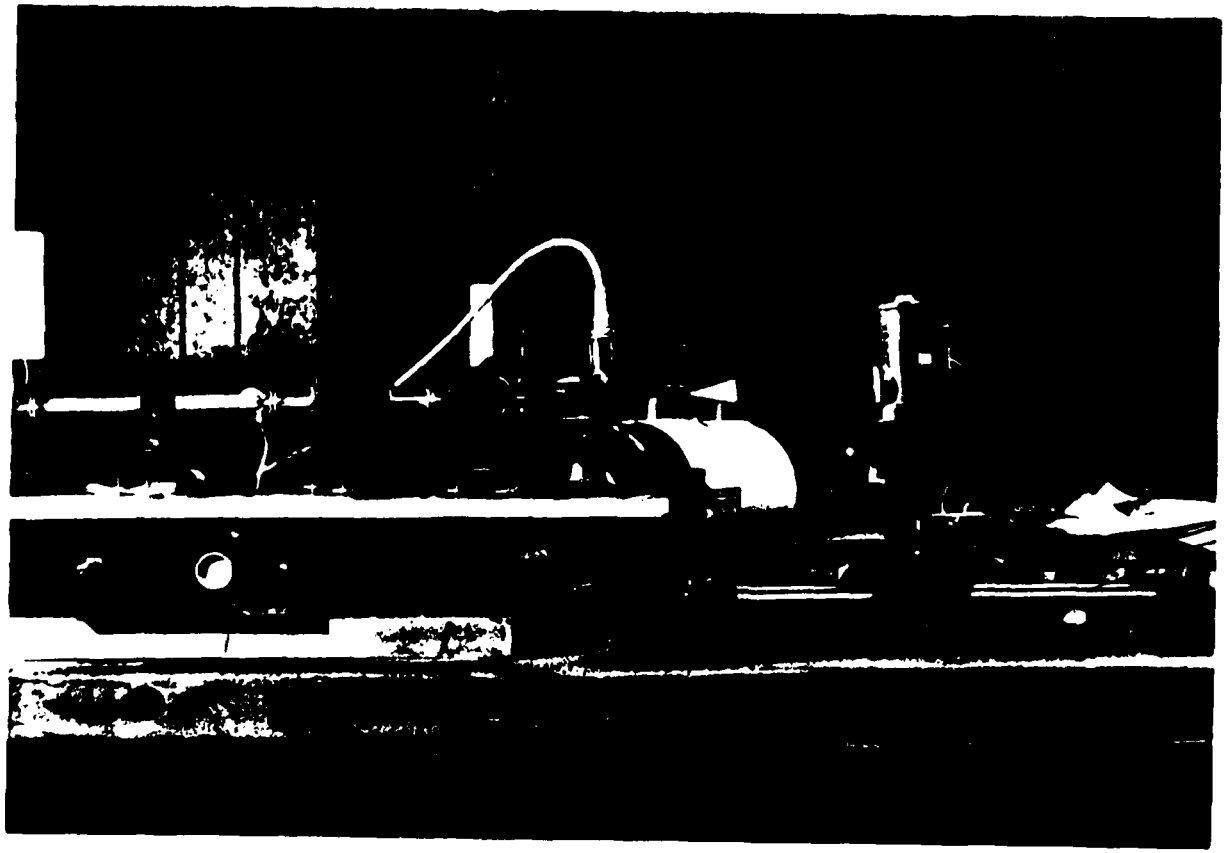

Figure 5. MMW Experimental Set-up

Another commonality throughout the experiment was the method used to measure the output of the IR detector and amplifier configuration. The output of the HgCdTe IR detector was connected to the input of a low noise voltage preamplifier. The output of each InSb detector was connected to the input of a current mode preamplifier. The output of each preamplifier was connected to a spectrum analyzer (HP3585A) capable of analyzing frequency components from 20-40 MHz. The spectral component of the detector output which corresponded to the fundamental frequency of the amplitude modulating (AM) waveform was monitored on the spectrum analyzer. The response of the detector and amplifier configuration was then determined by the level of the detected AM rate measured on the spectrum analyzer. In the majority of the IR detector tests, the orientation of the detector with respect to the transmitting horn was the same. Exceptions are noted when they occur. Normally, the metal dewar in which the detector was mounted was arranged so that its window was centered on the transmitting horn aperture center. Additionally, the dewar was oriented such that the surface of the window was parallel with the front of the horn aperture (reference Figure 6).

Several additional items are common to most of the tests (exceptions are noted). The pyramidal microwave horn was mounted to transmit a vertically polarized wave. The IR detectors were operated at 77K.

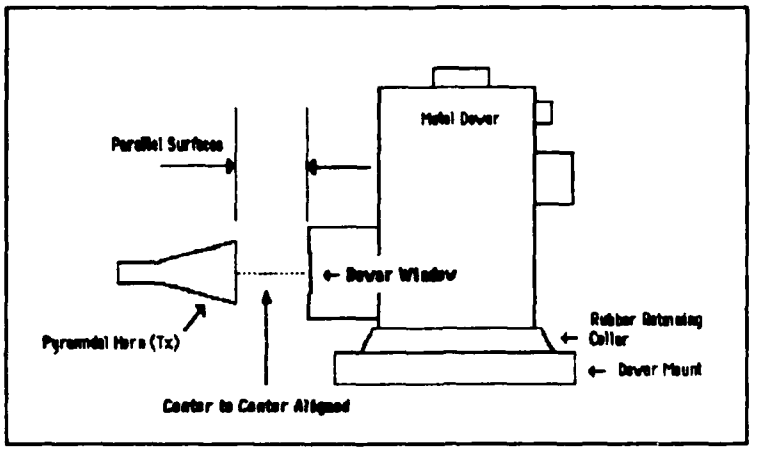

Figure 6. Dewar - Horn Orientation (Side View).

Phase I. (Field Characterization)

The available transmitter power was limited to less than 10 mW. As a result the IR detector response tests had to be conducted in the near-field of the transmitting antenna. The purpose of this test series was to sufficiently describe the power radiated such that ranges relatively free from rapid near-field variations could be identified. In an article by Wang on near-field measurement theory and practices, it is suggested that near-field variations due to evanescent waves are not significant if the separation from the test antenna is greater than several wavelengths (Wang, 1988; 751).

To characterize the fields, two experiments were performed. In the first, a receiving antenna identical in dimensions to the transmitting antenna was used to measure

the antenna power pattern. The transmitting antenna pattern was then inferred from the results based on the principle of reciprocity. The process was repeated at several distances until a point was obtained where the smoothness of the antenna pattern deteriorated.

In the second test, measurements of the on-axis fields from the near-field to the far-field were taken. The near and far-field definitions used throughout the experiments are shown pictorially in Figure 7 as defined by Yaghjian (Yaghjian, 1986: 33).

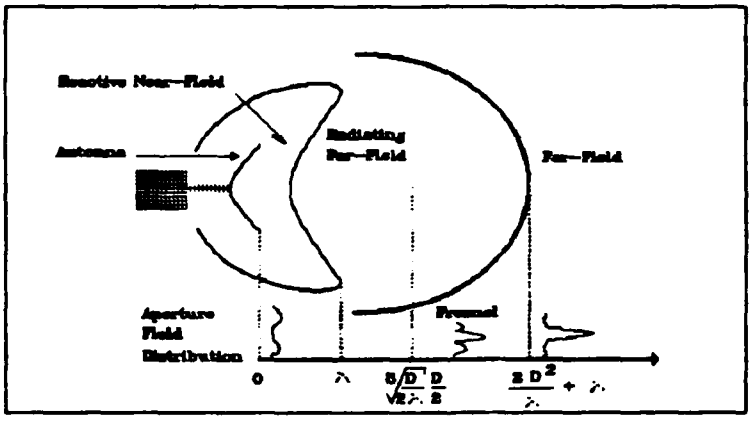

Figure 7. External Fields of Radiating Antenna (Yaghjian, 1986:33).

Antenna Power Patterns. The theoretical field patterns of the two transmitting pyramidal horns are plotted in Figures 8 and 9. Figure 8 is the principal E-plane pattern of the E band 20 dB horn. Figure 9 is the principal E-plane pattern of the Ka band 20 dB horn. The equations governing the principal plane patterns are given in Appendix C.

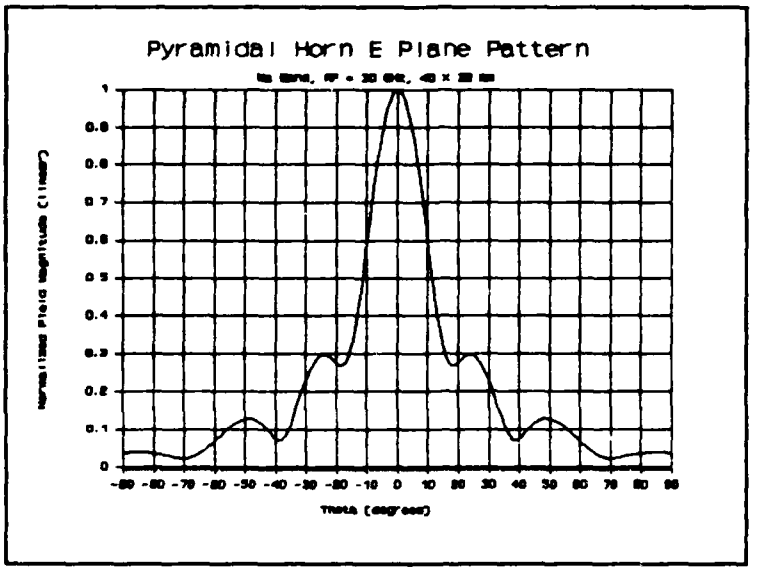

Figure 8. Principal E-plane Pattern of a 20 dB Ka Band Gain Pyramidal Horn.

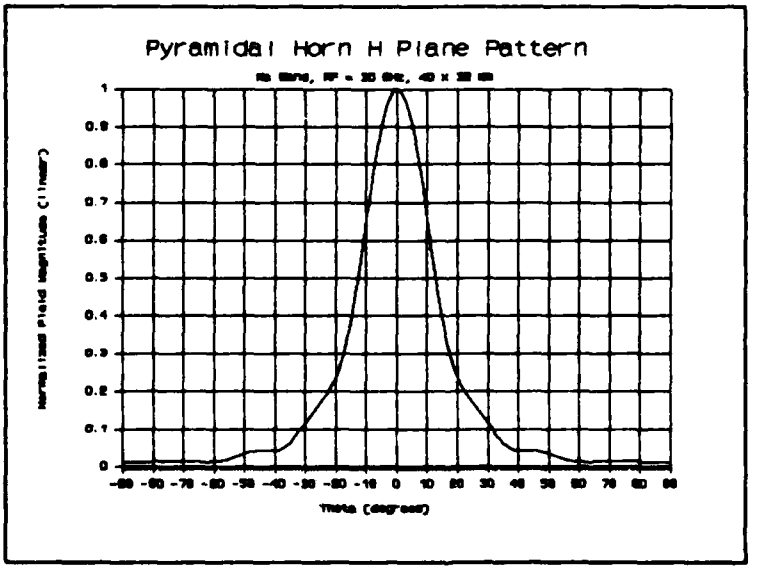

Figure 9. H-plane Pattern of a 20 dB Gain Ka Band Pyramidal Horn Antenna.

The 3 dB beamwidths and gains of the pyramidal horns can be estimated from (Stutzman and Thiele, 1981: 406- 413):

$$HP_H \approx 78 \frac{\lambda^\circ}{A} \quad (1); \qquad HP_E \approx 54 \frac{\lambda^\circ}{B} \quad (2)$$

$$G \approx \frac{2\pi}{\lambda^2} (AB) \quad (3)$$

where

A = Horn width at aperture

B = Horn height at aperture

The horn and waveguide dimensions along with the theoretical 3 dB bandwidths and gains are listed below in Table 3. The gains and beamwidths are calculated at sample frequencies of 30 GHz for the Ka band and 75 GHz for E band. The gain and beamwidth are frequency dependent parameters. Figure 10 illustrates the frequency dependent nature of the Ka-band horn over the frequency range of 26.5-40 GHz.

Table 3. Pyramidal Horn Dimensions, Gain, and Beamwidths

Band	A (mm)	B (mm)	Re (mm)	G dB	HP_H°	HP_E°
Ka	40	32	53	19.1	19.5	16.9
E	18	13.5	40	19.8	17.3	16.0

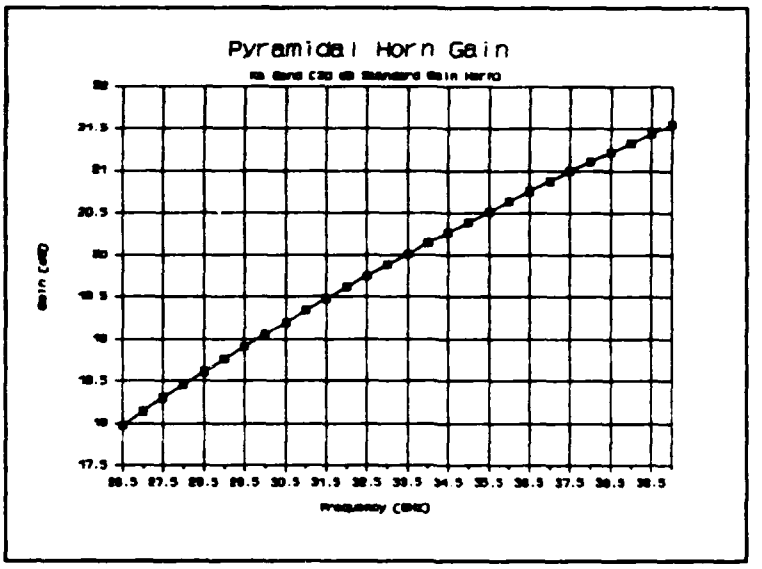

Figure 10. Gain of a 32 x 40 mm Pyramidal Horn Antenna.

Antenna pattern measurement was accomplished using a receiving horn identical in dimensions to that of the transmitting horn. A flat broadband detector was attached to the receiving horn and the detector output fed to the high impedance input of an oscilloscope. The horn and detector were mounted on a stand which could be rotated about its vertical axis in azimuth. The stand base was graduated in degrees so that the rotation could be easily noted. The stand was mounted on several wood blocks and placed on the movable sled of the rail-sled apparatus. The transmitting horn height was adjusted to match that of the receiving horn and their longitudinal axis aligned. The separation between horns was measured with a ruler and angular measurements taken in 1° increments. This was

repeated at several ranges in the near and far-field regions. The RF transmitted was unmodulated CW. The detector output voltage was measured on an oscilloscope.

The RF broadband detector used is a silicon Schottky-barrier diode with typical sensitivities (in the square law region) of 250 mV/mW and 500 mV/mW for the E and Ka bands respectively. The Hughes diodes exhibit a sensitivity flatness of ± 1.5 dB over the waveguide bandwidth (Millimeter Wave Products, 1985: 90). The Schottky-barrier diode operates in the square law region producing an output voltage that is linearly proportional to the input power. Thus, the output voltage of the detector was proportional to the power received by the receiving antenna so that the antenna power pattern could be measured directly.

On-axis Measurements. Theoretical predictions of the on-axis fields radiated by the pyramidal horn are provided in Figures 11 and 12. The equations describing the radiated fields are provided in Appendix C (Jull, 1981: 50-66). As can be seen in the figures, the rapid variations associated with the near-field dampen out within a range of several wavelengths.

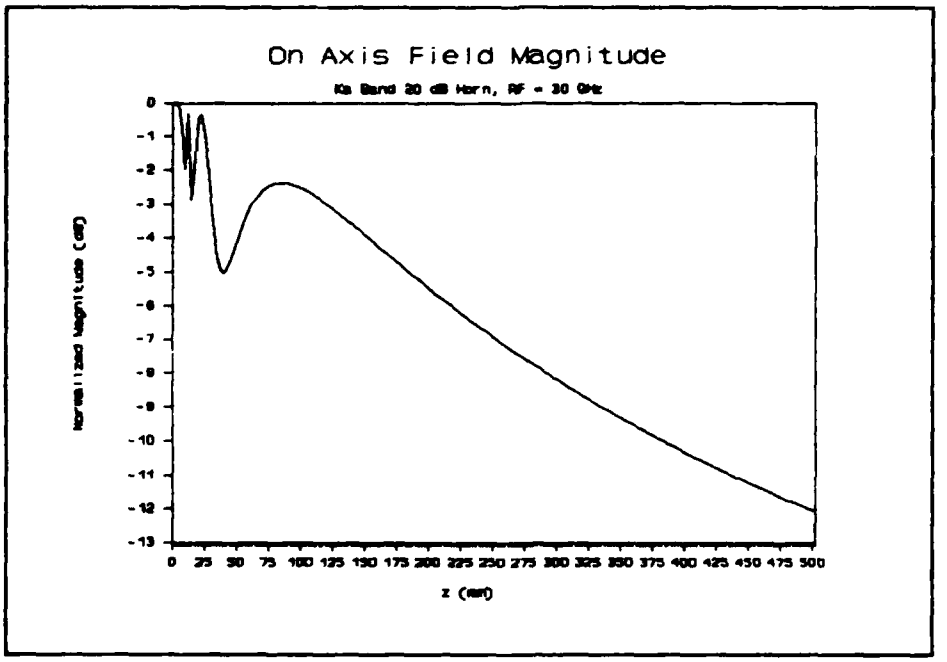

Figure 11. On-axis Fields of a 32 x 40 mm Ka Band Pyramidal Horn Antenna.

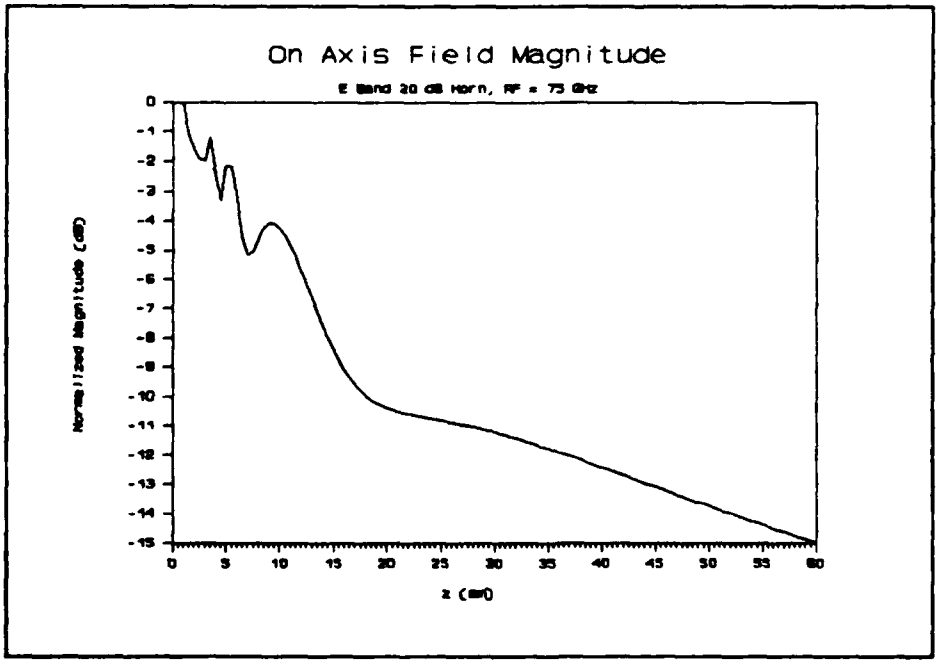

Figure 12. On-axis Fields of a 13.5 x 18 mm E Band Pyramidal Horn.

In the measurement of the on-axis fields, the test set-up was identical to that of the power pattern measurement with the exception that the antenna and flat broadband detector were mounted on a stationary stand. The receive antenna was oriented for maximum signal strength. The angular position was fixed for the maximum signal. Detector voltage measurements were taken on-axis for separations of several centimeters to ranges in the far-field. Voltage measurements were taken at distance increments of a quarter wavelength to observe near-field variations and horn interference effects of a frequency dependent nature.

Phase II. (IR Detector Response)

The purpose of Phase II was to determine if and how each IR detector responded to MMW energy. The tests ranged from initial checks for a response at any distance and frequency to the effects which would occur from having both a MMW and IR source simultaneously present in the detector FOV. Specifically, the tests found if a detector responded, where MMW energy coupled to the IR configuration, whether the detection mechanism was linear or nonlinear, if the response was present at a detector operating temperature of room temperature or 77K (or both or neither), if the MMW polarization affected the response, if an IR source in the detector FOV augmented the detected RF signal, and if interaction between the metal dewar and antenna was present.

Initial MMW Response. The task was to determine if each IR detector responded to MMW radiation at any RF, amplitude modulation rate, orientation, distance, or operating temperature. The modulation rate was chosen primarily to avoid multiples of 60 Hz and to provide a clean square wave as detected by a receiving horn and flat broadband RF detector.

The metal dewar containing the IR detector was placed on the dewar mount with the detector preamplifier placed on the mount base. The detector mount was placed on the movable sled of the rail-sled apparatus. The dewar window was then centered on the transmitting horn aperture as in Figure 6.

An RF with a relatively large power level was selected on the HP8620C. The IR detector preamplifier output was monitored on the spectrum analyzer at the modulation rate fundamental frequency for a response. If no response was noted, the horn to dewar separation was decreased and the output rechecked. This was repeated until the separation was less than 0.5 cm. If a response was not evident, the RF was varied in approximately 0.5 GHz intervals throughout the band. If a response was still not observed, the RF was returned to the original frequency. The dewar orientation was varied in tilt, azimuth, and elevation and the detector output monitored. The orientation which provided the maximum response was used for the remaining tests. If a response

was noted, spectral measurements of the detector output were compared with those taken under identical conditions with the RF off. To test the dependence of the IR detector on its operating temperature, the tests were reaccomplished on a different day with the detectors at room temperature.

Entry Point. The purpose of this experiment was to determine where the MMW energy was coupling to the detector and preamplifier combination. The only obvious coupling port to the IR detector was the dewar window. The simplest test was to block the aperture window in the metal dewar to observe if the detected signal was eliminated. This was accomplished by taping a quarter to a "sticky" and attaching the sticky to the front of the dewar. The "sticky" is a piece of paper with adhesive on one end and side of the paper (generally used for posting notes). The quarter was then placed over the window by attaching the adhesive portion of the "sticky" to the metal above the window. In this manner the quarter blocked the aperture but left the remaining dewar surface, preamplifier, and connecting cables exposed to the incident MMW energy. This proved to be the only "entry point test" required, as blocking the aperture with the quarter effectively eliminated the detected output.

Linearity. This experiment evaluated the IR detector MMW response mechanism for linear or nonlinear characteristics. The detector and amplifier were oriented as in the response test. With the in-line waveguide

attenuator set to 0 dB, the output of the detector was monitored on the spectrum analyzer and the power level of the modulation rate fundamental frequency noted. The attenuation was then increased by 1 dB and the power level measured. This was repeated several times. If a linear detection of the RF was occurring, a 1 dB change in the transmitted power would result in a 1 dB change in the detected signal. If a nonlinear process was involved, the change would be otherwise. A nonlinear square law process would result in a 2 dB change in the detected power for every 1 dB change in the transmitted power.

Polarization. The purpose of this test was to measure the polarization dependence of the IR detector MMW response. First, the transmitting antenna was oriented to transmit a vertically polarized wave. Then, the dewar was positioned to center the dewar window in the transmitting antenna main beam (reference Fig. 6). The separation was noted. The RF was turned on and the IR detector preamplifier response measured on the spectrum analyzer. The RF was turned off and a waveguide with a 90° twist was inserted between the directional coupler and transmitting antenna to obtain a horizontally polarized wave. The height of the jack supporting the transmitting hardware was adjusted to center the transmitting horn aperture on the dewar window center. The dewar orientation was checked to insure the window was still parallel to the aperture surface. The RF CW was

turned on and the frequency measured and adjusted if necessary. With the identical RF and AM rate, the detector output was measured on the spectrum analyzer.

Multiple Sources (HgCdTe). The purpose of this experiment was to observe the effect of placing an in-band IR source and a MMW source in the IR detector FOV simultaneously. The IR signal was generated with a blackbody (IR Blackbody Model 464 manufactured by Infrared Industries Inc.) and chopped at 673.9 Hz. The chopped signal was placed in the detector FOV by altering the beam's elevation and direction with a beam steering instrument. The beam steering instrument is essentially two high grade optical mirrors which provide a 90° change in direction to a beam incident upon the mirror's surface. Each mirror could be adjusted in elevation and azimuth by changing the position of the retaining rings which held the mirrors to a vertical post. The top mirror could be adjusted further through fine and coarse azimuth and tilt controls (reference Figure 3, Chapter 2).

Separation between the transmitting horn and dewar window was fixed. The dewar orientation was as in Figure 3. At this separation, the horn aperture blocked the detector FOV. However, the IR beam diffracted at the horn edges and effectively irradiated the dewar window and IR detector. The RF was fixed and the attenuator set at 0 dB to allow maximum power transfer to the transmitter antenna. Using

the above equipment setup, several tests were performed. The magnitude of the IR blackbody source and RF amplitude modulation rates were varied, and the AM rate was allowed to sweep over a finite range.

Dissimilar Magnitudes. First, the magnitude of the detected IR component at 673.9 Hz was adjusted to a level substantially greater (on the order of 50 dB) than that of the detected RF component. The AM rate of the RF was set to 200 Hz. With both the IR source and the modulated MMW energy incident upon the detector, the level of the detected RF component at 200 Hz was measured on the spectrum analyzer. The beam steering mirrors were then adjusted to remove the IR source from the detector FOV; this was verified by monitoring the 673.9 Hz chop rate on the spectrum analyzer. The level of the detected RF component was measured on the spectrum analyzer.

Next, the modulation rate was set to match that of the IR source chop rate. The steering mirrors were again adjusted to place the IR beam in the detector FOV and provide a signal at the chopper rate on the order of 50 dB greater than that of the detected RF signal. The level of the 673.9 Hz component (RF off) was measured on the spectrum analyzer. The RF was turned on and the combination provided by the detection of both the IR and MMW signals was measured on the spectrum analyzer.

Similar Magnitudes. With the RF off, the magnitude of the chopped IR signal 673.9 Hz component was reduced to the order of the detected RF level by adjusting the beam steering mechanism and monitoring the output signal on the spectrum analyzer. The RF was turned on and the level of the 673.9 Hz component measured.

Signal Combination. To observe if the detected RF signal and IR source signal combined in a linear or nonlinear manner, several test were performed. Linear and nonlinear effects were looked for by controlling the RF, AM rate, and IR signal magnitude. If the two signals combined in a nonlinear fashion, the mixing of the two signals would produce sum and difference frequencies in addition to the original fundamental frequencies of the chopper and RF amplitude modulation rate. If the signals combined in a linear or algebraic manner, the two signals would add together producing constructive and destructive interference without generating additional frequency components.

The level of the IR source was left at a level approximately equal to that of the detected RF signal. The modulation rate of the RF was reduced to 300 Hz. The spectrum analyzer resolution bandwidth was reduced to 3 Hz and the frequency scan set to 800 Hz. The center frequency was set to 600 Hz. With this setting, the spectrum analyzer displayed frequencies from 200 to 1000 Hz allowing the result of nonlinear mixing of the two signals to be observed

on the display. If mixing occurred, the fundamental frequencies (300 Hz and 673.9 Hz) and the sum and difference frequencies (373.9 Hz and 973.9 Hz) would be present in the spectral output of the IR detector preamplifier. With the RF off, a plot of the detected spectrum was made. The RF was then turned on and a plot of the detected spectrum made.

To examine the linear combination of signals, the RF AM rate was adjusted to 673.6 Hz. The spectrum analyzer resolution bandwidth remained at 3 Hz. The frequency span was reduced to 20 Hz. With the center frequency set at 673.9 Hz, the interference between the two signals was observed. As the phase of the two signals changed with respect to each other over time, the resultant interference varied between constructive and destructive effects.

Multiple Sources (InSb). The output of the blackbody was chopped and directed into the FOV of the large area InSb detector with the beam steering mirrors. Monitoring the detector preamplifier output level at the chopper frequency of 673.9 Hz on the spectrum analyzer, the beam steering mirrors were adjusted to produce a level of -85 dBm. The detector was oriented as in Figure 6 and irradiated with amplitude modulated CW RF. With an AM rate of 1085 Hz, the RF was varied through the Ka band and the preamplifier output monitored on the spectrum analyzer. The RF was turned off and the IR blackbody signal redirected to produce an output of 673.9 Hz with a magnitude of -22.6 dBm. The RF

was varied throughout the Ka band and the detector preamplifier output observed on the spectrum analyzer. The AM rate was then dropped to 200 Hz. The detector output was monitored for several RFs within the Ka band. None of the tests resulted in a detectable response to the incident MMW radiation.

Horn to Dewar Interactions. This test examined interactions between the transmitting horn and detector dewar. Previous tests with identical transmitting and receiving horns exhibited maxima and minima at locations correlated to half wavelength intervals. Similar variations were expected as the separation between the horn and dewar was altered. The metal dewar was oriented as in Figure 6. Beginning with a horn to dewar separation of a few wavelengths the dewar was positioned for a response maximum. The output of the detector preamplifier was measured on the spectrum analyzer. The separation was increased in increments of quarter wavelengths. The detector preamplifier output was measured at each increment.

Phase III. (RF and AM Rate Response)

Once it was established that an IR detector responded to MMW radiation, the response was characterized for differing modulation rates and RFs. The output of the detector preamplifier was measured on the spectrum analyzer for incident RFs (constant AM rate) spanning the Ka and E

MMW bands. Then a value of RF was chosen for which the IR detector exhibited a strong response and the AM rate varied.

RF Response. The purpose of this test was to measure the demodulated RF response of the IR detector and amplifier combination at RFs within the Ka and E millimeter wave bands.

The IR detector and dewar were set up as illustrated in Figure 6. The separation between the horn and dewar was held at a constant distance (± 1 cm) during the test. In the Ka band RF response test, it was necessary to compensate for multiple reflections between the transmitting horn and metal dewar. The reflections caused maxima and minima in the detector preamplifier signal output as a function of distance. To compensate for this, the separation was allowed to vary as the RF changed in order to locate a maximum response. The absolute separation was kept to within ± 1.0 cm. In the corresponding E band test, a separation was chosen such that the maxima and minima present in the detector output were minimized; for the E band test, the separation was held constant. The RF values were incremented by 0.5 GHz across the sub-bands. During each RF response test, the amplitude modulation rate was kept constant. The detector preamplifier output was measured on the spectrum analyzer. The RFs were measured using a Hughes in-line waveguide frequency meter and HP432A Power meter; as the frequency selected on the frequency

meter was tuned in on the HP8620C Sweep Oscillator, the power indicator on the HP432A would dip. The transmit power was measured at each RF.

The AM rate, horn to dewar separation, and dewar orientation were all chosen to maximize the output of the IR detector and preamplifier. The AM rate was selected based on the ability of the RF modulator to produce a clean square wave as detected with a broadband RF detector and receiving horn; this required a fairly low AM rate of 100-400 Hz. The second requirement for the AM rate was the absence of interfering noise at the same frequency. The dominant noise sources in the IR detector output were caused from florescent and incandescent lights. The radiation from the light sources caused large signal responses in the detector output at frequency multiples of 60 Hz. This was reduced by turning off the lights in the half of the room where the test was conducted. The horn to dewar separation was selected to provide a sufficient IR detector response across the MMW band under test.

AM Rate Response. The purpose of this test was to measure the response of the IR detector and preamplifier combination vs different AM rates. The RF and horn to dewar separation were held constant. The detector dewar was oriented as in Figure 6. With the RF on, the AM rate was set to a specific value and the detector output monitored and measured on the spectrum analyzer. The spectrum

analyzer display center frequency was set to each AM rate selected. The AM rate was changed and the process repeated. The level of the transmitted power was measured at each AM rate. The MMW modulator did not respond uniformly across the range of AM rates which were measured; equipment specifications indicated limitations in modulator response to external rates less than 1 kHz.

IV. Results

Introduction

Of the three IR detectors tested, only the HgCdTe detector and preamplifier combination exhibited a response to incident MMW radiation. When subjected to the same tests, the InSb detectors did not produce a measurable response. To summarize, the HgCdTe detector demonstrated a response which is:

- Frequency dependent
- Polarization dependent
- Characterized by square law detection
- Temperature dependent (detector must be cooled)
- Independent of IR sources within the system field-of-view

The results will be presented in the same order in which the experimental procedures were developed. Phase I (preliminary test environment characterization) results will be presented first. Then the results of the individual tests in which the manner of the IR detection occurs (Phase II) will be discussed. Last, the MMW response of the detector versus RF and amplitude modulation rate will be presented.

Phase I.

In the first set of tests, the radiated MMW microwave power in the Ka band was examined by measuring the antenna power pattern and magnitude of the on-axis fields.

Antenna Patterns. The antenna power pattern of the Ka band pyramidal horn was first measured at a range (far-field) of 101 cm, RF of 33 GHz, and vertical polarization. After measuring the pattern in the far-field, several intermediate ranges were selected for pattern measurements. The received RF was detected by a flat broadband detector operating in the square law region. Because of the square law behavior, the output voltage of the detector is directly proportional to the received power. Thus, the output voltage versus azimuth angle represents the power pattern of the receive horn. The power pattern of the transmit horn is inferred from the results by the reciprocity theorem (Stutzman and Thiele, 1981: 45).

Figure 13 illustrates the measured power pattern at a range of 101 cm. The vertical scale indicates the normalized output voltage from the broadband detector. The voltage was normalized with respect to the received detector voltage at 0° azimuth and 0° elevation. The elevation was held constant while the azimuth was varied. The measured half power beamwidth is 16° (measured at the point where the normalized detector voltage decreases to 0.5). The theoretical half power beamwidth is 15.3°.

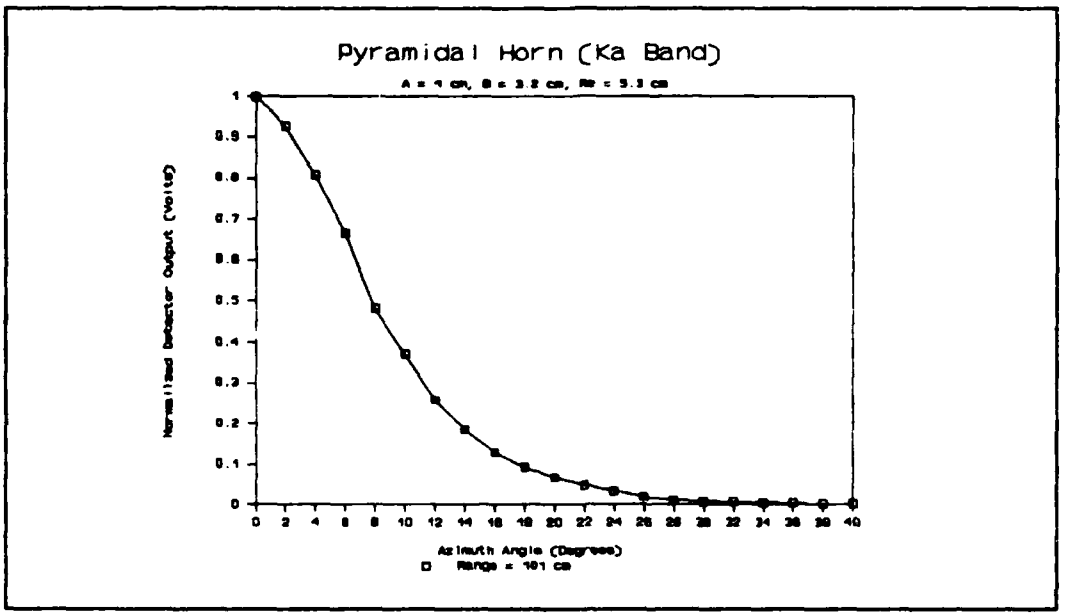

Figure 13. Measured Power Pattern of the Ka Band Pyramidal Horn. Range = 101 cm.

The receive antenna power pattern was measured at several intermediate ranges. Figure 14 displays the measured patterns. The measured patterns were relatively smooth at each range. Only a slight perturbance is evident in the pattern when the range is decreased to 5 cm.

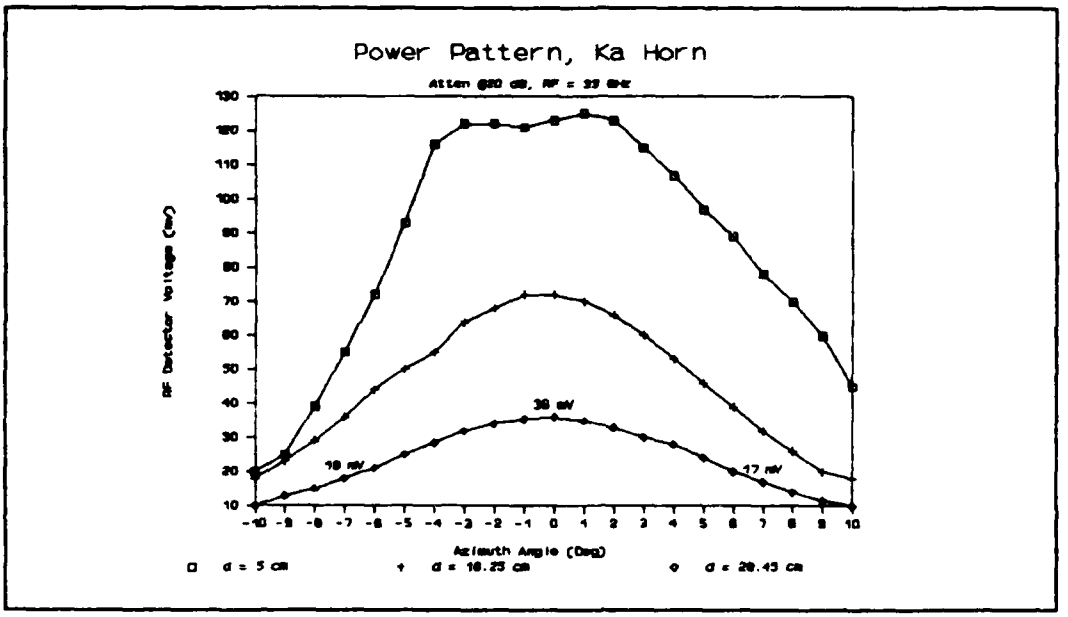

Figure 14. Power Pattern Measurements of the Ka Pyramidal Horn. Ranges = 5.00, 16.25, and 29.45 cm.

On-axis Magnitude. The theoretical values for the on-axis fields illustrated that the rapid near-field variations diminished within a separation of 7.5 cm for the Ka band and 2.0 cm for the E band pyramidal horns (reference Figures 11 and 12). Measurements of the on-axis power magnitudes were done in the Ka band at 33 GHz. The results are displayed in Figure 15.

The results in Figure 15 show rapid fluctuations in the on-axis fields at distances exceeding that predicted by theory. The fluctuations are clearly related to the RF wavelength. Maxima are located a $\lambda/4$ from adjacent minima. Consecutive maxima are separated by $\lambda/2$ as are consecutive minima. The fluctuations are most likely due to multiple

reflections which exist between the transmit and receive antenna. Newell discusses similar effects between near-field probes and antennas under test for on-axis fields and attributes the cause to multiple reflections between the antenna and probe (Newell, 1988: 765). The periodic variations will be a factor in IR detector measurements. For a given RF, the position of the IR detector will affect the received signal strength. However, the locations of the maxima and minima may not be at the same location or as clearly defined as that of the antennas. Reflections from the metal dewar will occur at its face and from within the interior located behind the window.

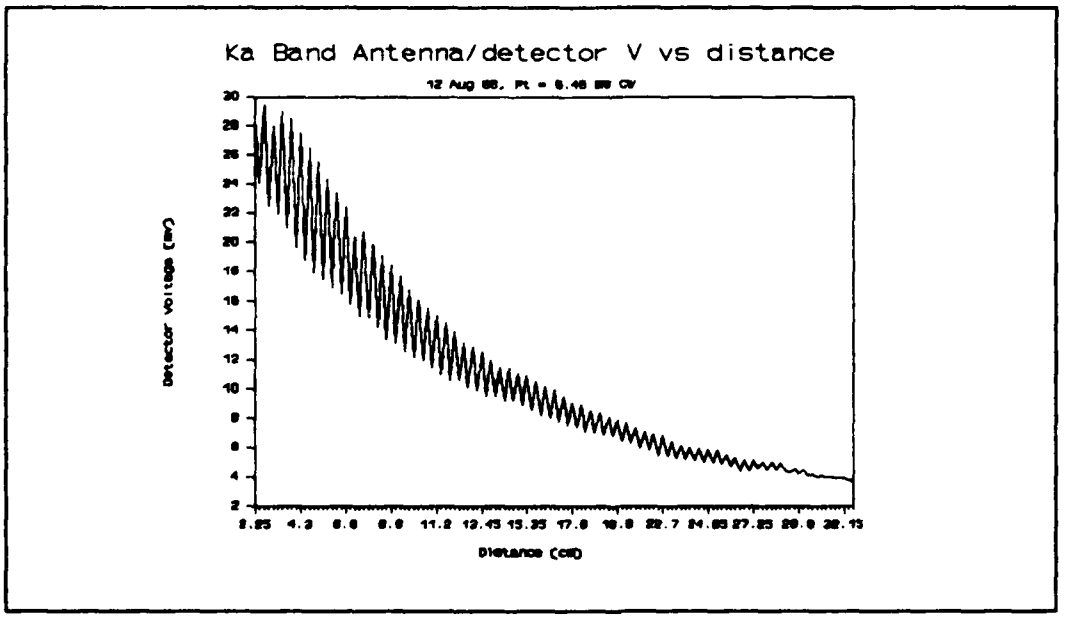

Figure 15. Ka Band Pyramidal Horn On-axis Power Measurements.

Antenna pattern and on-axis power measurements were not accomplished in the E band. Rather, the conclusions gained from the Ka band measurements were used to infer the E band results. As the measured Ka band antenna patterns and beamwidths matched the theoretical values quite well (within 1°), the theoretical values for the E band were accepted as actual. The periodic $\lambda/2$ power fluctuations measured in the Ka band, caused by multiple reflections between antennas, was deemed a factor which would have to be accounted for in both Ka and E band measurements.

Phase II. (IR Detector Response)

Results will be presented only for the HgCdTe IR detector tests. No response which could be correlated to MMW radiation was observed for the InSb detectors.

Initial Response. Measurements were accomplished with the HgCdTe detector cooled to 77K. With the RF set to 32.78 GHz, the AM rate to 200 Hz (square wave), and the transmit horn to dewar separation set to 34 cm, the output of the IR detector and preamplifier was monitored on the spectrum analyzer. The power indicated on the HP432A at the coupled port of the output directional coupler was -11.62 dBm. This corresponded to a radiated power of 28.6 dBm providing a power density at 34 cm of 50 $\mu W/ cm^2$. The radiated power was computed from:

$$P_t(dBm) = P_m + 20_{DC} + Cf + 10Log(2*\pi*A*B) - 20Log(\lambda) \quad (4)$$

where,

P_t = maximum power radiated by the antenna

P_m = power indicated by power meter

Cf = thermistor correction factor

A = Horn aperture width

B = Horn aperture height

λ = Transmitted wavelength (free space)

20_{DC} = Coupling factor (directional coupler)

Power densities were estimated from

$$S(mW/cm^2) = P_t/(4\pi R^2) \qquad (5)$$

where

S = power density at a distance R

P_t = maximum radiated power

R = distance in cm

Figure 16 displays the response measured on the spectrum analyzer. The vertical scale indicates power level in dBm referenced to 50 Ω. The top graticule corresponds to a reference of -25.0 dBm. The relevant spectrum analyzer settings are annotated on the display: RBW - resolution bandwidth, VBW - video bandwidth, Span - frequency span, ST - time required for one complete scan of the frequency span, and Center - center frequency of span. "Marker" or "counter" indicates the frequency component being measured. When the "counter" position is selected, an internal frequency counter is used to measure the signal frequency. The readout accuracy of the "marker" is ± 0.2 % of the

frequency span ± the resolution bandwidth. The "counter" accuracy is greater than that of the marker position depending on the signal amplitude. For a signal 20 dB greater than other signals and noise within the resolution bandwidth setting, the "counter" position can provide accuracies of ± 0.3 Hz (HP Test and Measurement Catalog, 1988: 108). The amplitude displayed directly below the marker frequency is the level of the frequency component indicated. In Figure 16, the amplitude of the 200 Hz component corresponding to the detected AM rate of the incident RF is -97.4 dBm.

In Figure 16, an output at 200 Hz is present corresponding to a detected output from the HgCdTe detector, dewar, and preamplifier combination. Outputs at 60 Hz, 120 Hz, and 240 Hz are also evident. The 60 Hz multiples are due to interference from stray radiation caused by incandescent and florescent lighting.

To verify the output observed as a result of the incident RF, the RF was turned off and another plot of the detected spectrum made using identical test conditions. Figure 17 illustrates the result. The spectral outputs at 60 Hz multiples are still present. The 200 Hz component was reduced by 9.8 dB, leaving only random noise at 200 Hz.

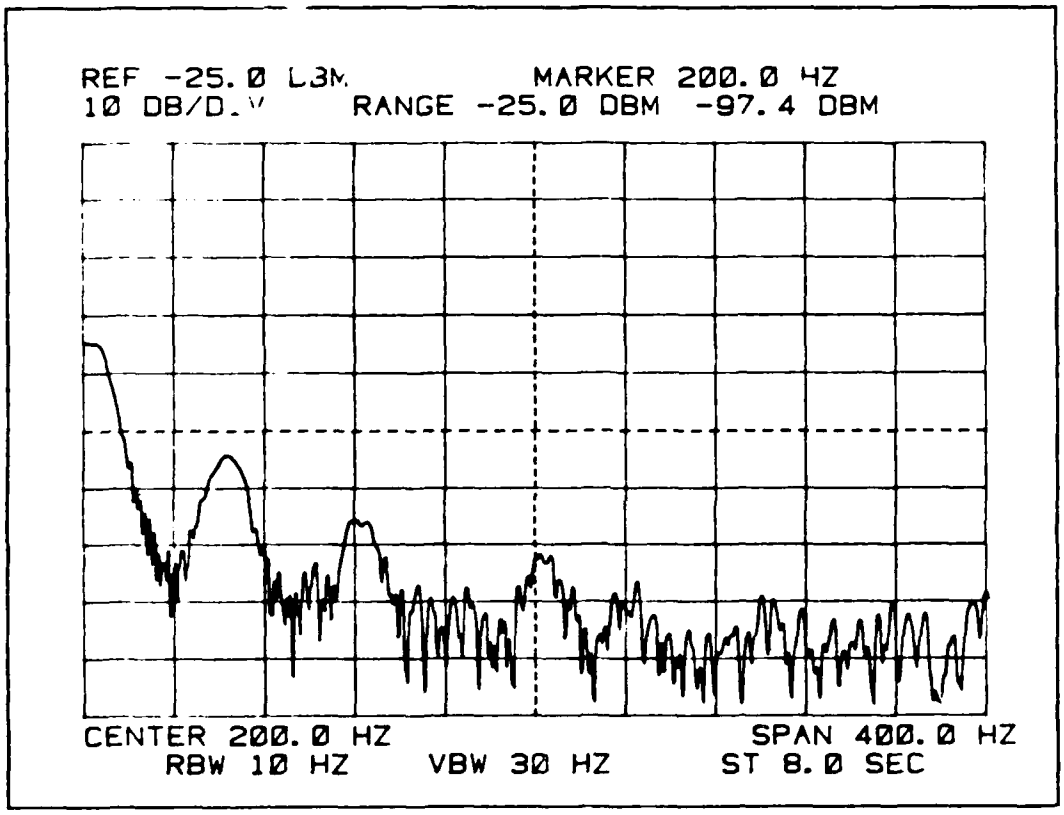

Figure 16. Spectral Output of The HgCdTe Detector and Preamplifier Output. RF = 32.78 GHz, AM = 200 Hz, separation = 34 cm.

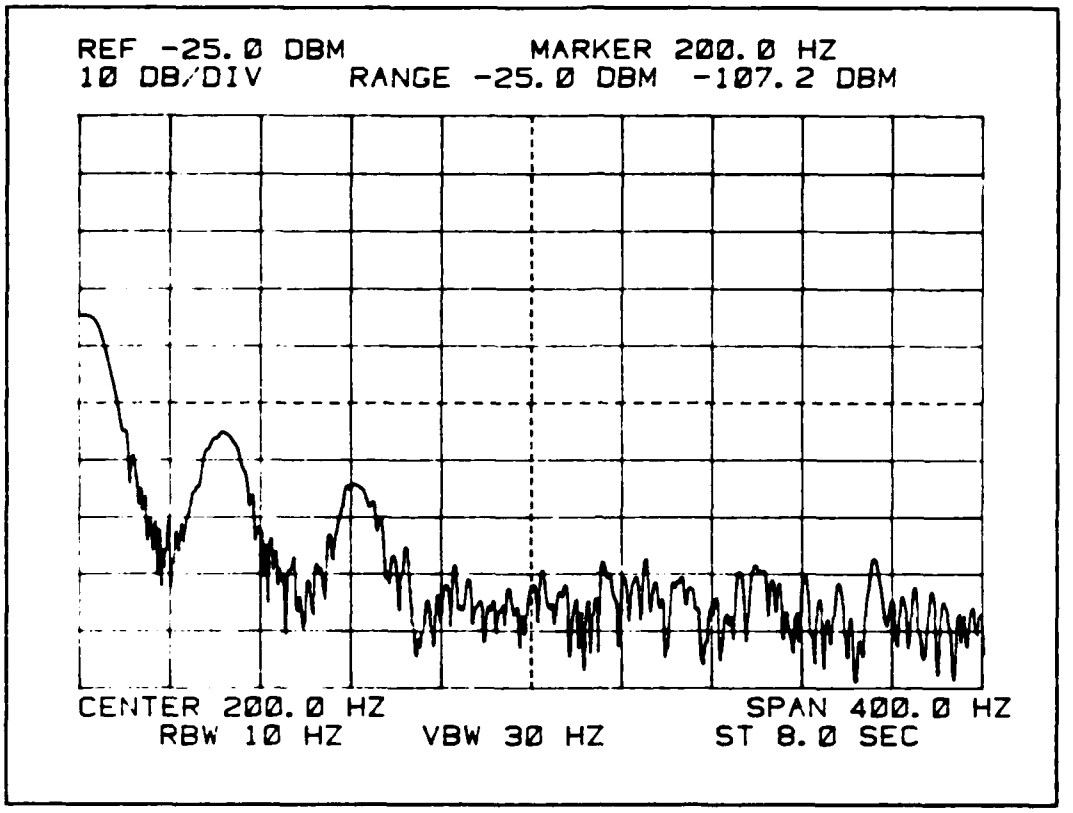

Figure 17. HgCdTe Detector and Preamplifier Spectral Output. RF = off, separation = 34 cm.

Interference from lighting was verified by measuring the IR detector output with the overhead lights on and off. Figure 18 displays the detector output with the florescent lights directly overhead. The level of the 120 Hz component was measured at -74.5 dBm (reference Figure 18). The overhead lights were then turned off and another plot made. The results are shown in Figure 19. The level of the 120 Hz component is -88.6 dBm. A relative advantage of 14.1 dB was obtained by turning the overhead lights off.

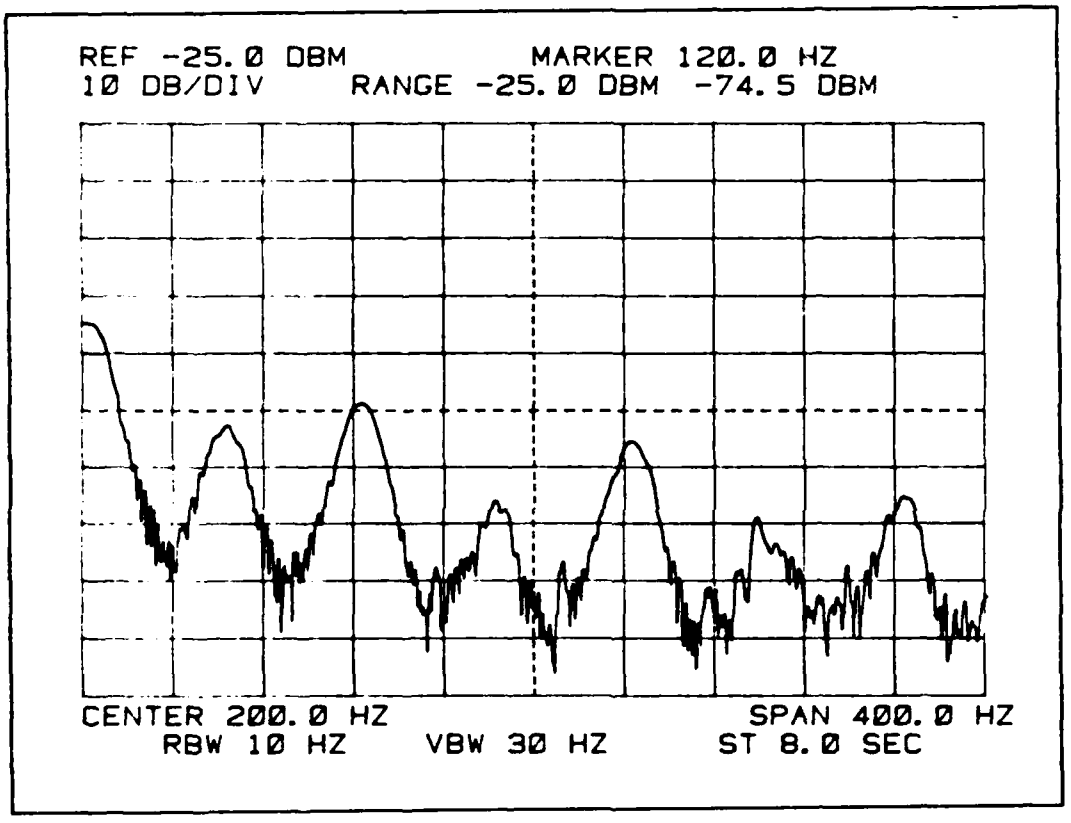

Figure 18. HgCdTe Detector and Preamplifier Spectral Output With Overhead Florescent Lights On. RF = Off.

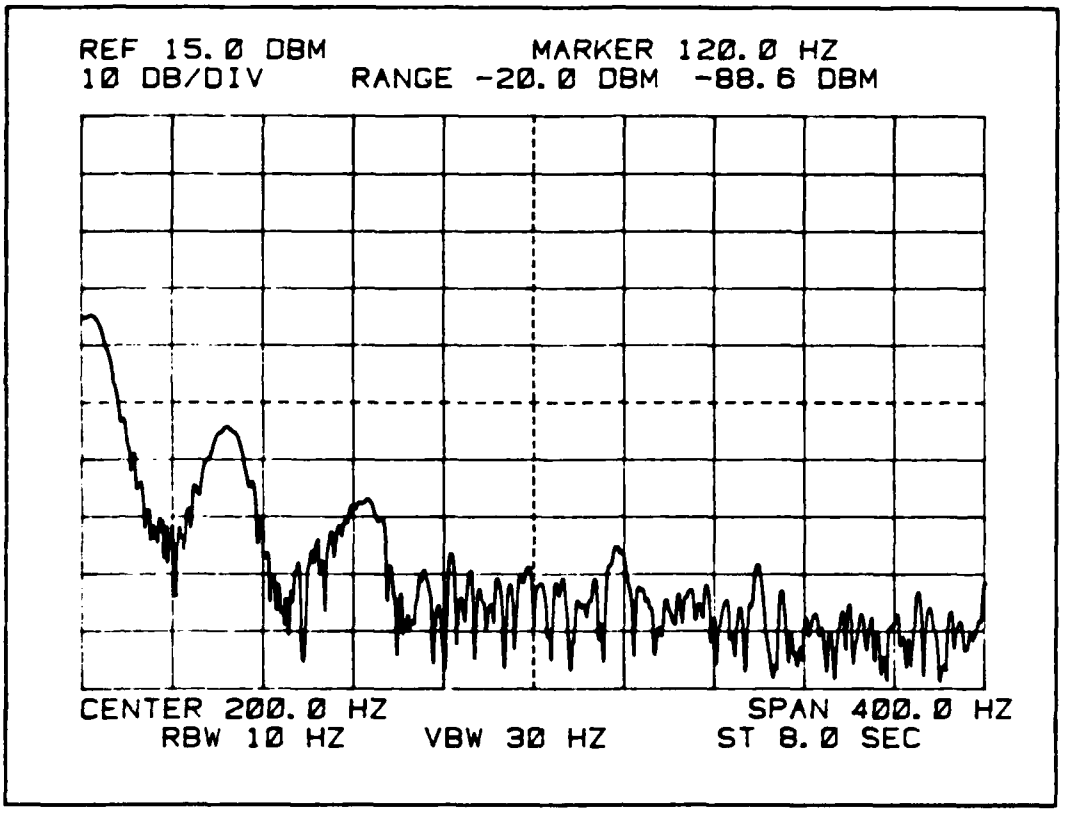

Figure 19. HgCdTe Detector and Preamplifier Spectral Response With The Overhead Lights Off. RF = Off.

A plot of the response with the RF at 90 GHz is displayed in Figure 20. Figure 21 is a time and amplitude response for the same RF, separation, and AM rate as Figure 20. The separation between the transmitting horn and the dewar window is 4 cm. The power output is unknown as the thermistor mount for the E-band was not operational. As in Figure 16, the MMW polarization is vertical. The display of Figure 20 clearly indicates a response of -75.2 dBm at the AM rate of 200 Hz. Interference from stray lighting causes the 120 Hz response.

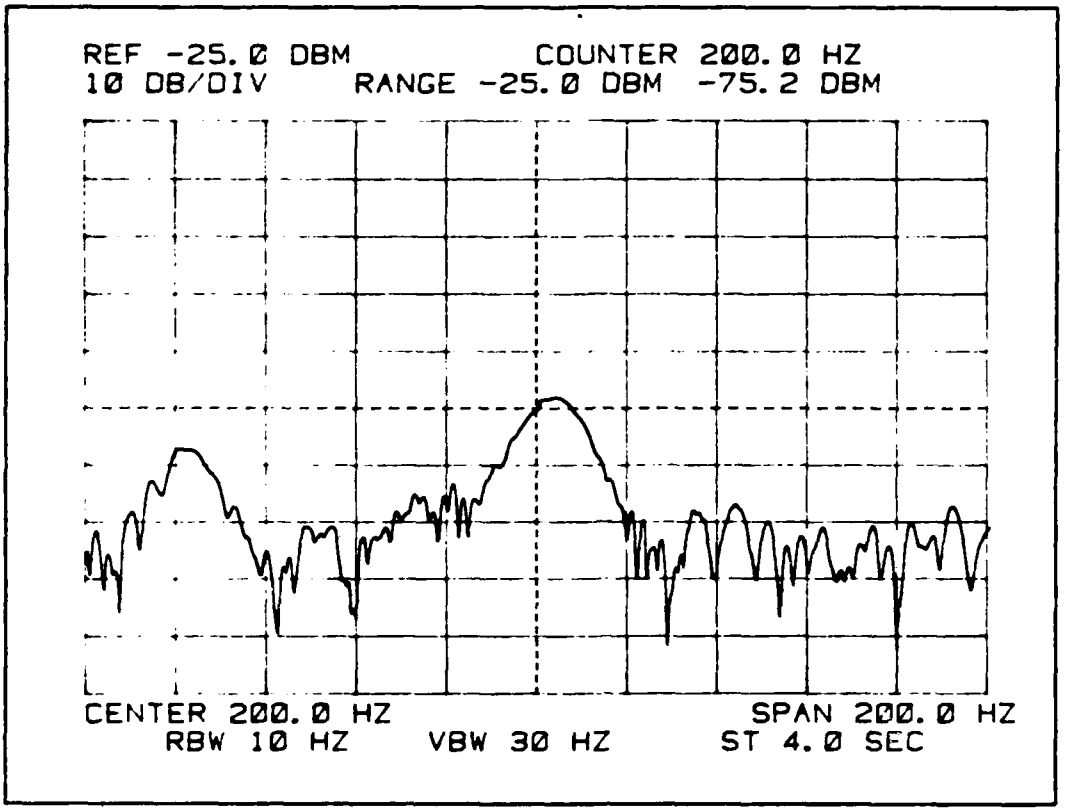

Figure 20. HgCdTe Detector and Preamplifier Spectral Output. RF = 90 GHz, AM = 200 Hz, Range = 4 cm.

Additional plots were made at different RFs, distances, and AM rates to substantiate the MMW response for different conditions. The results are similar to those displayed in Figures 16 and 20 and are included in Appendix D.

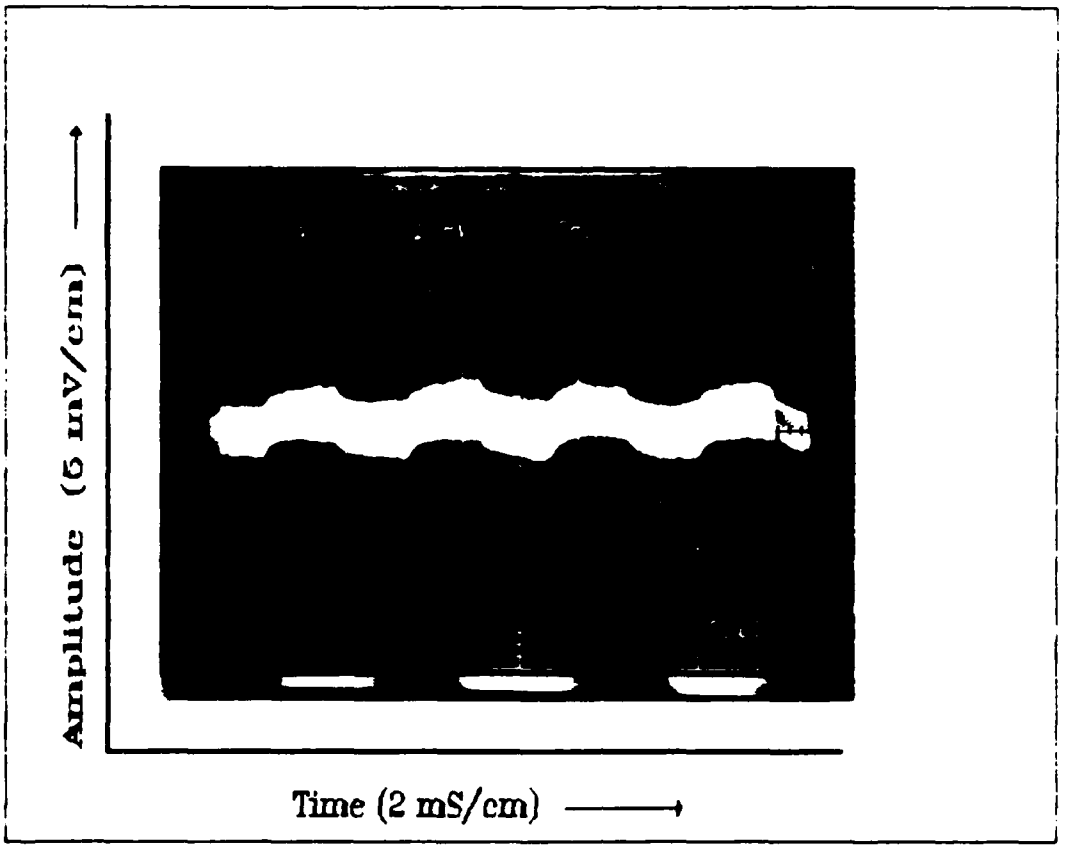

Figure 21. Time and Amplitude Response of the HgCdTe Detector and Amplifier. RF = 90 GHz, AM = 200 Hz, Range = 4 cm.

Entry Point. The most obvious place for MMW energy to couple to the IR detector was through the dewar window. To verify this, a simple test was performed in which the IR detector output was measured with the dewar window uncovered and then blocked. Figure 22 is a spectrum analyzer plot of the IR detector and preamplifier response with the window unobstructed. Figure 23 is a spectrum analyzer plot of the IR detector and preamplifier output at the same separation,

RF, and AM rate but with the window obstructed by a coin (quarter). Figure 22 displays an output of -75.8 dBm at the AM rate of 200 Hz. With the window blocked by the quarter, the output is eliminated, leaving only noise.

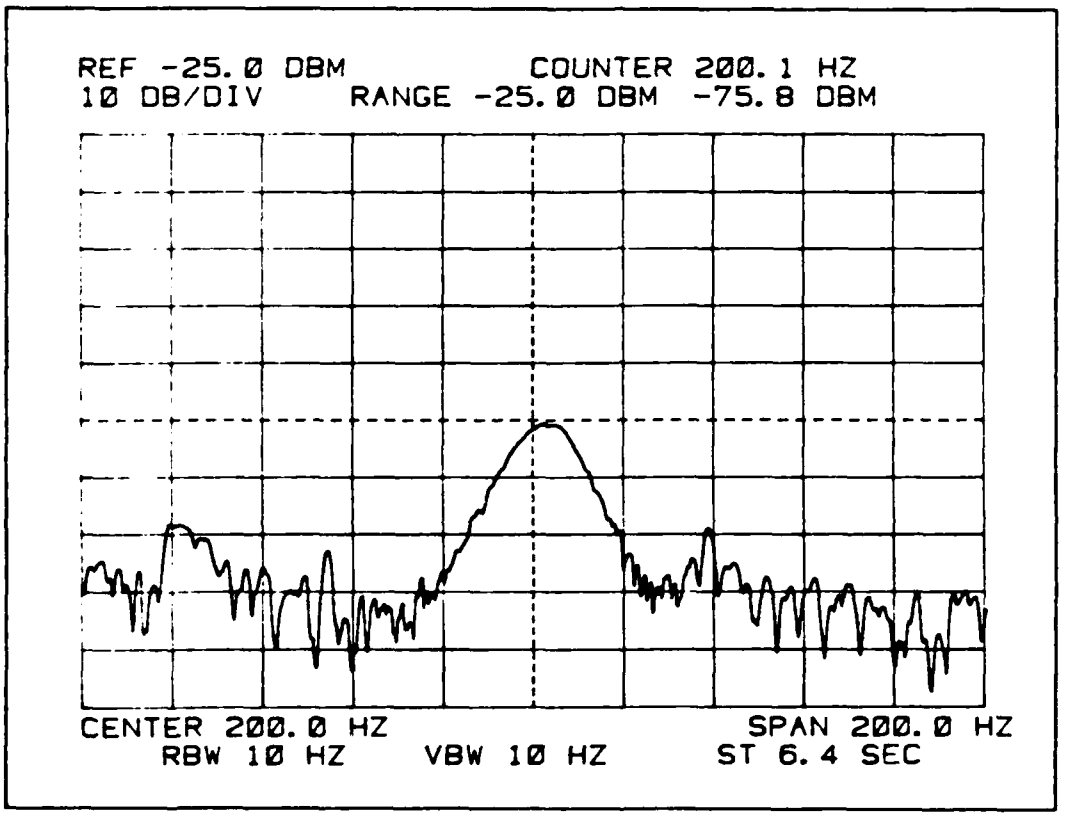

Figure 22. HgCdTe Detector and Preamplifier Spectral Response. RF = 33 GHz, AM = 200 Hz, Range = 5 cm.

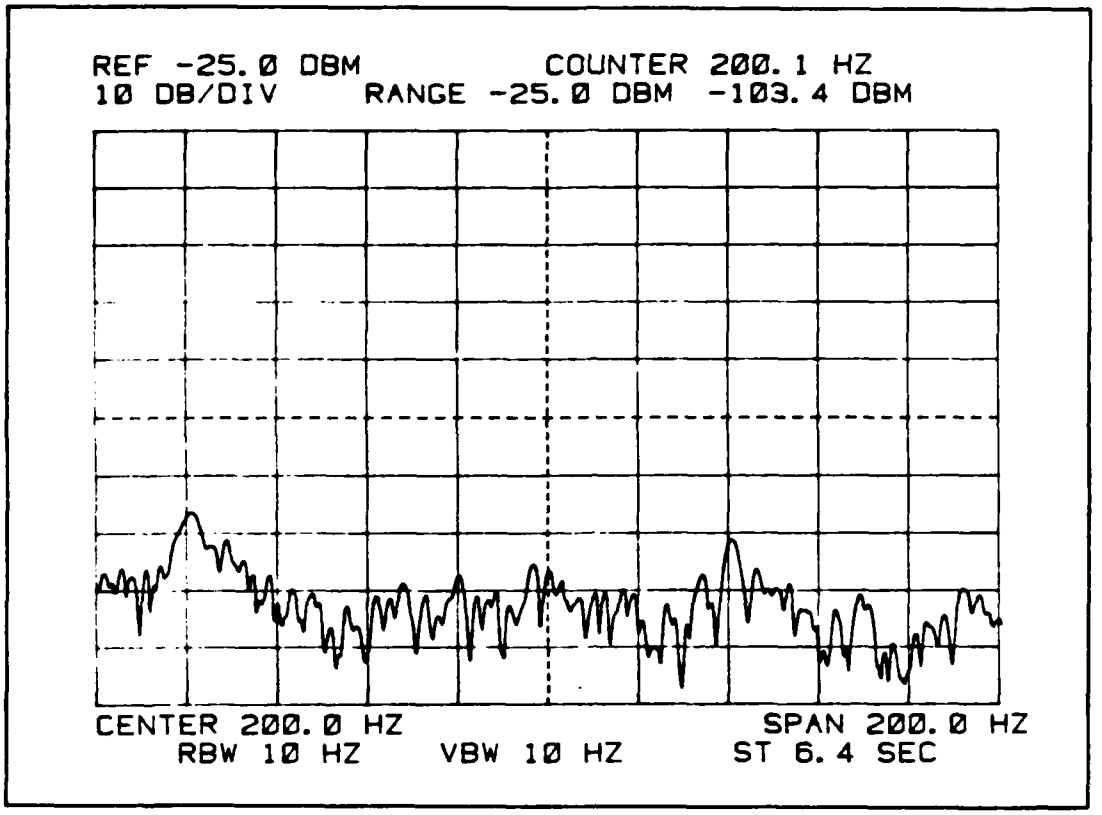

Figure 23. HgCdTe Detector and Preamplifier Spectral Output With The Dewar Window Blocked By A Coin (Quarter). RF = 33 GHz, AM = 200 Hz, Range = 5 cm.

The simplicity and efficiency of the "25 ¢" test was such that it was repeated throughout the experiment to verify that the incident RF was coupling to the detector element through the window and not to the connecting cables or other portions of the dewar or preamplifier. Each time the test was applied, the result was the same. Blocking the window aperture eliminated the MMW response.

Linearity. The test purpose was to determine if the MMW response of the IR detector was square law, linear, or otherwise. The test was performed in both the Ka and E bands. In each test, only the setting of the precision waveguide attenuator was varied. The RF, AM rate, and separation were constant.

The results of the linearity test in the Ka band are tabulated in Table 4 and displayed graphically in Figure 24. The RF was set to 33 GHz, the AM rate to 200 Hz, and the separation to 5 cm. The spectrum analyzer settings were: ST = 6.4 sec, RBW = 10 Hz, VBW = 10 Hz, Center = 200 Hz, and Span = 200 Hz. Five readings were taken for each setting of the attenuator and the mean and standard deviation reported. The difference between the averaged measured detector responses was in turn averaged. The average change in the detected output for each 1 dB change in attenuator setting was 1.94 ± 0.3 dB. This indicates a square law response from the IR detector to incident MMW radiation. The raw data is attached in Appendix E.

Table 4. Ka Band Linearity Data (HgCdTe Detector Output)

Atten. (dB)	Mean Resp. dBm	σ dBm	Δx dB	Power Meter (dBm)
0	-76.6	0.16	-	-12
1	-78.6	0.21	2.0	-13
2	-80.9	0.29	2.3	-14
3	-82.4	0.16	1.5	-15
4	-84.4	0.15	2.0	-16
5	-86.3	0.4	1.9	-17

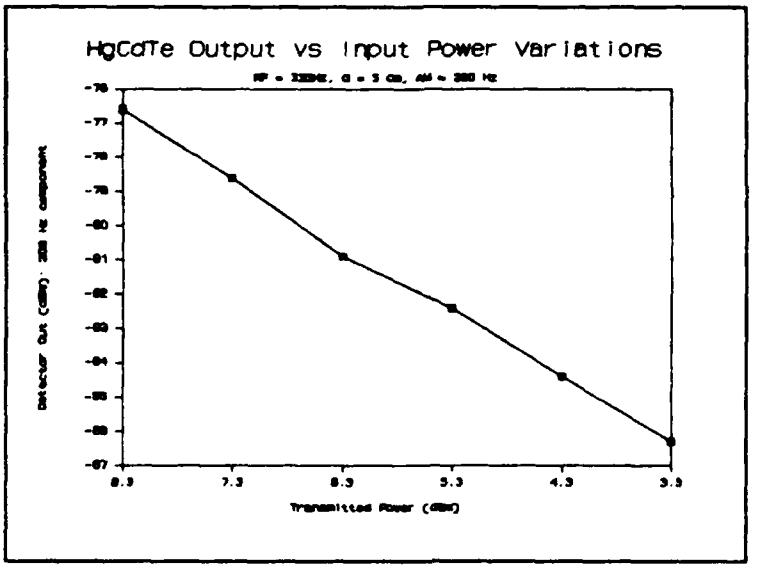

Figure 24. HgCdTe Detector and Preamplifier Response vs MMW Power Variations. RF = 33 GHz, Range = 5 cm, AM = 200 Hz.

A similar linearity test was conducted in the E band at 75.0 GHz. The separation was set to 4.0 cm and the AM rate was set to a 1000 Hz square wave. For each setting of the in-line precision attenuator, five readings were taken. The average and standard deviation of each attenuator setting along with the attenuator settings are tabulated in Table 5. The results in Table 5 indicate an average difference in the power level of the IR detector preamplifier output of 1.05 dB ± 0.57 dB for each change in the attenuator setting of 0.5 dB. Figure 25 displays the results graphically. The E band results, in agreement with the Ka band results, indicate a square law response mechanism.

Table 5. Linearity Test, RF = 75.0 GHz

Atten. dB	Mean Resp. dBm	σ dB	Δx dB
0.0	-85.8	0.4	-
0.5	-86.6	0.6	0.8
1.0	-87.0	0.8	0.4
1.5	-89.1	0.7	2.1
2.0	-90.4	1.2	1.3
2.5	-91.2	0.9	0.8
3.0	-92.5	1.0	1.3
3.5	-92.9	1.1	0.4
4.0	-94.2	0.9	1.3

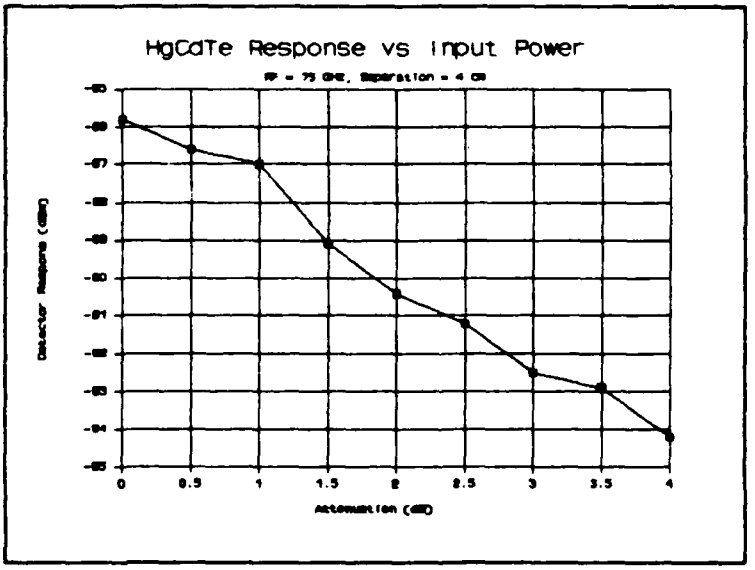

Figure 25. HgCdTe Detector and Preamplifier Response vs Input Power Variations. RF = 75 GHz, Range = 4 cm, AM = 1000 Hz.

Polarization. To check the dependence of the HgCdTe MMW response to the polarization of the incident RF, a 90° waveguide twist was inserted before the transmit antenna to change the polarization to horizontal. Figure 26 shows the detector response to a vertically polarized wave at 28.0 GHz amplitude modulated at 200 Hz, with the horn to dewar separation set at 7.5 cm. The polarization was changed to horizontal using the 90° twist. The power meter indication remained constant at -17.5 dBm for both polarizations. Separation was set to 7.5 cm and the RF remeasured using the frequency meter. Figure 27 illustrates the result. When the polarization was changed to horizontal, the detected response vanished.

Figures 26 and 27 illustrate a strong dependence of the HgCdTe detector to the polarization of the incident MMW. A check of other RFs revealed a response at horizontal polarization. With the polarization at horizontal, the RF was changed to 29.43 GHz. A response was observed on the spectrum analyzer with an average level of -97.1 ± 1.3 dBm at 200 Hz. Blocking the aperture with a quarter eliminated the response confirming MMW coupling through the dewar window.

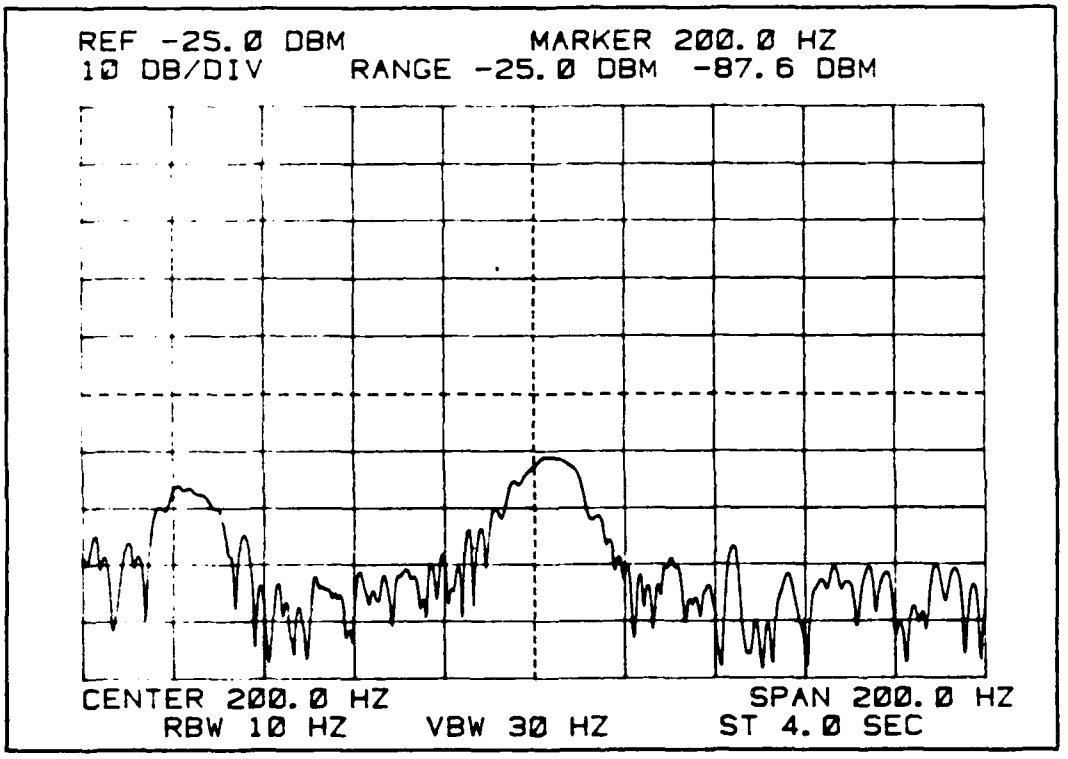

Figure 26. HgCdTe Detector and Preamplifier Spectral Response. RF = 28.0 GHz, AM = 200 Hz, Range = 7.5 cm, Vertical Polarization.

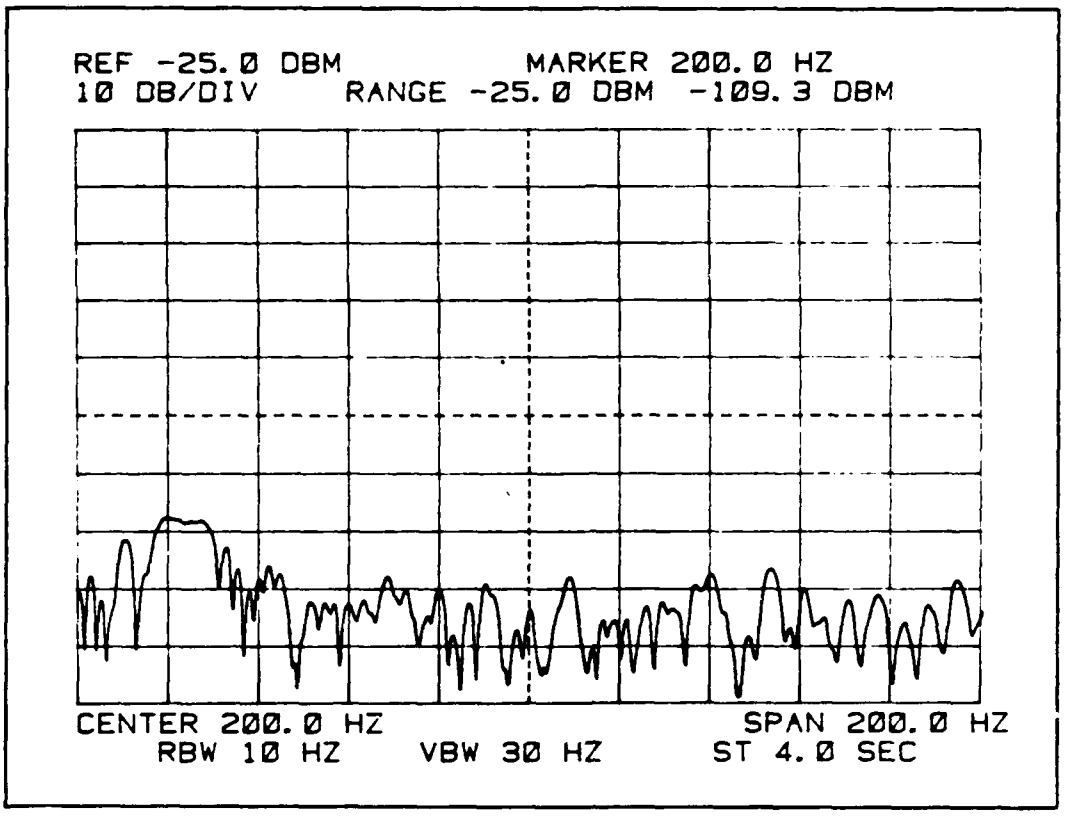

Figure 27. HgCdTe Detector and Preamplifier Spectral Response. RF = 28.0 GHz, AM = 200 Hz, Range = 7.5 GHz, Horizontal Polarization.

Cross polarization measurements were performed with the transmit antenna arranged for horizontal polarization. The receive antenna was adjusted for first vertical and then horizontal polarization and the received power measured. At 28.0 GHz a ratio of the received voltage for vertical to horizontal polarization of the receive antenna was -51.8 dB. At 29.4 GHz, the ratio was -46.0 dB. The ratio of the cross polarized components is not constant across all frequencies. This could explain in part the lack of a response from the IR detector for a horizontal polarization at 28 GHz while a

response of -97.1 dBm is present with vertical polarization at an RF of 29.43 GHz. The 46 dB ratio at 29.4 GHz indicates a cross polarized component which is 5.8 dB greater than the relative value of the cross polarized component at 28 GHz. Given a square law response mechanism in the IR detector, the detected response would be 11.6 dB lower at 28 GHz than the response at 29.4 GHz. This would put the IR detector response at a power level of -108.7 dBm. This level would be unmeasurable from that of the noise.

Temperature. In this test, the IR detectors (both HgCdTe and InSb detectors) were operated at room temperature. None of the detectors produced a response to the incident MMW radiation regardless of the RF frequency, dewar orientation, or horn to dewar separation. Plots of the HgCdTe detector responses with and without RF incident upon the detector were made and are included in Appendix D.

Multiple Sources. In this series of experiments, radiation from an IR blackbody source (chopped at 673.9 Hz) as well as MMW radiation were placed in the IR detector FOV. Both the HgCdTe and InSb detectors were tested. As in previous tests, only the HgCdTe detector responded to the incident MMW radiation. All responded to the chopped IR source. Only the HgCdTe MMW responses will be discussed.

Sources of Dissimilar Magnitude. The magnitude of the response to the IR source was monitored and the beam steering mechanism adjusted to provide an IR source magnitude significantly higher than that of the detected MMW response.

The IR signal was adjusted to provide a detected signal at 673.9 Hz of -37.6 dBm as measured on the spectrum analyzer. The AM rate of the 28.0 GHz MMW source was set to 200 Hz. The horn to dewar separation was 8.6 cm. The output from each component (200 Hz and 673.9 Hz) was measured on the spectrum analyzer. The spectrum analyzer settings were set to: RBW = 10 Hz, VBW = 30 Hz. The center frequency was readjusted to measure each component. Five readings of the detected RF component were taken and the result averaged. The level of the detected RF component at 200 Hz was -86.2 ± 0.6 dBm. The blackbody radiation was then removed from the detector field-of-view (verified by monitoring the spectrum analyzer response at 673.9 Hz). The detected RF component level without the blackbody source present was -86.3 ± 0.3 dBm. The presence of the IR source did not effect the level of the detected MMW signal when the modulation rates of the two signals differed significantly.

The chopped blackbody source was again placed within the detector field-of-view. The detector response to the chopped signal with no RF present was -37.6 dBm at 673.9 Hz as measured on the spectrum analyzer. The AM rate of the

MMW signal was adjusted to 673.9 Hz and the RF set to 28.0 GHz. The resulting detector response at 673.9 Hz was -37.6 dBm (spectrum analyzer measurement).

Similar Magnitude Sources. The IR source was arranged to provide a detector response of -86.1 dBm at 673.9 Hz as measured on the spectrum analyzer. The AM rate of the 28.0 GHz MMW source was set to 673.9 Hz. The spectrum analyzer settings were: Center = 673.9 Hz, RBW = 10 Hz, VBW = 30 Hz. The level of the combined response at 673.9 Hz was -83.0 ± 0.2 dBm. With the rates and levels of the two sources matched, the simultaneous presence of both signals doubled the output power of the IR detector as measured at 673.9 Hz on the spectrum analyzer.

The AM rate of the 28.0 GHz MMW source was adjusted to 673.7 Hz to provide an intentional interference between the signal rates. The spectrum analyzer settings were changed to: Center = 673.9 Hz, RBW = 3 Hz, VBW = 10 Hz. The level of the detected response was -87.4 ± 2.4 dBm. The magnitude of the standard of deviation (2.4 dBm) indicates the destructive and constructive interference between the two sources which were present in the detected signal. The AM rate was changed to 674.8 Hz and the test repeated. The raw data is tabulated in Table 6.

Table 6. Simultaneous IR and MMW Sources of Similar Magnitudes and Modulation Rates (673.7 and 673.9 Hz).

AM Rate(Hz)	673.9 Hz Component (dBm)	x ± σ(dBm)
673.9	-85.2, -87.0, -88.7, -90.2 -84.8, -88.7, -84.5, -90.1	- 87.4 ± 2.4
674.8	-84.8, -89.1, -84.8, -89.9 -85.1, -84.6, -88.4, -87.2	- 86.7 ± 2.2

To examine whether the observed interference is primarily due to both signals being within the spectrum analyzer resolution bandwidth or due to a nonlinear mixing of the two signals, the AM rate was separated from the chop rate. The separation was greater than that of the spectrum analyzer resolution bandwidth. If the signals combined in a nonlinear fashion internally, difference or beat frequencies should be evident in the output spectrum.

The 28.0 GHz MMW source AM rate was set to 300 Hz. The spectrum analyzer center frequency was set to 600 Hz and the span set to 800 Hz. The spectrum analyzer display frequency range was from 200-1000 Hz. If sum and different frequencies were present at 373.9 and 973.9 Hz they could be observed on the display. Figure 28 illustrates the detector spectral response with only the chopped blackbody source present. The level cf the 673.9 Hz component is -86.9 dBm. Figure 29 shows the detector output with the MMW source present. The level of the 300 Hz component is -88.6 dBm; the level is essentially the same as that observed with the

chopped blackbody source adjusted to provide a relatively much larger level. Figure 29 demonstrates that no sum and difference signals are present which would result if a nonlinear mixing of the two signals occurred.

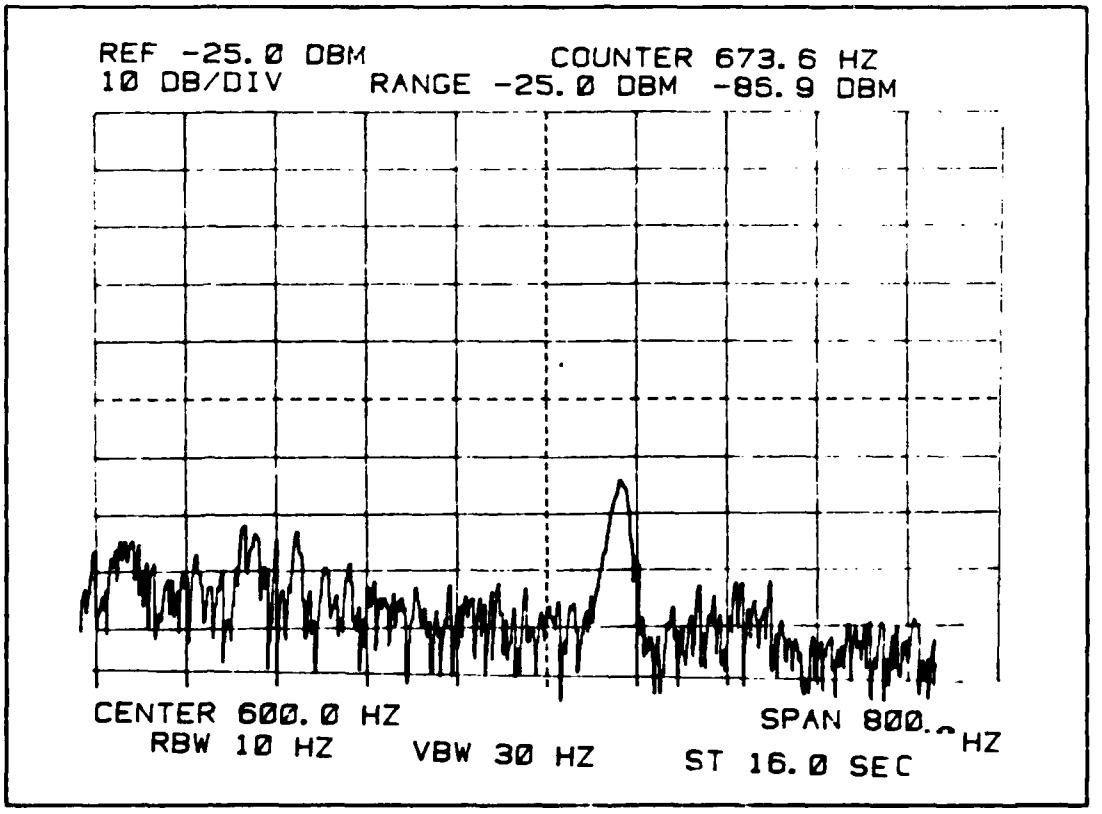

Figure 28. HgCdTe Detector and Preamplifier Response To A Chopped (673.9 Hz) IR Blackbody Source. RF = Off.

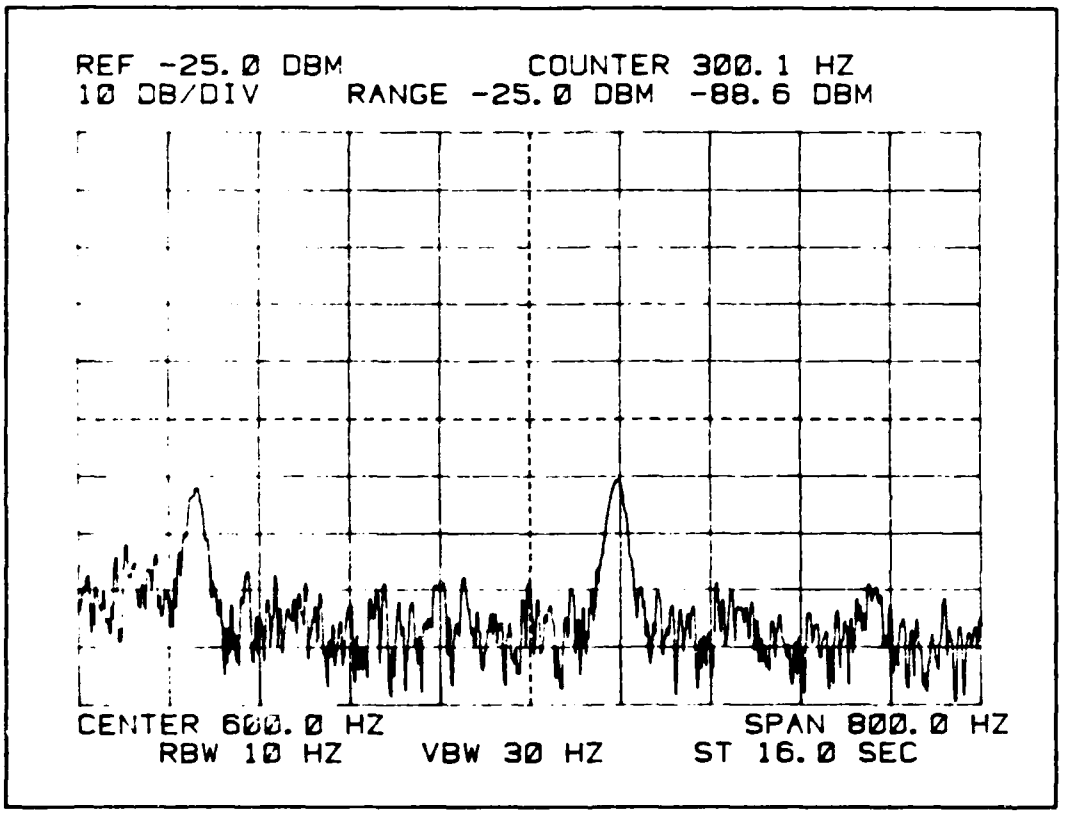

Figure 29. HgCdTe Detector and Preamplifier Spectral Response To A Chopped (673.9 Hz) IR Blackbody Source and A 28.0 GHz MMW Source Modulated at an AM Rate of 300 Hz. Range = 8.6 cm.

Figure 30 is a plot of the detected spectrum with the spectrum analyzer centered on 973.9 Hz. No measurable component is present at 973.9 Hz.

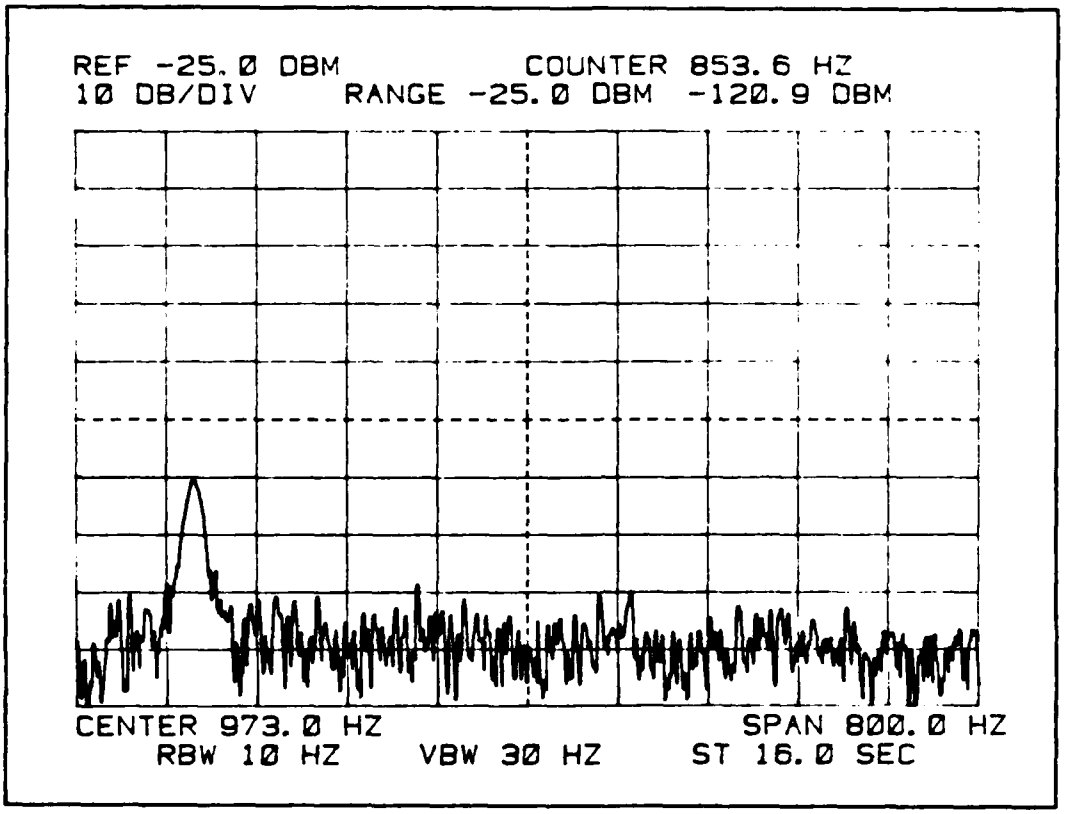

Figure 30. HgCdTe Detector and Preamplifier Spectral Response With Simultaneous IR and MMW Sources Present. Chop Rate and Level = 673.9 Hz @ -86.9 dBm, AM Rate = 300 Hz @ -88.6 dBm, Range = 8.6 cm.

Figure 31 is a plot of the detector output spectrum with the level of the chopped component increased. The level of the detected MMW component at 300 Hz remained at -88.6 dBm. Again, no evidence of mixing is present in the displayed spectrum.

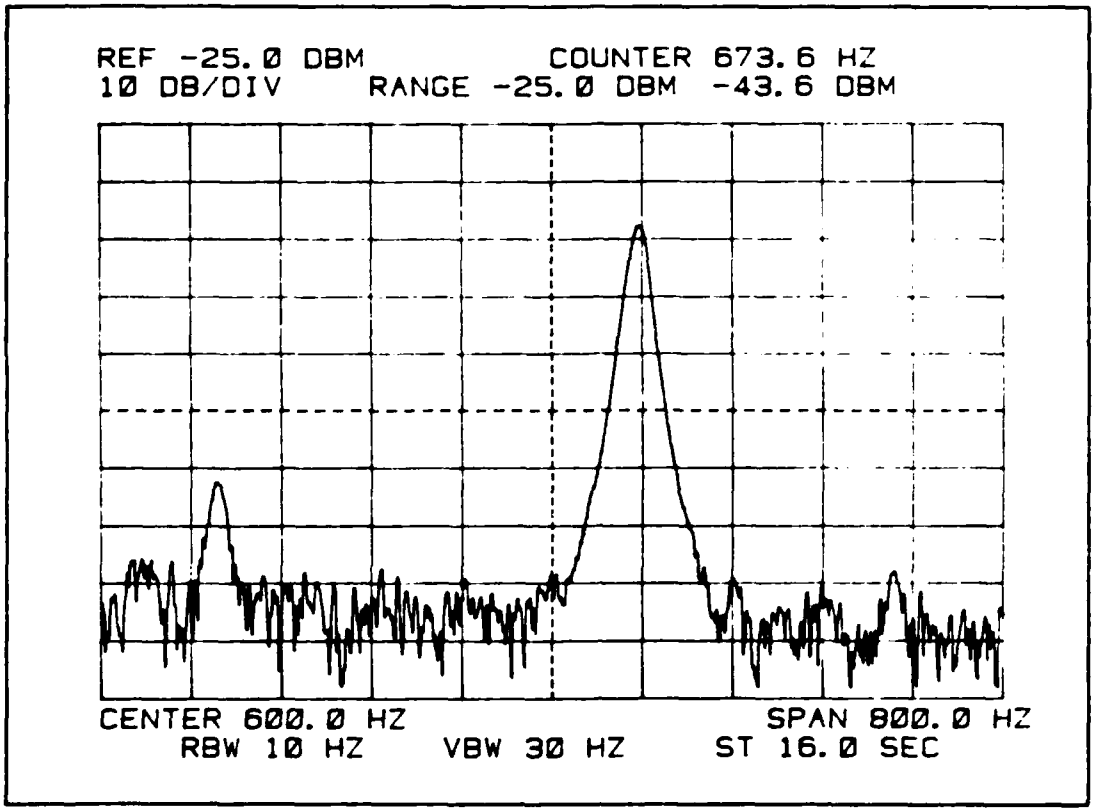

Figure 31. HgCdTe Detector and Preamplifier Spectral Response With an IR and MMW Source Present Simultaneously. Chop Rate = 673.9 Hz, AM rate = 300 Hz, Pyramidal Horn to Dewar Separation = 8.67 cm.

The lack of interference when the modulation rates of the IR and MMW sources are separated by more than the spectrum analyzer resolution bandwidth imply that the constructive and destructive interference observed is due to the integration of the two signals within the spectrum analyzer resolution bandwidth. The results suggest a linear combination of the two signals in the output current of the detector. This implies that the detection mechanisms by which the IR and MMW radiation produce a detector response

are different and separate. Previous tests demonstrated a nonlinear square law response mechanism for the detection of the MMW radiation within the IR detector. If both the MMW and IR sources produced a detector response by the same square law mechanism, sum and difference frequencies would have occurred in the output. The results indicate that the two signals exist in linear combinations within the detector output current and may cause interference if the two signals are separated in modulation frequency by an amount that is less than the integration bandwidth of processing circuitry.

Figure 32 illustrates the result when both signals are within the resolution bandwidth of the spectrum analyzer. The beam steering mirrors were adjusted to provide a level of -90 dBm at 673.9 Hz in the cutput of the detector. The 28.0 GHz MMW source AM rate was set to 673.6 Hz. Two traces of the detected spectral response were stored and plotted on the spectrum analyzer. Destructive interference is evident in the display.

Horn and Dewar Interaction. Measurements of the on-axis radiated power exhibited periodic fluctuations caused by multiple reflections between the receive and transmit horn. Similar results were expected between the transmit horn and metal dewar.

Figure 33 illustrates the output of the HgCdTe detector and preamplifier as a result of 75 GHz MMW irradiation amplitude modulated at a rate of 1000 Hz. The separation

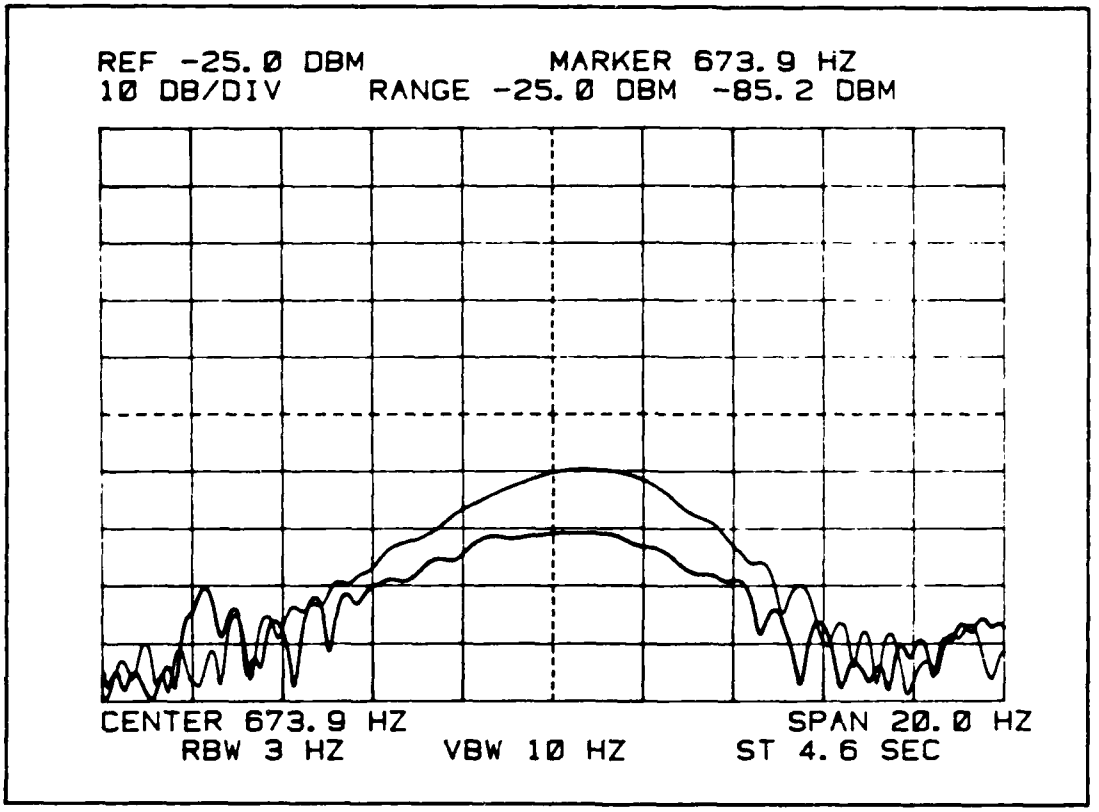

Figure 32. HgCdTe Detector and Preamplifier Response With an IR and MMW Source Simultaneously Present. Blackbody Chop Rate = 673.9 Hz, AM rate = 673.6 Hz, RF = 28.0 GHz, Range = 8.6 cm.

between the dewar and transmit horn was changed in 1 mm increments. This provided a response measurement at every $\lambda/4$ increment in separation. Five or more measurements of the detected response at 1000 Hz on the spectrum analyzer were taken at each distance. The average results for each distance are displayed in Figure 33. Periodic fluctuations in the amplitude of the detected signal are present out to a separation of approximately 4 cm. For distances in excess of 4 cm, the amplitude decreases monotonically.

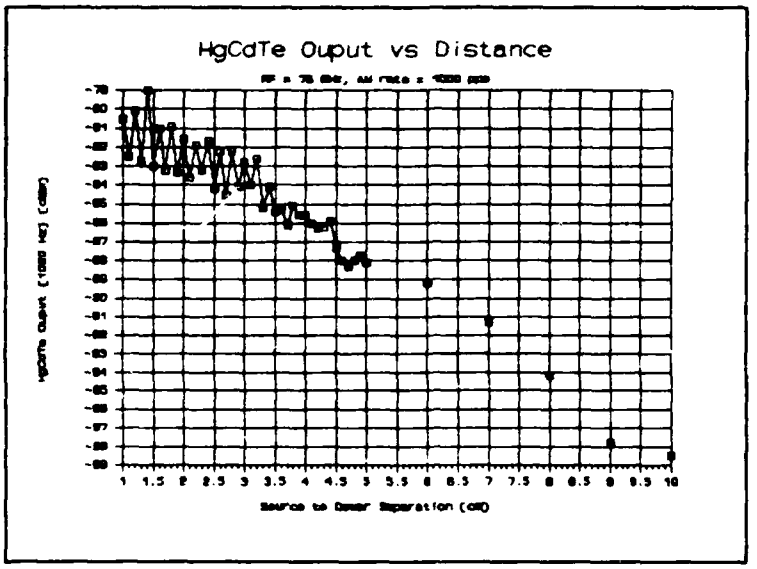

Figure 33. HgCdTe Detector and Preamplifier Spectral Response vs The Transmitting Horn to Metal Dewar Separation. RF = 75 GHz, AM = 100^G

Phase III. RF and AM Rate Response

RF Response. The measurement of the HgCdTe detector RF response was complicated by multiple reflections between the metal dewar and transmit horn. RF power levels were not sufficient to permit far-field measurements where multiple reflections could be minimized. As a result, periodituations in the received signal strength were present.

In the Ka band, the separation was allowed to vary by ± 1.0 cm from 6.0 cm. In this manner, an attempt was made to locate a signal maximum before a reading was taken. The

variation in separation would cause errors in attempting to maintain a power level consistent with a fixed range. However, the error in received signal strength levels due to the separation error would be less in magnitude than that caused by taking a reading in the location of a minimum. In the E band, fluctuations due to multiple reflections became less significant after a distance of approximately 4 cm was obtained. As a result, the separation remained fixed as the RF was varied in the E band.

Another factor complicating the RF response measurements was the variation in transmitter power versus RF. To compensate for this, the detector responses were adjusted for changes in transmitted and radiated power. The radiated power was estimated based on the power meter reading, thermistor correction factor, and calculated antenna gain as a function of frequency. The responses were adjusted based on a square law response detection mechanism within the HgCdTe detector and the peak power transmitted within the MMW band . For example, if the estimated radiated power at a particular RF was 1 dB lower than that of the peak RF power, an adjustment factor of 2 dB was added to the detector response. Both the raw and adjusted data are reported (Appendix F). Multiple response readings were taken at each RF and the results averaged. The IR detector responses were adjusted based on the mean data values.

The accuracy of the adjustment process is not good. Several factors detract from the accuracy. The first is the lack of reflection and transmission coefficients for the transmit horns, directional couplers, thermistor mount, and flat broadband RF directional coupler. The capability was not present to determine these values for the MMW band used. Rather than attempt to estimate the values, transmission coefficients of 1.0 were assumed. As a result, the estimated values for the transmitted and radiated power and the power differences themselves as a function of frequency will not be correct. Another factor is the frequency response of the MMW hardware. The directional couplers have a coupling flatness of ± 0.7 dB across the bands and the E band broadband detectors have a sensitivity flatness ranging from ± 1.1 to 1.5 dB across the band. Aside from the rated gains and physical dimensions, the pyramidal horn frequency response specifications are unknown.

In the Ka band, the response adjustments to transmitter power variations were based on the power meter readings obtained using the thermistor and HP432A meter. In view of the magnitude of the errors which are present, the effect of the thermistor correction factors are minimal. Because of this, the correction factors in the Ka band were averaged and the mean value used for correction. The antenna gain was calculated based on established antenna theory predictions relating antenna dimensions and transmitter

wavelength to antenna performance (reference Eq (3) and Appendix C). The IR detector response adjustment was then calculated based on the estimated maximum radiated power as in Eq (4).

In the E band, the thermistor was inoperational. In an attempt to equalize the detector response for power variations, a flat broadband RF detector was attached to the coupled port of the output directional coupler. The voltage output of the RF detector was measured at each RF using an oscilloscope. The output of the RF detector is proportional to the RF power incident upon it. The relative changes in voltage were interpreted as relative changes in transmitter power. The IR detector response could then be adjusted based on the relative changes.

Figure 34 displays the raw and adjusted HgCdTe detector response readings in the Ka band. During the course of the experiment, the middle sub-band of the Ka band became inoperational. As a result, some tests could not be conducted in the 30-35 GHz frequency range. In Figure 34, the RF results displayed in the range from 30-35 GHz suffer from this equipment outage. The measurements were taken during some of the initial tests. Only single readings were taken at each frequency. No averaging was accomplished. However, the data is valid and included for completeness. The raw and processed data is included in Appendix F.

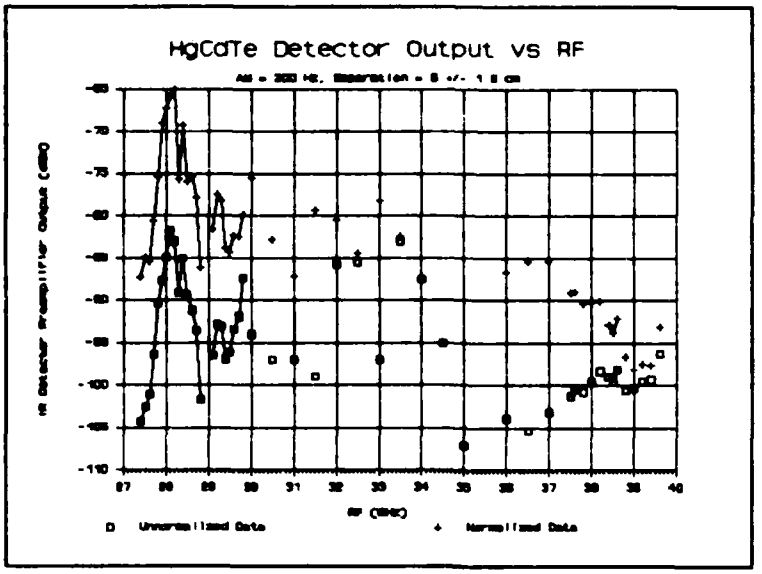

Figure 34. HgCdTe Detector and Preamplifier Output as a Function of The MMW RF. Range = 6.0 ± 1.0 cm. AM = 200 Hz.

Figure 35 illustrates the RF response of the HgCdTe detector and preamplifier for the E band. The interference due to multiple reflections was not as severe as that experienced for the Ka band. The RF response measurements were accomplished at a range of 4 cm in the E band. This corresponds to a separation of 10 wavelengths at 75 GHz or 16% of the far-field distance (based on a maximum horn aperture dimension of 22.5 mm corresponding tc the aperture diagonal).

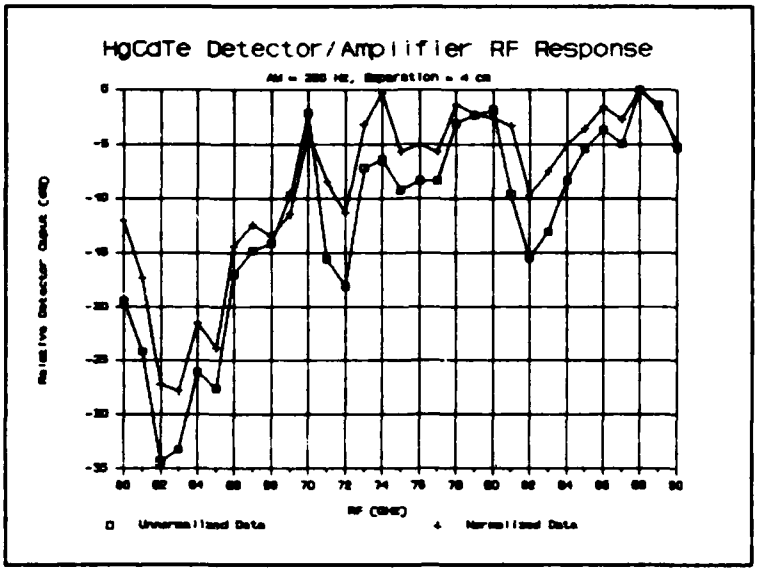

Figure 35. HgCdTe Detector and Preamplifier RF Response. AM = 200 Hz, Range = 4 cm.

The E band data was equalized for power variations based on the received peak to peak voltage of the broadband RF detector attached to the coupled port of the output directional coupler. Manufacturer's data for the specific detector was not located; the detector serial number did not match that of the data sheets. Instead, the typical response of 250 mV/mw in the E band as listed in the Hughes Microwave catalog was used (Millimeter Wave Products, 1985: 91). The measured RF detector voltage was converted to mW. Then, the peak transmitter power for the RF response test was determined. The coupling factor of 20 dB and antenna gain for each frequency were added to the calculated RF

detector power. The difference between the estimated peak radiated power and the individual power was calculated. The difference (in dB) was multiplied by two to allow for the square law response and added to the measured IR detector response.

$$P_{det} + 2(P_{t,max} - P_t) = P_{norm} \quad (6)$$

$$P_t = 10\log(V_{det}/.250) + 20 \text{ dB} + G_{Horn} \quad (7)$$

$$P_{t,max} = \text{maximum of } P_t \quad (8)$$

where,

P_{det} = Measured IR detector output (dBm)

V_{det} = Output RF detector voltage (volts P-P)

P_{norm} = Normalized IR detector output (dBm)

G_{Horn} = Antenna gain at the RF (dB)

P_t = Maximum radiated power at the RF (dBm)

AM Response. This test examined the HgCdTe detector response at an RF of 89.0 GHz while the amplitude modulation rate was varied. The results are not conclusive when viewed with respect to the relative response at one rate compared to another. Rather, the results demonstrate the detector response across a range of AM rates. The RF modulator was only rated to 1000 Hz. However, external modulation rates up to 30 KHz were tested. The modulator functioned through the range of rates tested, but the sharpness and depth of modulation decreased markedly as the AM rate increased. Both the raw and adjusted data are included in Appendix F.

A broadband RF detector was used to monitor the transmitter power at the coupled port of the output directional coupler. The RF detector output voltage dropped off as the AM rate was increased. Specifications regarding the effect of modulation rate upon the detector were not available. The assumption was made that the effect was negligible. The magnitude of the RF detector output voltage was monitored at each AM rate and recorded. Figure 36 illustrates the RF detector output peak to peak voltage measured at each AM rate. The output voltage is flat to a frequency of approximately 1 KHz and then falls off in a manner similar to a single pole filter.

The output voltage from the RF detector was used in an attempt to compensate the value of the HgCdTe response. The same method of compensation was used as for the E band RF response test. The results are displayed in Figure 37. Both the adjusted and raw data are displayed. For AM rates less than 1 KHz, the RF detector voltage magnitude remained constant. As a result, for frequencies less than 1kHz the adjusted and raw data values for the HgCdTe response are the same. However, the response still tapers off with as the AM rate increases. It is possible then, that the MMW response of the HgCdTe detector does decrease rather quickly with the increasing AM rate until an AM rate of approximately 2 KHz is reached. When the AM rate approaches about 2 KHz, the adjusted AM response of the IR detector flattens.

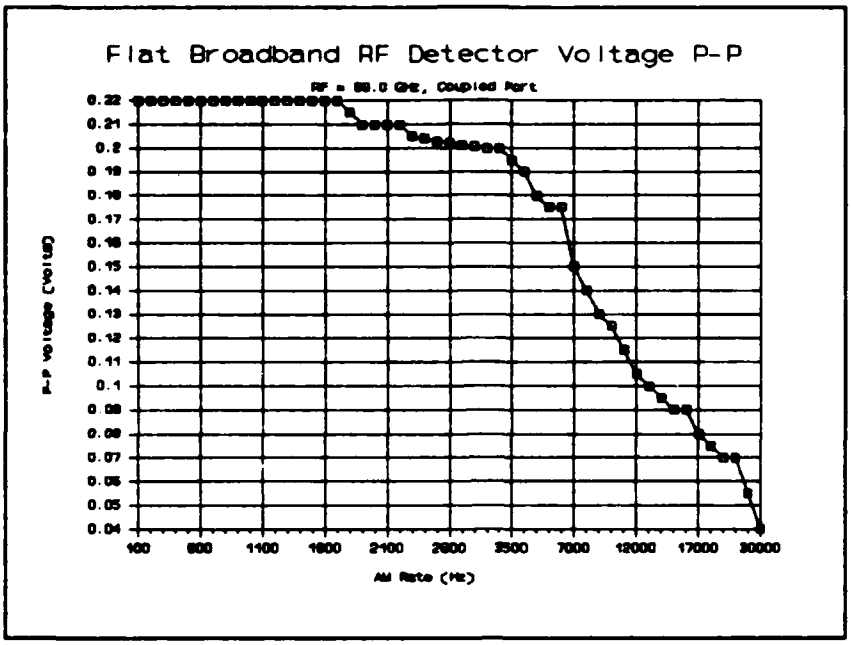

Figure 36. Peak to Peak Voltage Output of The Broadband RF Detector. RF = 89.0 GHz.

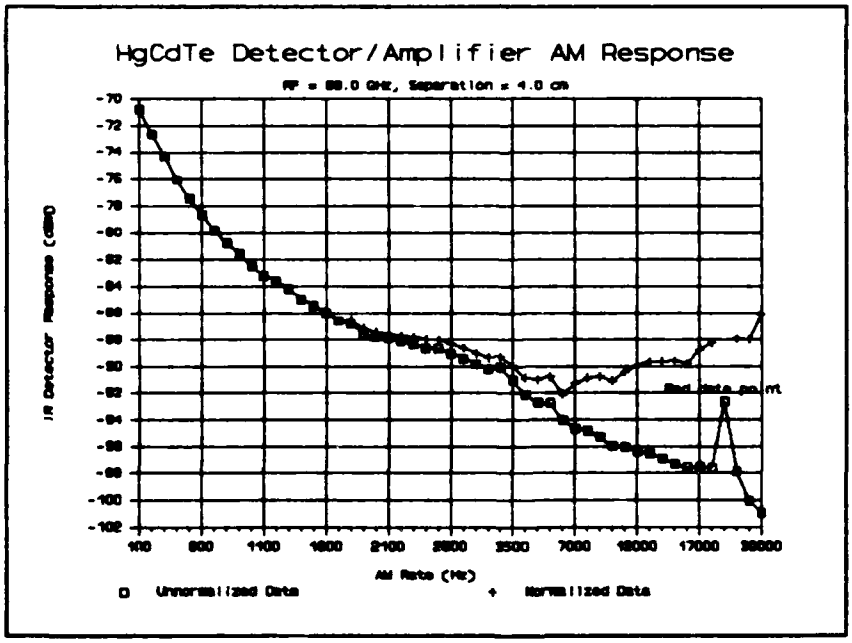

Figure 37. HgCdTe Detector and Preamplifier Response vs AM Rate. RF = 89.0 GHz, Range = 4 cm.

V. Conclusions

Of the three IR detectors tested, only the HgCdTe detector, metal dewar, and preamplifier combination exhibited a response to incident MMW radiation in the frequency range of 26.5-40 and 60-90 GHz. When subjected to the same tests, the InSb detectors did not produce a measurable response. To summarize, the HgCdTe detector response to amplitude modulated MMW energy was characterized by:

- Frequency dependence - RF and modulation rate
- A square law detection process
- Polarization dependence
- Temperature dependence - The detector only responded when operated at 77 K.
- Independence from simultaneous IR signal detection processes

The HgCdTe detector exhibited a response to MMW energy which varied in strength depending on the frequency of the MMW. The detector response was stronger in the 28-33 GHz and 70-90 GHz frequency regions of the Ka and E bands. A specific quantization of the RF response was not accomplished. Multiple reflections between the dewar and transmit antenna, RF power variations, and incomplete data

regarding microwave hardware reflection and transmission coefficients prevented quantization.

The HgCdTe detector appeared to demonstrate a dependence on the AM rate of the incident MMW signal. Lower AM rates (100-500 Hz) produced the strongest responses. As in the case of the RF response, the AM rate response could not be quantified. The RF modulators used in both the E and Ka bands were also dependent upon the AM rate. The effects of the modulator and the IR detector could not be isolated.

The HgCdTe detector element was shown to be the mechanism producing the MMW response. With MMW energy incident upon the detector and dewar combination, blocking the window located in front of the detector successfully eliminated any measurable response. This test was performed repeatedly at many RFs. Each time, the test was successful. The second test to show that the HgCdTe element was indeed the mechanism to which MMW energy coupled was the temperature test. When the HgCdTe detector was operated at room temperature, no response to MMW energy was observed. When the HgCdTe was cooled to 77K, the detector readily responded to MMW energy.

The HgCdTe detector exhibited a stronger response to vertically polarized fields. At an RF frequency where the cross polarized component was minimum, the detector response was unmeasurable at a horizontal polarization. In contrast, the response to the vertically polarized component at the

same RF was 20 dB over that of the noise floor.

The MMW detection process was found to be square law in nature. Varying the MMW power in specific attenuation steps produced a change in the HgCdTe detector response of 2 dB for each 1 dB change in incident power. This was verified at RFs in both bands with the same results. The greatest separation at which a response was measured was 34 cm. A response of -97.4 dBm was measured from the output of the IR detector amplifier with an incident field at 32.78 GHz with a power density of 50 $\mu W/cm^2$. The amount of attenuation caused by the window material was unknown. If no attenuation was present, the 2 mm square detector element would have received 2 μW (assuming the physical and electrical area of the detector surface are equal). This would correspond to a power of -60 dBm. If the detection process remains square law as the incident signal decreases, a drop in the incident power of 5 dB would cause the detector response to drop 10 db to -107.4 dBm. A signal of this magnitude would be lost in the noise floor of the spectrum analyzer. Realizing that the window material does attenuate the signal and that the power density calculated does not take into account an imperfect match between the transmitting horn and the directional coupler, the conclusion can be made that the HgCdTe detector element will respond to incident MMW power levels less than 2 μW.

The placement of IR sources or radiation within the HgCdTe detector field-of-view had no effect on the detected MMW signal. The chopped IR and AM MMW signal were simultaneously present. Mixing did not occur. Only when the chop and AM rate were both within the resolution bandwidth of the spectrum analyzer did interference of the two signals take place. The independence of the IR and MMW signals demonstrate that the two signals are detected by different processes. The detection process for the MMW signal was shown to be a nonlinear square law process. If the mechanisms were the same, the signals would combine in the detection process in a nonlinear fashion. This in turn would cause a mixing effect which would produce sum and difference frequencies in the spectral output.

Recommendations

Additional research should be performed to quantify the demonstrated MMW response of HgCdTe detectors. If dual IR and MMW sensor systems are fielded, the radiation of the IR detector element by the active MMW component could pose a serious threat to the IR detection process.

If additional research is performed, several equipment problems should be circumvented. First, more transmitter power is needed. Performing the tests in the far-field would reduce multiple reflections between the test device and the transmitter antenna. Second, the scattering

parameters of the microwave hardware should be determined. The equipment necessary to measure the scattering parameters was not available in the MMW bands. This is necessary, if the reflection and transmission coefficients of the hardware are to be accurately determined. RF response peaks were experienced. However, it could not be ascertained whether the peaks were due to the detector response or microwave hardware characteristics. Third, lighting is a problem. The detectors are very sensitive to the 60 Hz and 120 Hz spectral components produced by the florescent and incandescent lighting. While this was reduced for the experiment, it was never eliminated. A laboratory in which the lighting can be eliminated should be located. Fourth, RF modulators are available with wider modulation bandwidths. If additional research is done, the modulators should be purchased to allow quantization of the AM response. Fifth, a lens antenna should be used in place of the pyramidal horn. The plane wave produced by the horn would reduce the far-field requirement; reflections would still have to be considered.

Only InSb and HgCdTe IR devices were tested during this experiment. Other IR detector materials are commercially available and should be tested. Detector arrays should also be considered. The larger combined detector area and multiple elements may make the array more susceptible to MMW irradiation than that of the single element.

Appendix A: Equipment Specifications

Sweep Control Plug-in Specifications

	Ka (26.5-40 GHz)	E (60-90 GHz)
Triple Head Option Sweep Bandwidth (GHz min)	Full Band	Full Band
Power Output (mW min)		
with Mod/Lev Loop	2 (2)	2
without Mod/Lev Loop	3 (65.8)	3
Temperature Stability (MHz/°C typical)	5	12
Leveled Output Flatness (± dB)	1.5	1.5
Modulation Depth (dB typical)	20	20
Maximum External Modulation Rates (kHz)	1.0	1.0
External Modulation Voltage (+V)	5	5
RF Blanking (dB typical)	20	20
Linearity (± % typical)	1	1
CW Frequency Calibration Accuracy	0.1%	0.1%

Note: The values listed in parenthesis are measured values obtained from equipment data sheets.

Modulator Specifications

	Ka (26.5-40 GHz)	E (60-90 GHz)
Forward Insertion Loss @ low state (dB minimum)	1.5 (0.9)	2.0 (1.8)
Isolation @ Low Insertion Loss State (dB minimum)	20 (30)	xx (30)
1000 Hz on-off ratio (dB)	>20 (29.1)	>20 (28.2)
Input/Output VSWR (maximum)	1.5:1 (1.3:1)	1.5:1 (1.2:1)
Bias Current (mA maximum)	500 (290)	500 (260)

Directional Coupler Specifications

	Ka (26.5-40 GHz)	E (60-90 GHz)
Coupling Value (dB)	3, 6, 10, 20, 30, 40	3, 6, 10, 20, 30, 40
Coupling Flatness (± dB)	0.7	0.7
Insertion Loss (dB max)	0.7	1.4
Directivity (dB min)	40	40
Main Line VSWR (max)	1.05:1	1.08:1
Secondary Line VSWR (max)	1.1:1	1.1:1

Frequency Meter Specifications

	Ka (26.5-40 GHz)	E (60-90 GHz)
Accuracy (% maximum)	0.12	0.20
Scale Increment (MHz)	20	50
VSWR (maximum)	1.3:1	1.5:1
Insertion Loss (dB)	1.0	1.5

Attenuator Specifications

	Ka (26.5-40 GHz)	E (60-90 GHz)
Attenuation Range	0-50	0-50
Accuracy (dB/%)	0.1/2.0	0.1/2.0
VSWR (maximum)	1.15:1	1.25:1
Insertion Loss (dB maximum)	0.5	1.0
Rated Power (W maximum)	0.5	0.3

Thermistor Correction Factors (Ka Band)

Frequency (GHz)	Correction Factor
26.5	+0.15
28.0	+0.45
31.0	+0.30
34.5	+0.35
37.0	+0.10
40.0	+0.10

Broadband Detector Sensitivities

Detector Serial #/Band	Flatness (dB max)	Sensitivity (mV/mW min)
21/E	+/- 1.5	350
26/E	+/- 1.1	1500
26/Ka	+/- 1.5	2100

HgCdTe Detector Test Data

Test Conditions

Black Body Temp: 500°K	Noise Bandwidth: 6 Hz.
Background Temp: 295°K	Overall Gain: 460
Detector Temp: 77°K	Field-of-View: 60°
Flux Density: 1.8 $\mu W/cm^2$	Filter: None
Chopping Freq: 900 Hz	Window: ZnS
Detector Size: 2.0 mm sq.	Dewar Style: M-108

Electrical Measurements

	1 kHz	10 kHz
Signal (mV)	1.35	1.35
Noise (mV)	0.0035	0.0019
S/N	386	711
$D^*_{BB}(500, 10\ kHz, 1)\ cm\text{-}Hz^{1/2}\text{-}W^{-1}$	0.26	0.48×10^{10}
$D^*_{\lambda}(\lambda p, 10\ kHz, 1),\ cm\text{-}Hz^{1/2}\text{-}W^{-1}$	0.60	1.11×10^{10}
Responsivity, R_{λ}, $V\text{-}W^{-1}$	94	94

Detector Resistance: 16 Ω

Optimum Bias Current: 30 mA

Cut-off Wavelength: 14.5 μm

Liquid Nitrogen Hold Time: 6+ Hours

InSb Detector (J10 Series) Typical Specifications

Typical Specifications

(Infrared Detectors, 1982: 2)

Peak Wavelength	5.0 μm
Operating Temp.	77K
Peak D*	$>1x10^{11}$ cm $Hz^{\frac{1}{2}}W^{-1}$
Peak Responsivity	>2.0 A/W
Capacitance	450 pf/ mm^2
Time Constant	0.1 to 1.0 μs
Dynamic Impedance (Dependent on detector size)	10kΩ to 100MΩ
Short Circuit Current	5 - 10μA/mm^2
Open Circuit Voltage	50 - 120mV
Standard Sizes (diameter)	0.1, 0.25, 1, 2, 4, 7 mm

Model 700 Preamplifier Specifications

Feedback Resistor (Ω)	10K, 100K, 1M, 10M
Transimpedance Gain (dB V/A)	40, 50, 60, 70
Max Output	±10V into 1KΩ
Bandwidth (dependent on size of feedback resistor)	DC to 200kHz

Input Offset Voltage	1.0mV
Shorted Input Noise	$15nV/Hz^{\frac{1}{2}}$
Input Noise Current	$0.01pA/Hz^{\frac{1}{2}}$
Power Requirement	± 10V to ± 13V

Appendix B: Equipment Listing

Microwave Equipment

Name	Ka Band Model #	E Band Model #
Sweep Oscillator	HP8620C	HP8620C
Full Band MM-Wave Sweeper Control Plug-in (Triple Head IMPATT Source)	47721H-1010	47725H-1110
Modulator	45211H-1000	45215H-1000
Directional Coupler	45321H-1010	45325H-1010
Directional Coupler	45321H-1220	44345H-310
Broadband Detector	47321H-1111	47325H-1100
Broadband Detector	47321H-1111	47325H-1100
Precision Attenuator	45721H-1000	45725H-1000
Frequency Meter	45711H-1000	45715H-1000
Thermistor Mount	45771H-1100	45775H-1100
90° Waveguide Twist	45411H-1090	Not Used
Terminator	45611H-1000	45615H-1000
Waveguides	45500H-0100	47723H-1110
Pyramidal Horn (20 dB)	Unknown	DBA-520-20
Laboratory Jack	NRC Model 280	NRC Model 280

IR Equipment

Name	Model
IR Blackbody	Infrared Industries Inc. Model 464
IR Temperature Controller	Infrared Industries Inc. Model 101B
Chopper	EG&G PARC Model 125A
Beam Steering Instrument	NRC Model 650

Test Equipment

Name	Model
Dual Trace Oscilloscope	Tektronix 7844
Plug-ins:	
Vertical Amplifier	Tektronix 7A16
Vertical Amplifier	Tektronix 7A19
Delaying Time Base	Tektronix 7B71
Dual Time Base	Tektronix 7B92
Oscilloscope Cart	Tektronix 204
20 - 40MHz Spectrum Analyzer	HP3585A
Plotter	HP9872A
Calculator/Controller	HP9825A
Thermal Printer	HP9876A
Power Meter	HP432A
Scope Camera	Tektronix C53
Two Channel Frequency Synthesizer	HP3326A

IR Test Objects

Name	Model
HgCdTe IR Detector	Judson J15, S/N 8567
HgCdTe Bias/Preamplifier	Judson 000, S/N 166
InSb IR Detector (large area)	Judson J10, S/N 8568
InSb Preamplifier	Judson 700, S/N 7282
InSb IR Detector	Judson J10, S/N 8752
InSb Preamplifier	Judson PA-700, S/N 7333A
Dual D.C. Power Supply	Harrison 6205B
IR Detector Mount	N/A, Constructed on Site
Sliding Cart (rail sled)	Testech M58-1

Miscellaneous Equipment

Name	Description
Aluminum I-beam	Base for the laboratory jack
Plywood 7" x 3/4" x 41"	Platform to support microwave hardware
Measuring Tape	Lufkin 3m steel measuring tape
Plastic Ruler	C-Thru English/metric ruler W-20
Plastic Funnel	Plastic funnel with aluminum shaft for applying liquid nitrogen into the IR metal dewars
Plastic Thermos	1-quart plastic thermos for handling liquid nitrogen
Line Level	2" level

Appendix C: Radiated Fields of a Pyramidal Horn

The following development of the radiated fields of a pyramidal horn is taken largely from "Aperture Antennas and Diffraction Theory" by Jull. First, the geometrical relationships between the horn dimensions will be developed. Next, the equations for the far-field pattern of the antenna will be given. Then, the far-field restriction will be dropped and the magnitude of the on-axis fields in the near-field will be developed.

Several assumptions are necessary for the development. First, the horn aperture is contained in the x-y plane. Propagation occurs in the $z > 0$ space. Second, the aperture field is polarized in the x direction. Third, the aperture fields are assumed to be zero outside of the aperture space. As a result, integration over the aperture fields is limited to the physical extent of the aperture. Fourth, in the waveguide feed to the horn, only the dominant TE_{01} mode is present. The horn orientation and coordinate system used is shown in Figure 38.

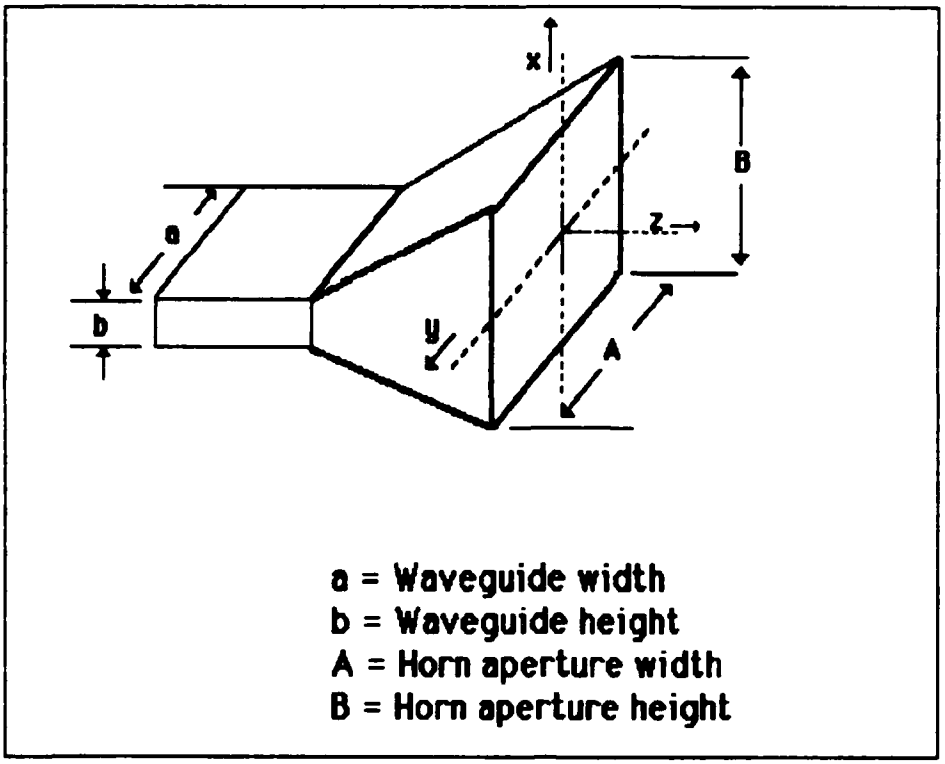

Figure 38. Pyramidal Horn Orientation and Coordinate System.

Dimensions

The known dimensions were the waveguide height and width obtained from manufacturers literature (Millimeter Wave Products, 1985: 144). The measured dimensions of the horns were the aperture height and width and the distance between the horn aperture and mating waveguide. The remaining dimensions were calculated from the geometrical relationships. Figure 39 illustrates the E-plane geometry. Figure 40 illustrates the H-plane geometry.

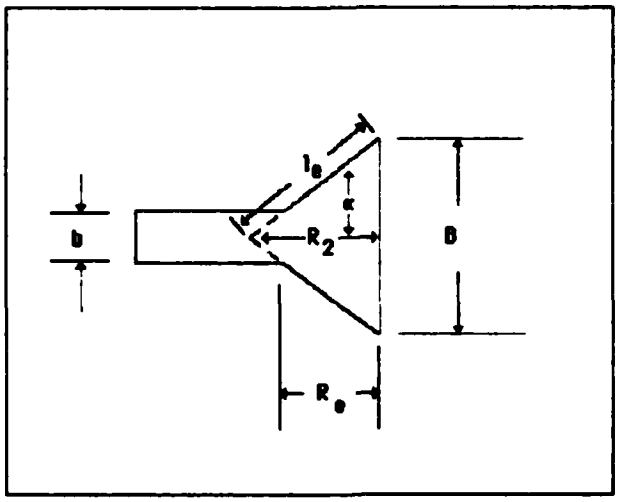

Figure 39. E-Plane Horn Geometry.

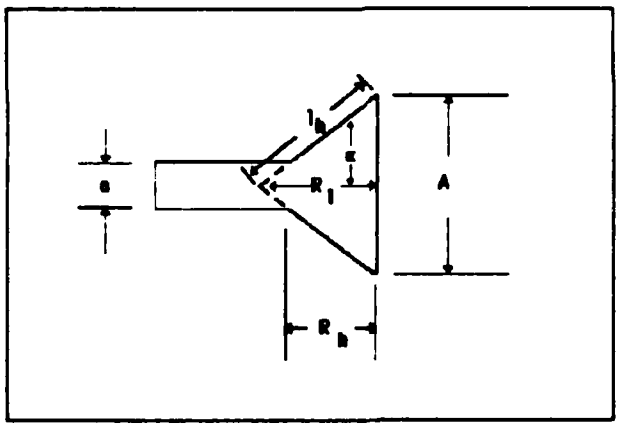

Figure 40. H-Plane Horn Geometry.

From Figure 39, the following relationships hold:

$$\tan\alpha = \frac{(B - B)/2}{R_e} = \frac{B/2}{R_2} \qquad (9)$$

$$\frac{B - b}{2 R_e} = \frac{B}{R_2} \qquad (10)$$

$$R_2 = \frac{B}{(B - b)} R_e \qquad (11)$$

Similarly, from Figure 40,

$$R_1 = \frac{A}{(A - a)} R_h \qquad (12)$$

$$l_e = \left[R_2^2 + \frac{B^2}{4}\right]^{1/2} \qquad (13)$$

$$l_h = \left[R_1^2 + \frac{A^2}{4}\right]^{1/2} \qquad (14)$$

Far-field Pattern

Beginning with the fields radiated by a rectangular aperture placed in the x-y plane, Jull gives the radiated electric field for an x-polarized aperture field as (Jull, 1981: 18):

$$\vec{E}(r,\theta,\phi) = \vec{A} \int E(x,y)\exp\left[jk(x \sin\theta\cos\phi + y \sin\theta\sin\phi)\right]dx\,dy \qquad (15)$$

$$\vec{A} = \vec{A}(r,\theta,\phi) = j \frac{\exp(-jkr)}{2\lambda r} (1 + \cos\theta) \times (\hat{\theta}\cos\phi - \hat{\phi}\sin\phi) \quad (16)$$

Integration is performed over the physical extent of the antenna aperture. It is assumed that the phase and amplitude of the aperture field is separable with respect to the aperture coordinates. Then,

$$E(x,y) = E_1(x)\, E_2(y) \quad (17)$$

$$\vec{E}(r,\theta,\phi) = \vec{A} \int E_1(x) \exp(jk_1 x)\, dx \times \int E_2(y) \exp(jk_2 y)\, dy \quad (18)$$

$$k_1 = k \sin\theta \cos\phi \quad (19a)$$

$$k_2 = k \sin\theta \sin\phi \quad (19b)$$

$$k = 2\pi/\lambda \quad (19c)$$

Because the path length from the horn apex to the aperture changes with the aperture position, the phase of the aperture field changes across the aperture. Figure 41 illustrates the geometry for the phase variation.

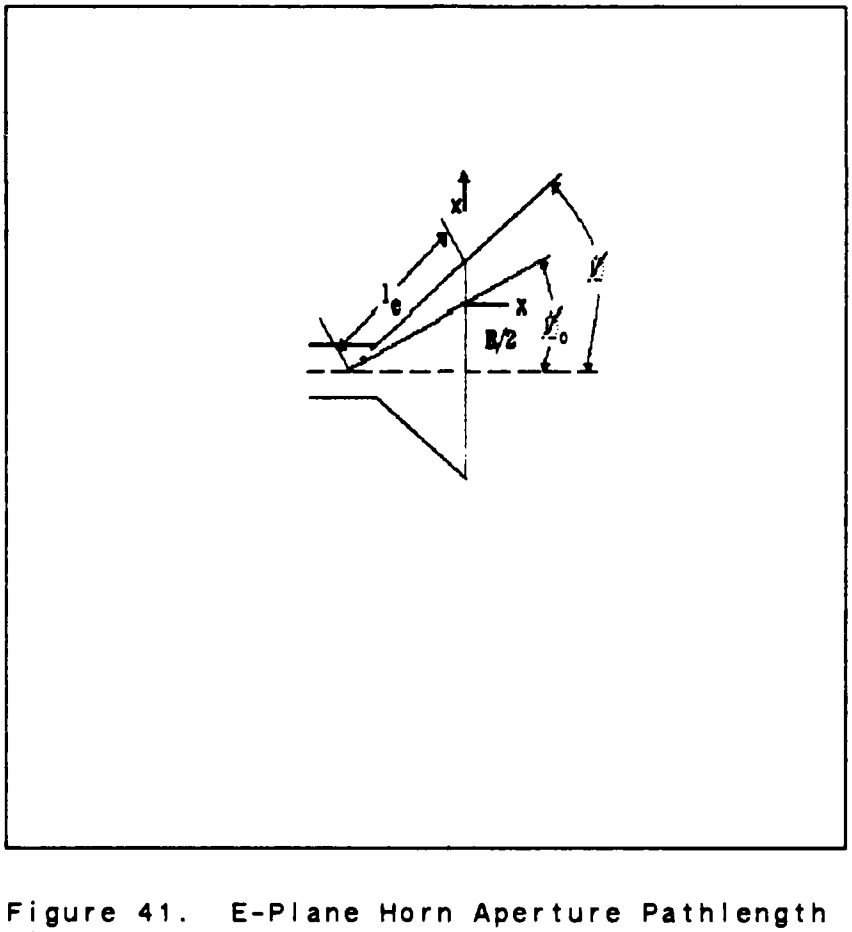

Figure 41. E-Plane Horn Aperture Pathlength Differences (Jull, 1981: 55).

ξ = pathlength

ψ = phase change from aperture center

$$\xi = \left[R_2^2 + x^2\right]^{1/2} \qquad (20a)$$

where,

$$R_2 = l_e \cos\phi. \qquad (20b)$$

$$(1+x)^{1/2} \approx 1 + x/2 - x^2/(2\cdot4)$$

$$+ 1\cdot3x^3/(2\cdot4\cdot6) - \ldots \quad (21)$$

$$-1 \leq x \leq 1$$

(Spiegel, 1968: 110)

For small x,

$$(1 + x)^{1/2} \approx 1 + x/2 \quad (22)$$

Then,

$$\xi \approx R_2 \left\{1 + \left[\frac{x}{R_2}\right]^2\right\}^{1/2} \approx R_2 [1 + 0.5(x/R_2)^2] \quad (23)$$

Phase at aperture center = kR_2 (w.r.t. apex)

Phase at a distance x from aperture center = kx

$$\psi = k(\xi - R_2) \approx kx^2/(2R_2) \quad (24)$$

Similarly, the phase variation in the H-plane is

$$\Psi \approx ky^2/(2R_1) \quad (25)$$

Note: Jull replaces R_2 with l_e for small values of ϕ..

The aperture field becomes,

$$E(x,y) = E_0 \cos(\pi y/A) \exp\left\{-jk\left[[x^2/(2R_2)] + [y^2/(2R_1)]\right]\right\} \quad (26)$$

where E_0 = field amplitude at aperture center

Substituting Eq (26) in Eq (18) (the aperture field), the far-field radiation pattern becomes (integration limits are over the physical extent of the antenna aperture):

$$\vec{E}(r,\theta,\phi) = \vec{A} \int \exp\left[-jk[x^2/(2R_2) - x\sin\theta\cos\phi]\right] dx$$

$$X \int \cos(\pi y/A) \exp\left[-jk[y^2/(2R_1) - x\sin\theta\sin\phi)\right] dy \quad (27)$$

The integrals in Ea (27) are reduced to Fresnel integrals. The resulting normalized E-plane ($\phi = 0°$) radiation pattern is (Jull, 1981: 32 -34, 56):

$$|E_{e,n}(r,\theta)|^2 = \left[\frac{1 + \cos\theta}{4}\right]^2 X \frac{\left[C(u_2) - C(u_1)\right]^2 + \left[S(u_2) - S(u_1)\right]^2}{C^2(u) + S^2(u)} \quad (28)$$

$$u = B/(2\lambda R_2)^{1/2} \quad (29a)$$

$$u_{2,1} = \pm u - [2R_2/\lambda]^{1/2}\sin\theta \quad (29b)$$

Letting $l_h \approx l_h \cos\phi$, ie R_1, the normalized H-plane of the horn ($\phi = \pi$) becomes (Jull, 1981: 33-34, 58):

$$E_{H,n}(r,\phi) = \frac{1 + \cos\theta}{2} \quad \frac{I(k \sin\theta)}{I(0)} \tag{30}$$

$$I(k \sin\theta) = 0.5[l_h \lambda/2]^{\frac{1}{2}} \left\{ \left[\exp\{j l_h \lambda/(4\pi) \right. \right.$$

$$\times [k \sin\theta\sin\phi + (\pi/A)]^2\}$$

$$\left. \times \{C(v_2) - C(v_1) - j[S(v_2) - S(v_1)]\} \right]$$

$$+ \left[\exp\{j l_h \lambda/(4\pi)[k \sin\theta\sin\phi - (\pi/A)]^2\} \right.$$

$$\left. \left. \times \{C(w_2) - C(w_1) - j[S(w_2) - S(w_1)]\} \right] \right\} \tag{31}$$

$$v_2^1 = \pm \left[\frac{A}{(2 l_h \lambda)} \right]^{\frac{1}{2}} - \frac{k \cdot \sin\theta\sin\phi}{2\pi} (2 l \lambda)^{\frac{1}{2}}$$

$$- \frac{1}{A} [0.5\, l_h \lambda]^{\frac{1}{2}} \tag{32}$$

$$w_2^1 = \pm \left[\frac{A}{(2 l_h \lambda)} \right]^{\frac{1}{2}} - \frac{k \sin\theta\sin\phi}{2\pi} (2 l \lambda)^{\frac{1}{2}}$$

$$+ \frac{1}{A} [0.5\, l_h \lambda]^{\frac{1}{2}} \tag{33}$$

$$I_2(0) = [0.5\lambda l_h]^{1/2} \exp\left[j\lambda \frac{l_h \pi}{(4A^2)}\right]$$

$$X \{C(v)-C(w)-j[S(v)-S(w)]\} \qquad (34)$$

$$v_w = \pm \frac{A}{(2\lambda l_h)^{1/2}} + \frac{1}{A}\left[\frac{\lambda l_h}{2}\right]^{1/2} \qquad (35)$$

The Fresnel integrals are defined by (Stutzman and Thiele, 1982: 567):

$$C(x) = \int_0^x \cos(\tau^2 \pi/2)\, d\tau \quad , C(-x) = C(x) \qquad (36)$$

$$S(x) = \int_0^x \sin(\tau^2 \pi/2)\, d\tau \quad , S(-x) = -S(x) \qquad (37)$$

Near-field On-axis Fields

To estimate the near-field effects on the radiated fields, the equation for the aperture field, Eq (26), is modified to include a quadratic phase variation (reference Figure 7) to simulate the first order effects of the non-planar fields radiated in the near-field (Jull, 1981: 32). Combining quadratic phase variations in both the x and y directions yields a phase variation of (Jull, 1981: 59):

$$\exp\left[\frac{-j\pi}{r\lambda}(x^2 + y^2)\right] \qquad (38)$$

Including the phase factor given by Eq (38) in the aperture field of Eq (26) yields the near-field principal plane patterns when I_e and I_h are replaced by: (Jull, 1981: 59,60):

$$I_e \Rightarrow \frac{r I_e}{(r + I_e)} \tag{39}$$

$$I_h \Rightarrow \frac{r I_h}{(r + I_h)} \tag{40}$$

The on-axis fields were then estimated for near-field ranges by evaluating Eqs (28) and (30) for z, Θ, and $\phi = 0$ and with the substitutions provided by Eqs (39) and (40).

The numerical values obtained for both the near and far-field patterns were obtained by implementing Eqs (28) and (30) (with the appropriate substitutions) on a Zenith Z-248 computer (80286 microprocessor) using MathCAD™.

Appendix D: Spectrum Analyzer Data Plots

This appendix includes additional data regarding the MMW response of the HgCdTe detector and preamplifier. The plots included are similar to those presented in the body of the text. Some of the parameters have been changed to illustrate a wider aspect of the IR detector response.

Figure 42 is the HgCdTe detector and preamplifier response to 32.78 GHz MMW irradiation amplitude modulated at 200 Hz for a horn to dewar separation of 6 cm. The polarization of the incident RF is vertical. The power meter indication of the transmitted power at the coupled port was -10.2 dBm. This provides a maximum radiated power of 28.4 dBm assuming microwave transmission coefficients of 1 (reference Eq (4)). The power density at a range of 6 cm assuming a power fall off proportional to the inverse square law is 1.53 mW per square centimeter (reference Eq (1)). The detector preamplifier output was terminated into the 50 Ω spectrum analyzer signal input.

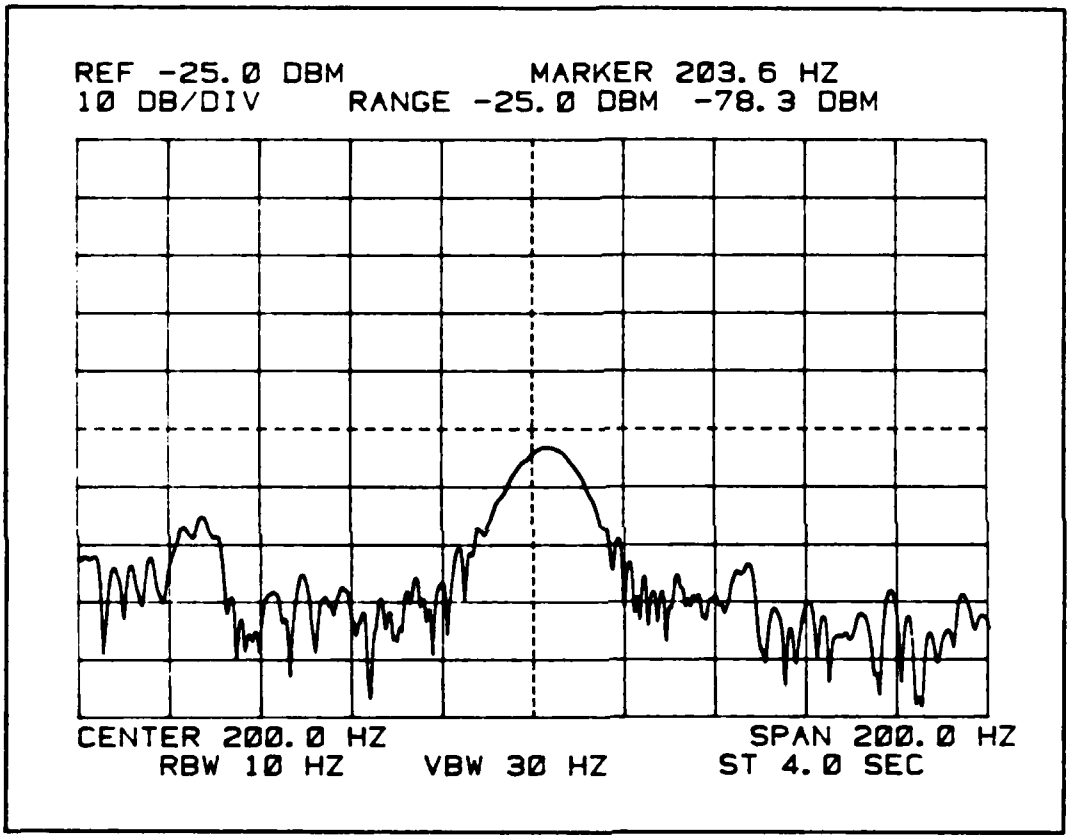

Figure 42. HgCdTe Detector and Preamplifier Spectral Response (RF = 32.78 GHz, AM = 200 Hz, Range = 6 cm).

Figure 43 is the spectral response of the HgCdTe detector and preamplifier at the same settings as that of Figure 42 with the exception that the RF power is off. The two plots clearly show the result of the MMW irradiation of the IR detector is a demodulated output at the rate of the modulating signal (200 Hz).

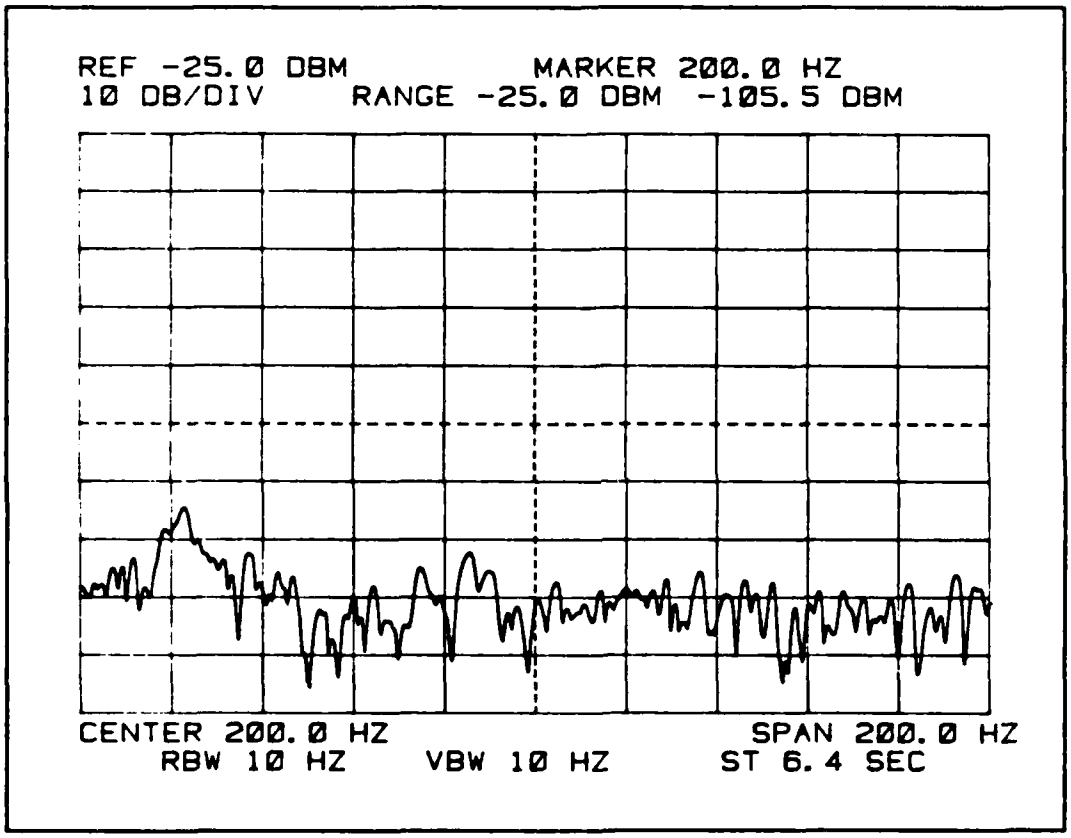

Figure 43. HgCdTe Detector and Preamplifier Spectral Response With No MMW Energy Incident. Range = 6 cm.

Figure 44 is the HgCdTe detector and preamplifier response when irradiated with a 28.0 GHz MMW signal amplitude modulated at 500 Hz. The horn to dewar separation is 7.5 cm. The power meter indication is -17.5 dBm providing a maximum radiated power of 21.4 dBm for a power density at 7.5 cm of 0.2 mW per square centimeter.

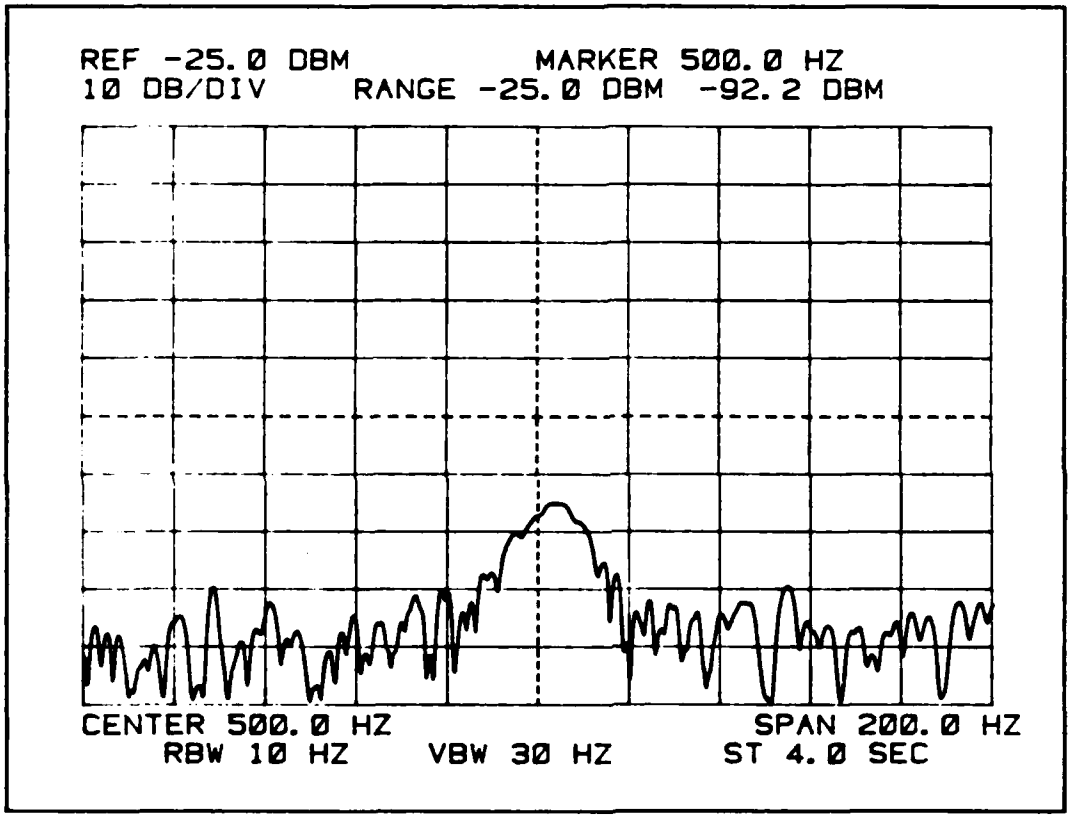

Figure 44. HgCdTe Detector and Preamplifier Response to 28.0 GHz MMW Energy at a Range of 7.5 cm. AM = 500 Hz.

Figure 45 is the HgCdTe response to a 28.0 GHz signal amplitude modulated at a 1 kHz rate. The separation and power settings are identical to that of Figure 44.

Figure 46 is identical to that of Figures 45 and 44 except that the amplitude modulation rate is 2 kHz.

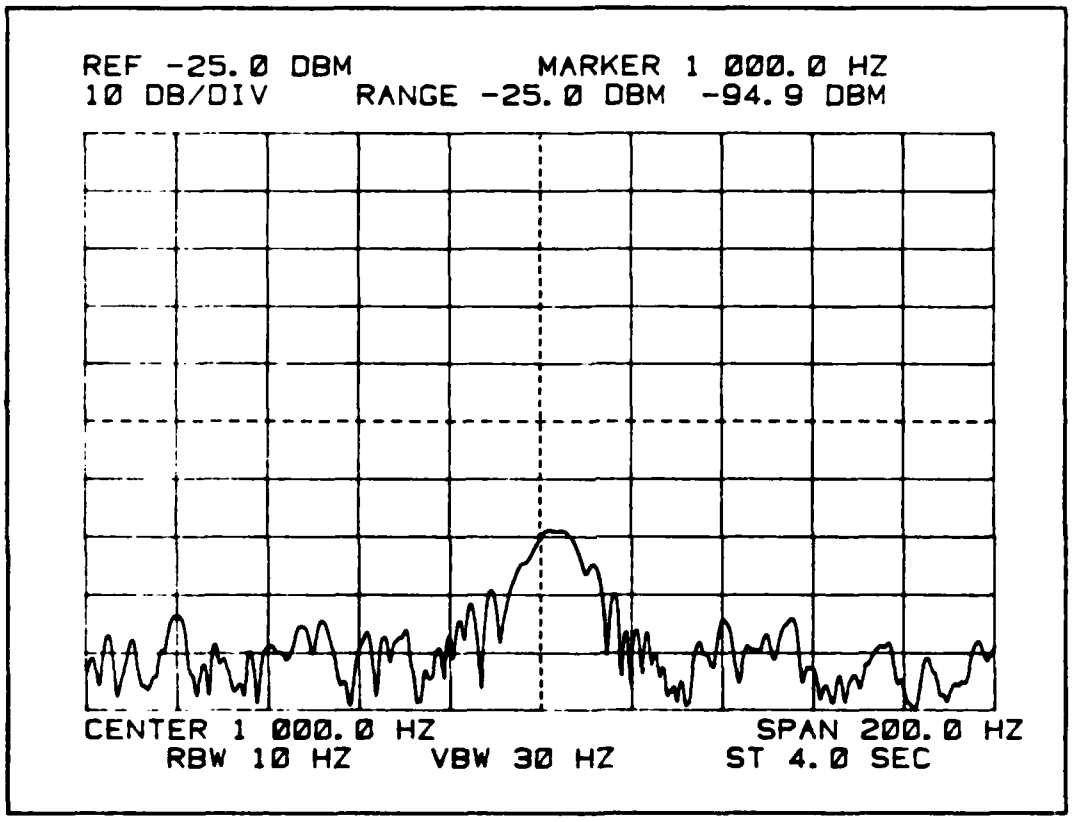

Figure 45. HgCdTe Detector and Preamplifier Response to 28.0 GHz MMW Energy Amplitude Modulated at 1 kHz. Dewar to Transmit Horn Separation is 7.5 cm.

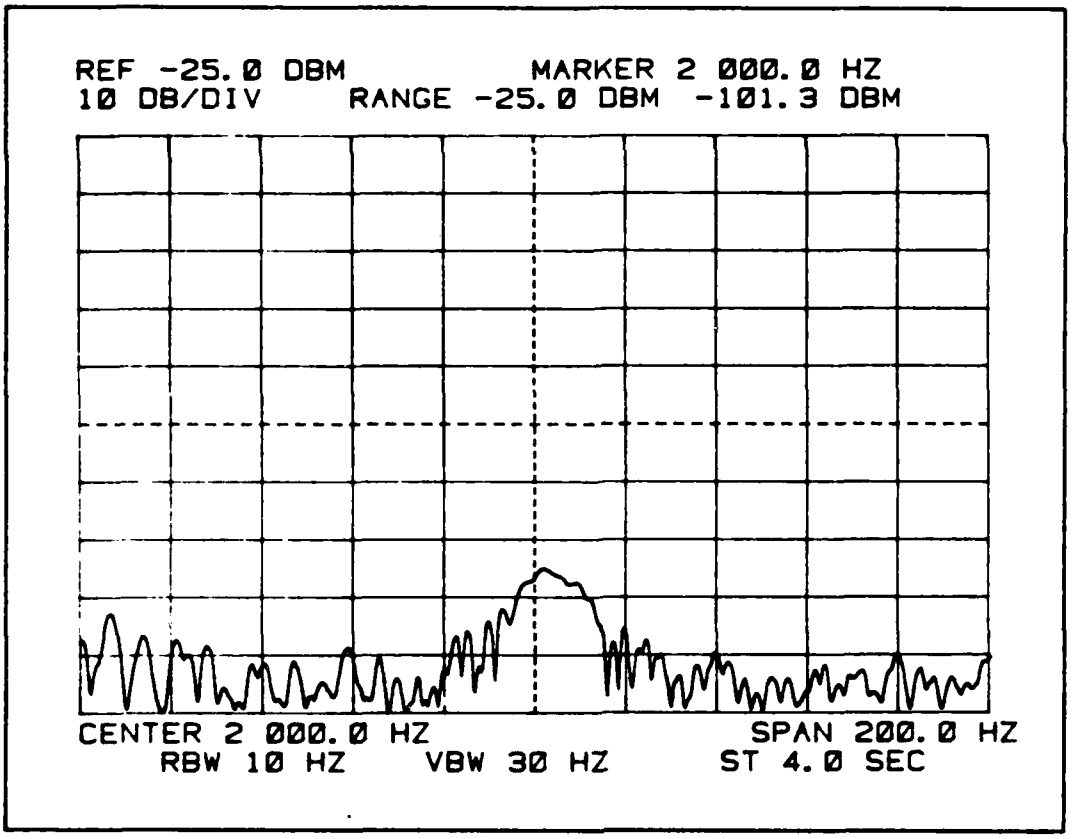

Figure 46. HgCdTe Detector and Preamplifier Response to 28.0 GHz MMW Energy Amplitude Modulated at 2 kHz. Separation is 7.5 cm.

Figures 47 and 48 show the HgCdTe detector and preamplifier output as displayed on the spectrum analyzer with the detector operated at room temperature. Figure 47 is the output with an amplitude modulated RF of 33 GHz incident on the detector. A 200 Hz squarewave was used to modulate the RF. The separation between the transmit horn and dewar window was 5 cm. The power meter indicated a level of -9.2 dBm at the coupled port of the output directional coupler for an estimated peak radiated power of

31 dBm. No response to the MMW energy was observed with the detector at room temperature. Figure 48 is the detector output with the RF off. There are no noticable differences between the displays.

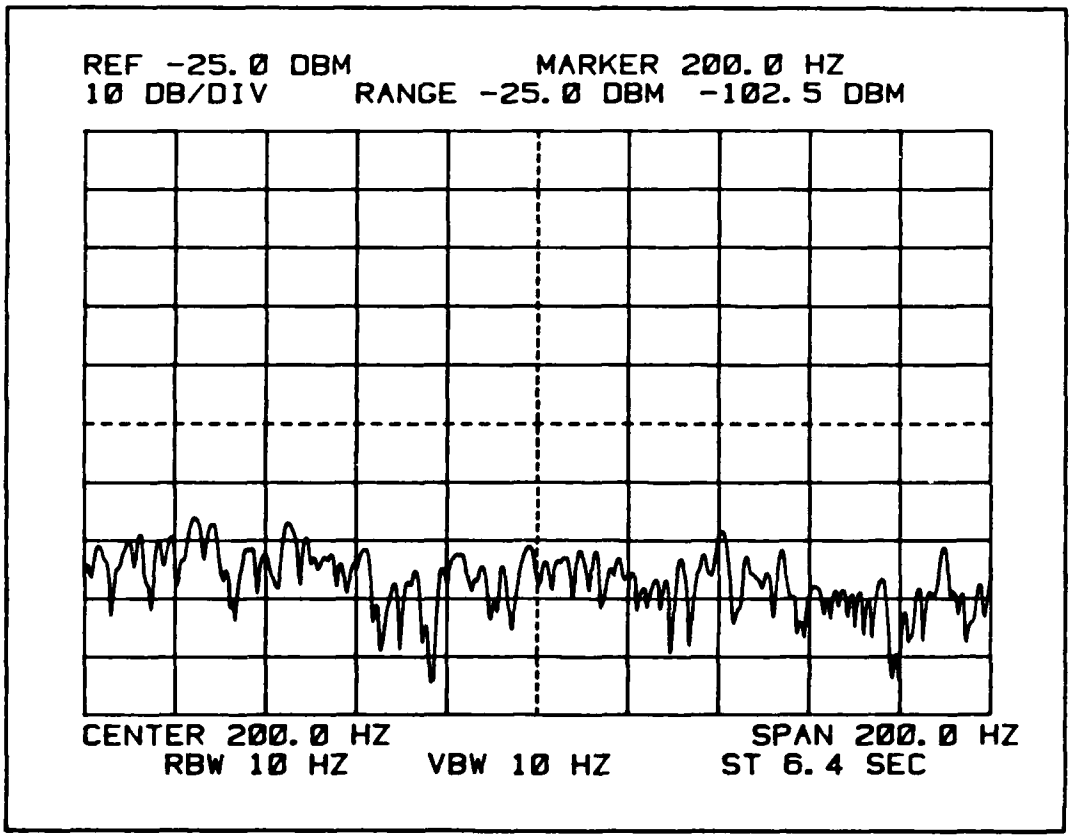

Figure 47. Uncooled HgCdTe Detector and Preamplifier Spectral Output. RF = 33 GHz, Separation = 5 cm.

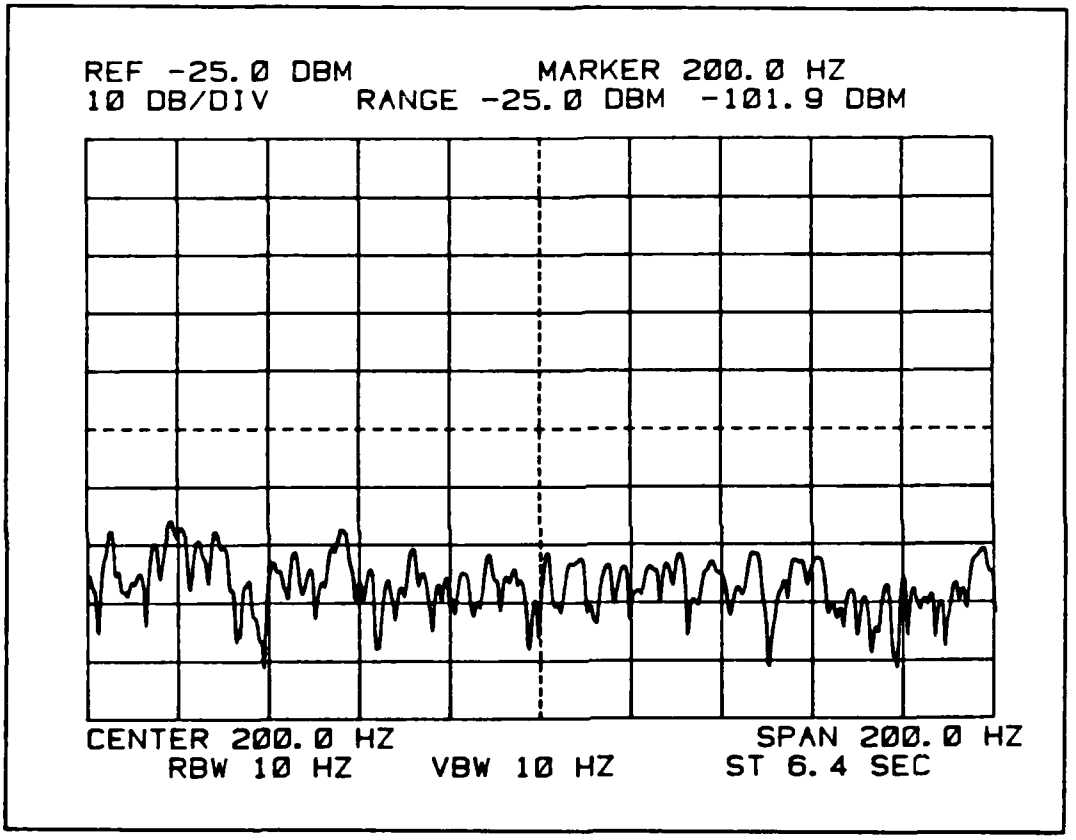

Figure 48. Uncooled HgCdTe Detector and Preamplifier Spectral Output With the RF Off. Separation = 5 cm.

Appendix E: Linearity Data

The following data was measured from the output of the HgCdTe IR detector preamplifier on an HP3582A Spectrum Analyzer. The IR detector dewar was separated from the transmitting antenna aperture by 4.0 cm. Data was measured at two RFs, 75.0 and 89.0 GHz. The RF was modulated at an amplitude modulation rate of 1000 Hz.

HgCdTe Detector Output Power @75 GHz

Atten. Setting (dB)	Average Response (dBm)	HgCdTe Detector Response Data (dBm)					
0.0	-85.8	-85.7	-85.1	-86.0	-86.1	-86.0	
0.5	-86.6	-85.8	-86.9	-86.4	-87.3	-86.6	
1.0	-87.0	-87.5	-88.0	-86.6	-87.1	-85.8	
1.5	-89.0	-89.9	-88.9	-88.5	-89.7	-88.2	
2.0	-90.4	-89.8	-91.7	-89.6	-91.9	-88.8	-90.5
2.5	-91.2	-90.1	-90.4	-91.9	-92.2	-91.5	
3.0	-92.5	-92.1	-93.8	-91.1	-92.5	-93.1	
3.5	-92.9	-94.2	-92.9	-91.5	-92.7	-91.8	-94.2
4.0	-94.2	-95.1	-95.3	-93.6	-93.9	-93.2	

HgCdTe Detector Output Power @89 GHz

Atten. Setting (dB)	Average Response (dBm)	HgCdTe Detector Response Data (dBm)				
0.0	-82.1	-81.8	-82.0	-82.1	-82.3	-82.3
0.5	-82.8	-82.6	-82.8	-82.4	-83.3	-82.9
1.0	-83.6	-83.5	-84.1	-82.7	-84.4	-83.1
1.5	-84.5	-84.7	-84.6	-83.5	-85.1	-84.5
2.0	-85.6	-86.1	-84.6	-85.3	-86.6	-85.4

Appendix F: RF & AM Response Data

Ka Band HgCdTe Detector RF Response Data

RF (GHz)	Antenna Gain (dB)	Power Meter (dBm)	Max Power Radiated (dBm)	Unnorm Output (dBm)	Stand dev (dBm)	Normalized Output (dBm)
27.0	18.14					
27.1	18.17					
27.2	18.20	-19	19.4			
27.3	18.23					
27.4	18.27	-18.5	20.0	-104.3	2.9	-87.3
27.5	18.30	-18.8	19.7	-102.5	2.2	-85.0
27.6	18.33	-17.9	20.7	-101.1	2.4	-85.4
27.7	18.36	-18	20.6	-96.5	0.4	-80.6
27.8	18.39	-17.6	21.0	-90.3	0.9	-75.4
27.9	18.42	-19.5	19.2	-87.7	0.7	-69.0
28.0	18.45	-19	19.7	-84.9	0.4	-67.3
28.1	18.49	-18.2	20.5	-81.7	0.3	-65.8
28.2	18.52	-19.2	19.6	-83.0	0.3	-65.1
28.3	18.55	-17	21.8	-89.2	0.5	-75.7
28.4	18.58	-18.2	20.6	-85.0	0.4	-69.2
28.5	18.61	-17	21.8	-89.3	0.6	-76.0
28.6	18.64	-18.2	20.7	-91.1	0.8	-75.5
28.7	18.67	-18.2	20.7	-93.5	0.5	-77.9
28.8	18.70	-18.2	20.7	-101.7	1.4	-86.2
28.9	18.73					
29.0	18.76					
29.1	18.79	-18	21.0	-96.5	0.8	-81.6
29.2	18.82	-18.2	20.9	-92.8	1.0	-77.5
29.3	18.85	-18	21.1	-93.1	1.1	-78.2
29.4	18.88	-17.2	21.9	-97.0	1.9	-83.8
29.5	18.91	-16.5	22.6	-96.1	1.2	-84.4
29.6	18.94	-16.2	23.0	-93.4	1.2	-82.3
29.7	18.97	-15.4	23.8	-91.9	1.1	-82.5
29.8	19.00	-14.5	24.7	-87.4	0.7	-79.9
29.9	19.02					
30.0	19.05	-20	19.3	-94.0		-75.6
30.1	19.08					
30.2	19.11					
30.3	19.14					
30.4	19.17					
30.5	19.20	-18	21.4	-97.0		-82.9
30.6	19.23					
30.7	19.25					
30.8	19.28					
30.9	19.31					
31.0	19.34	-16	23.6	-97.0		-87.1
31.1	19.37					

Ka Band HgCdTe Detector RF Response Data

RF (GHz)	Antenna Gain (dB)	Power Meter (dBm)	Max Power Radiated (dBm)	Unnorm Output (dBm)	Stand dev (dBm)	Normalized Output (dBm)
31.2	19.39					
31.3	19.42					
31.4	19.45					
31.5	19.48	-21	18.7	-99.0		-79.4
31.6	19.51					
31.7	19.53					
31.8	19.56					
31.9	19.59					
32.0	19.61	-14	25.9	-85.8		-80.5
32.1	19.64					
32.2	19.67					
32.3	19.70					
32.4	19.72					
32.5	19.75	-12	28.0	-85.5		-84.5
32.6	19.78					
32.7	19.80					
32.8	19.83					
32.9	19.86					
33.0	19.88	-21	19.1	-97.0		-78.2
33.1	19.91					
33.2	19.93					
33.3	19.96					
33.4	19.99					
33.5	20.01	-12	28.3	-83.0		-82.5
33.6	20.04					
33.7	20.06					
33.8	20.09					
33.9	20.12					
34.0	20.14	-12	28.4	-87.5		-87.2
34.1	20.17					
34.2	20.19					
34.3	20.22					
34.4	20.24					
34.5	20.27	-12	28.5	-95.0		-95.0
34.6	20.29					
34.7	20.32					
34.8	20.34					
34.9	20.37					
35.0	20.39	-20.7	19.9	-107.1	1.7	-90.0
35.1	20.42					
35.2	20.44					
35.3	20.47					
35.4	20.49					
35.5	20.52					
35.6	20.54					
35.7	20.56					

Ka Band HgCdTe Detector RF Response Data

RF (GHz)	Antenna Gain (dB)	Power Meter (dBm)	Max Power Radiated (dBm)	Unnorm Output (dBm)	Stand dev (dBm)	Normalized Output (dBm)
35.8	20.59					
35.9	20.61					
36.0	20.64	-21	19.9	-103.9	1.8	-86.7
36.1	20.66					
36.2	20.69					
36.3	20.71					
36.4	20.73					
36.5	20.76	-22.5	18.5	-105.4	2.4	-85.4
36.6	20.78					
36.7	20.80					
36.8	20.83					
36.9	20.85					
37.0	20.88	-21.5	19.6	-103.2	2.0	-85.4
37.1	20.90					
37.2	20.92					
37.3	20.95					
37.4	20.97					
37.5	20.99	-18.8	22.4	-101.3	1.2	-89.1
37.6	21.02	-18.5	22.8	-100.5	2.0	-89.0
37.7	21.04					
37.8	21.06	-18	23.3	-100.8	2.7	-90.4
37.9	21.08					
38.0	21.11	-17.5	23.8	-99.5	3.0	-90.2
38.1	21.13					
38.2	21.15	-17	24.4	-98.3	1.3	-90.1
38.3	21.18					
38.4	21.20	-16	25.4	-99.0	1.2	-92.8
38.5	21.22	-15.8	25.7	-99.5	2.1	-93.8
38.6	21.24	-16	25.5	-98.2	1.3	-92.1
38.7	21.27					
38.8	21.29	-15	26.5	-100.6	0.7	-96.6
38.9	21.31					
39.0	21.33	-14.2	27.4	-100.4	1.5	-98.1
39.1	21.36					
39.2	21.38	-14.1	27.5	-99.5	1.7	-97.5
39.3	21.40					
39.4	21.42	-14	27.7	-99.3	3.1	-97.6
39.5	21.44					
39.6	21.47	-14.8	26.9	-96.3	0.9	-93.1
39.7	21.49					
39.8	21.51					
39.9	21.53					
40.0	21.55					

Ka Band HgCdTe Detector RF Response Data (Raw Data)

RF (GHz)	Raw Data (HgCdTe Detector Responses)				
27.0					
27.1					
27.2					
27.3					
27.4	-102.6	-104.6	-102.4	-109.1	-102.6
27.5	-102.3	-99.1	-104.1	-102.5	-104.6
27.6	-97.7	-100.1	-101	-103.9	-102.7
27.7	-96.4	-96.5	-96.4	-97.1	-95.9
27.8	-90.1	-90	-91.9	-89.8	-89.9
27.9	-87.6	-88.6	-87.8	-86.8	-87.2
28.0	-84.9	-85.3	-84.4	-85.2	-84.8
28.1	-81.7	-81.6	-82.2	-81.9	-81.3
28.2	-83.0	-83.4	-82.9	-83	-82.7
28.3	-89.4	-88.5	-89.8	-88.6	-89.6
28.4	-85.0	-84.8	-84.5	-85.5	-85.3
28.5	-88.6	-89.9	-88.9	-89.8	-89.5
28.6	-90.4	-92.6	-90.5	-91.2	-91.2
28.7	-93.3	-93.8	-92.9	-93.5	-94.1
28.8	-100.9	-100.2	-102.6	-103.1	
28.9					
29.0					
29.1	-95.7	-96.5	-97.6	-95.9	-97
29.2	-93.3	-91.1	-93.8	-93.5	-92.5
29.3	-93.0	-92.2	-93.5	-92.1	-95.1
29.4	-96.3	-98.2	-95.6	-96.1	-100.3
29.5	-98.1	-95.2	-96.7	-96.1	-95.9
29.6	-93.4	-94.1	-92.8	-91.9	-92.9
29.7	-91.3	-93.3	-90.9	-90.7	-92.2
29.8	-87.1	-86.6	-87.8	-86.7	-88.3
29.9					
30.0	-94.0				
30.1					
30.2					
30.3					
30.4					
30.5	-97.0				
30.6					
30.7					
30.8					
30.9					
31.0	-85.0				
31.1					
31.2					
31.3					

Ka Band HgCdTe Detector RF Response Data (Raw Data) (continued)

31.4					
31.5	-99.0				
31.6					
31.7					
31.8					
31.9					
32.0	-85.8				
32.1					
32.2					
32.3					
32.4					
32.5	-85.5				
32.6					
32.7					
32.8					
32.9					
33.0	-97				
33.1					
33.2					
33.3					
33.4					
33.5	-83.0				
33.6					
33.7					
33.8					
33.9					
34.0	-87.5				
34.1					
34.2					
34.3					
34.4					
34.5	-95.0				
34.6					
34.7					
34.8					
34.9					
35.0	-106.7	-106.4	-107	-110	-105.6
35.1					
35.2					
35.3					
35.4					
35.5					
35.6					
35.7					
35.8					
35.9					
36.0	-105.9	-101.7	-102.7	-103.7	-105.7

Ka Band HgCdTe Detector RF Response Data (Raw Data) (continued)

36.1					
36.2					
36.3					
36.4					
36.5	-106.8	-106.4	-105.8	-106.7	-101.2
36.6					
36.7					
36.8					
36.9					
37.0	-101.3	-102.8	-102.1	-106.5	-104.9
37.1					
37.2					
37.3					
37.4					
37.5	-101.8	-100.4	-100	-103.2	-100.4
37.6	-99.0	-102.4	-102.5	-98	-100.5
37.7					
37.8	-99.9	-97.9	-104.1	-103.8	-98.3
37.9					
38.0	-102.2	-95.6	-97.2	-98.2	-100.5
38.1					
38.2	-97.8	-99.7	-96	-98.8	-99
38.3					
38.4	-97.6	-97.6	-98.9	-100.4	-99.8
38.5	-97.0	-99.9	-98.2	-98.5	-103
38.6	-98.9	-99.9	-98	-98.5	-95.9
38.7					
38.8	-100.2	-101.6	-100.3	-100.9	-100
38.9					
39.0	-99.3	-100.9	-98.7	-99.2	-101.8
39.1					
39.2	-101.4	-96.8	-99.5	-100	-99.8
39.3					
39.4	-99.3	-96.5	-96.5	-97.3	-103.1
39.5					
39.6	-97.8	-94.9	-96.1	-96.4	-96.3
39.7					
39.8					
39.9					
40.0					

E Band HgCdTe Detector RF Response Data

RF (GHz)	RF Det Voltage (P-P)	Horn Gain (dB)	IR Out Unnorm (Mean) (dBm)	Standard Deviation	Normalized Averaged (dBm)
60	0.2	17.85846	-89.75	0.546808	-80.4233
61	0.21	18.00203	-94.4166	0.856543	-85.8009
62	0.195	18.14327	-104.64	2.415160	-95.6630
63	0.23	18.28224	-103.514	4.407731	-96.2491
64	0.245	18.41903	-96.3428	1.912116	-89.9000
65	0.26	18.55370	-97.8714	1.178578	-92.2141
66	0.29	18.68631	-87.3285	0.482059	-82.8849
67	0.29	18.81693	-85.0857	0.357903	-80.9033
68	0.34	18.94561	-84.4666	0.683130	-81.9233
69	0.44	19.07241	-79.9833	0.183484	-79.9330
70	0.43	19.19739	-72.44	0.194935	-72.44
71	0.15	19.32060	-85.8571	0.502849	-76.9560
72	0.151	19.44208	-88.3666	0.492612	-79.7662
73	0.2	19.56189	-77.54	0.114017	-71.6202
74	0.153	19.68007	-76.7833	0.147196	-68.7731
75	0.2	19.79666	-79.56	0.151657	-74.1097
76	0.2	19.91170	-[illegible]7	0.244948	-73.4798
77	0.21	20.02525	-78.7	0.1	-74.1307
78	0.23	20.13732	-73.4	[illegible]308220	-69.8450
79	0.27	20.24797	-72.6	0.1	-70.6590
80	0.29	20.35723	-72.18	0.083666	-71.0782
81	0.125	20.46513	-79.92	0.178885	-71.7243
82	0.13	20.57171	-85.78	0.576194	-78.1381
83	0.13	20.67699	-83.36	0.181659	-75.9287
84	0.165	20.78102	-78.64	0.357770	-73.4875
85	0.19	20.88381	-75.72	0.130384	-71.9985
86	0.18	20.98540	-73.98	0.083666	-69.9920
87	0.175	21.08582	-75.22	0.130384	-71.1882
88	0.22	21.18508	-70.28	0.044721	-68.4344
89	0.225	21.28323	-71.7	0.122474	-70.2459
90	0.2	21.38028	-75.62	0.130384	-73.3370

E-Band HgCdTe Detector RF Response Raw Data

RF(GHz)	Data (Detector Output in dBm)					
60	-89.3	-89.4	-90.8	-89.5	-89.7	-89.8
61	-94.5	-93.8	-93.9	-95.9	-93.6	-94.8
62	-101	-106	-107.4	-103.9	-104.9	
63	-102.8	-96.6	-109.0	-107.4	-99.1	-104.8
64	-96.0	-99.1	-97.2	-92.7	-96.8	-96.3
65	-97.1	-97.1	-99.6	-98.7	-98.8	-96.3
66	-88.3	-87.3	-87.0	-87.1	-86.8	-87.4
67	-85.2	-84.7	-85.5	-85.3	-85.3	-84.5
68	-83.9	-84.0	-84.1	-84.3	-84.8	-85.7
69	-80.1	-79.9	-80.1	-79.9	-79.7	-80.2
70	-72.5	-72.7	-72.5	-72.2	-72.3	
71	-85.6	-86.6	-85.4	-85.4	-85.5	-86.4
72	-88.2	-89.0	-88.5	-88.8	-88.0	-87.7
73	-77.4	-77.7	-77.5	-77.5	-77.6	
74	-76.9	-76.8	-76.8	-76.8	-76.5	-76.9
75	-79.6	-79.6	-79.7	-79.6	-79.3	
76	-78.4	-79	-78.6	-78.6	-78.9	
77	-78.6	-78.6	-78.8	-78.8	-78.7	
78	-73.1	-73.2	-73.4	-73.9	-73.4	
79	-72.6	-72.5	-72.5	-72.7	-72.7	
80	-72.1	-72.2	-72.2	-72.1	-72.3	
81	-79.8	-80.2	-79.8	-79.8	-80.0	
82	-86.3	-86.1	-84.9	-86.1	-85.5	
83	-83.3	-83.6	-83.2	-83.5	-83.2	
84	-78.4	-78.4	-79.2	-78.8	-78.4	
85	-75.6	-75.8	-75.7	-75.9	-75.6	
86	-74.0	-74.1	-74	-73.9	-73.9	
87	-75.2	-75.4	-75.3	-75.1	-75.1	
88	-70.3	-70.3	-70.3	-70.2	-70.3	
89	-71.5	-71.8	-71.7	-71.7	-71.8	
90	-75.8	-75.5	-75.7	-75.6	-75.5	

AM Response Data

The raw and processed data for the E band test is displayed below. The test was performed at an RF of 89 GHz. At 89 GHz, the gain of the 18 x 13 mm pyramidal horn was calculated to be 21.3 dB. The transmitted power was estimated using a flat broadband RF detector with an assumed sensitivity of 250 mV/mW (typical value).

HgCdTe Detector AM Response Data (Mean, Adjusted Results)

AM Rate (Hz)	RF Det Volts p-p	Power at max (dBm)	Mean Det. Output (dBm)	Std dev (dBm)	Adjusted ave (dBm)
100	0.22	40.7	-70.8	0.152	-70.8
200	0.22	40.7	-72.6	0.089	-72.6
300	0.22	40.7	-74.3	0.084	-74.3
400	0.22	40.7	-76.1	0.114	-76.1
500	0.22	40.7	-77.4	0.130	-77.4
600	0.22	40.7	-78.6	0.270	-78.6
700	0.22	40.7	-79.8	0.130	-79.8
800	0.22	40.7	-80.8	0.148	-80.8
900	0.22	40.7	-81.5	0.114	-81.5
1000	0.22	40.7	-82.5	0.187	-82.5
1100	0.22	40.7	-83.2	0.055	-83.2
1200	0.22	40.7	-83.5	0.167	-83.5
1300	0.22	40.7	-84.2	0.265	-84.2
1400	0.22	40.7	-85.0	0.130	-85.0
1500	0.22	40.7	-85.4	0.152	-85.4
1600	0.22	40.7	-86.0	0.173	-86.0
1700	0.22	40.7	-86.6	0.536	-86.6
1800	0.215	40.6	-86.8	0.134	-86.6
1900	0.21	40.5	-87.5	0.719	-87.1
2000	0.21	40.5	-87.8	0.893	-87.4
2100	0.21	40.5	-87.9	0.316	-87.5
2200	0.21	40.5	-88.1	0.200	-87.7
2300	0.205	40.4	-88.4	0.134	-87.7
2400	0.204	40.4	-88.6	0.192	-88.0
2500	0.203	40.4	-88.7	0.277	-88.0
2600	0.202	40.4	-89.0	0.303	-88.3

AM Response Data (continued)

AM Rate (Hz)	RF Det Volts p-p	Power at max (dBm)	Mean Det. Output (dBm)	Std dev (dBm)	Adjusted ave (dBm)
2700	0.201	40.3	-89.4	0.570	-88.6
2800	0.2005	40.3	-89.8	0.671	-89.0
2900	0.2	40.3	-90.2	0.683	-89.4
3000	0.2	40.3	-90.1	0.467	-89.2
3500	0.195	40.2	-91.0	0.367	-90.0
4000	0.19	40.1	-92.1	0.335	-90.8
4500	0.18	39.9	-92.7	0.245	-91.0
5000	0.175	39.7	-92.7	1.782	-90.7
6000	0.175	39.7	-94.1	0.219	-92.1
7000	0.15	39.1	-94.6	0.349	-91.3
8000	0.14	38.8	-94.8	0.303	-90.9
9000	0.13	38.4	-95.3	0.689	-90.7
10000	0.125	38.3	-96.0	0.396	-91.1
11000	0.115	37.9	-96.0	0.460	-90.4
12000	0.105	37.5	-96.4	0.148	-90.0
13000	0.1	37.3	-96.5	0.100	-89.7
14000	0.095	37.1	-96.9	0.354	-89.6
15000	0.09	36.8	-97.3	0.738	-89.5
16000	0.09	36.8	-97.6	0.451	-89.8
17000	0.08	36.3	-97.6	0.451	-88.8
18000	0.075	36.1	-97.6	0.187	-88.3
19000	0.07	35.8	-92.7	4.696	-82.7
20000	0.07	35.8	-97.9	0.856	-87.9
25000	0.055	34.7	-100.0	0.781	-88.0
30000	0.04	33.3	-100.9	0.622	-86.1

HgCdTe Detector AM Response Raw Data

AM Rate (Hz)	IR Detector Output (raw data)				
100	-70.7	-70.6	-71	-70.7	-70.8
200	-72.5	-72.7	-72.7	-72.7	-72.6
300	-74.2	-74.4	-74.3	-74.3	-74.2
400	-75.9	-76.1	-76.1	-76.2	-76
500	-77.4	-77.2	-77.5	-77.5	-77.5
600	-78.6	-78.6	-78.4	-79.1	-78.5
700	-79.8	-79.7	-79.9	-79.7	-80
800	-81	-80.8	-80.6	-80.7	-80.8
900	-81.7	-81.5	-81.4	-81.5	-81.6
1000	-82.7	-82.6	-82.5	-82.2	-82.5
1100	-83.2	-83.1	-83.2	-83.2	-83.1
1200	-83.5	-83.8	-83.6	-83.4	-83.4
1300	-83.8	-84.5	-84.3	-84.1	-84.3
1400	-85.1	-85.1	-84.9	-85	-84.8
1500	-85.4	-85.7	-85.4	-85.3	-85.4
1600	-86.3	-85.9	-85.9	-86	-85.9
1700	-86.5	-86.1	-86.4	-87.5	-86.4
1800	-86.9	-86.9	-86.7	-86.7	-86.6
1900	-88.8	-87.2	-87.3	-87.2	-87.1
2000	-89.3	-87.6	-87	-87.3	-87.9
2100	-87.7	-87.6	-88	-88.4	-87.8
2200	-88.3	-88.3	-88.1	-87.9	-87.9
2300	-88.2	-88.5	-88.3	-88.3	-88.5
2400	-88.6	-88.7	-88.8	-88.3	-88.7
2500	-88.4	-88.8	-88.5	-89.1	-88.6
2600	-88.9	-89.5	-88.7	-88.9	-89.1
2700	-90.2	-89	-88.9	-89.1	-89.8
2800	-89.8	-90.9	-89.1	-89.7	-89.5
2900	-90.2	-91.3	-89.5	-89.8	-90.1
3000	-89.4	-90.3	-89.8	-90.2	-90.6
3500	-91.4	-91.3	-91	-90.8	-90.5
4000	-92.4	-92.2	-91.6	-92	-92.4
4500	-92.4	-92.5	-93	-92.8	-92.8
5000	-92.6	-91.4	-92.9	-95.6	-91.1
6000	-94.3	-93.9	-93.9	-93.9	-94.3
7000	-94.4	-94.4	-94.7	-95.2	-94.4
8000	-95.2	-94.6	-94.9	-94.8	-94.4
9000	-94.2	-95.1	-95.5	-95.8	-95.9
10000	-95.6	-95.8	-96.5	-96.3	-95.7
11000	-96.3	-95.8	-96	-96.6	-95.4
12000	-96.4	-96.2	-96.6	-96.3	-96.4
13000	-96.6	-96.6	-96.4	-96.4	-96.5
14000	-96.9	-96.6	-96.5	-97.2	-97.3
15000	-96.2	-97.9	-96.9	-97.9	-97.6
16000	-97.5	-98.3	-97.2	-97.2	-97.6

HgCdTe Detector AM Response Raw Data (continued)

AM Rate	IR Detector Output (raw data)				
17000	-97.5	-98.3	-97.2	-97.2	-97.6
18000	-97.5	-97.6	-97.6	-97.4	-97.9
19000	-87.8	-97.8	-94.3	-95.8	-87.6
20000	-97.6	-98.9	-96.9	-98.6	-97.3
25000	-99.7	-100.5	-101.1	-99.5	-99.2
30000	-101.2	-100.9	-101.7	-100	-100.8

Bibliography

Adams, A.T., et al. "On the Coupling of Electromagnetic Energy Through Apertures," Symposium and Technical Exhibition on Electromagnetic Compatibility, 1st Proceedings, EMC 1975: 363-367, (May 1975).

Benser, E.T., et al. "IR/MMW Dual-Mode, Common Aperture Optics," InFrared Technology XIII, Volume 819, edited by Irving J. Spiro. 288 - 296. Bellingham, WA: SPIE-The International Society for Optical Engineering, August 1987.

Bhartia, P. and I.J. Bahl. Millimeter Wave Engineering and Applications, New York: John Wiley & Sons, 1984.

Boyd, Robert w. Radiometry and the Detection of Optical Radiation. New York: John Wiley & Sons, 1983.

Emmons, R.B., et al. "Infrared Detectors: An Overview," Selected Papers on Infrared Design, edited by R. Barry Johnson and William L. Wolfe. Proc. SPIE 512: 601-610 (1985).

EMP Interaction 2-1, EMP Interaction: Principles, Techniques, and Reference Data (A Compleat Cancatenation of Technology From the EMP Interaction Notes). AFWL-TR-80-402. edited by K.S.H. Lee. Kirtland AFB, NM: Air Force Weapons Laboratory, December 1980.

Graves, B.D., et al. "On the Electromagnetic Field Penetration Through Apertures," Symposium and Technical Exhibition on Electromagnetic Compatibility, 1st Proceedings, EMC 1975: 511-515, (May 1975).

HP Test and Measurement Catalog. Product Catalog, 5954-7706D. Palo Alto, Ca.: Hewlett-Packard Co., 1988.

Infrared Detectors. Product Catalog, unnumbered. EG&G Judson, Montgomeryville, PA, undated.

Judson. Product Catalog, unnumbered. Judson, Montgomeryville, PA, undated.

Jull, Edward V. "Aperture Antennas and Diffraction Theory," Electromagnetic Wave Series, Volume 10, edited by Clarricoats, P.J.B., G. Millington, E. Shearman, and J.R. Wait. New York: The Institute of Electrical Engineers, 1981.

Justice, Susan. Sales Administrator. Telephone interview. EG&G Judson, Montgomeryville, PA, 13 July 1987.

Kruse, Paul W., et al. Elements of Infrared Technology: Generation, Transmission, and Detection. New York: John Wiley & Sons, 1962.

May, John J. Jr. and M.E. Van Zee. "Electro-Optic and Infrared Sensors," Microwave Journal, 26: 121-127 (Sept 1983).

Millimeter-Wave Products. Product Catalog, unnumbered. Hughes Aircraft Company, Microwave Products Division, Torrence, CA, January 1985.

Newell, Allen C. "Error Analysis Techniques for Planar Near-Field Measurements," IEEE Transactions on Antennas and Propagation, 36: 754-768 (June 1988).

Reedy, Edward K. and George W. Ewell. "Millimeter Radar," Infrared and Millimeter Waves, Volume 4, edited by Kenneth J. Button and James C. Wiltse. New York: Academic Press, 1981.

Sega, Ronald M. and John D. Norgard. "Expansion of an Infrared Detection Technique Using Conductive Mesh in Microwave Shielding Applications," Infrared Technology XIII, edited by Irving J. Spiro. Proc. SPIE 819: 213-219 (1987).

Spiegel, Murray R. "Mathematical Handbook of Formulas and Tables," Shaum's Outline Series. New York: McGraw-Hill Book Company, 1968.

Stutzman, Warren L. and Gary A. Thiele. Antenna Theory and Design. New York: John Wiley & Sons, 1981.

Taylor, Michael J.H. Missiles of the World. New York: Charles Scribner's Sons, 1980.

Wang, Johnson J.H. "An Examination of the Theory and Practices of Planar Near-Field Measurement," IEEE Transactions on Antennas and Propagation, 36: 746-753 (June 1988).

Weber, Bruce A. and Stanley M. Kulpa. The Extension of [Hg,Cd]Te Detector Technology to the Near-Millimeter Spectral Region. U.S. Army Electronics Research and Development Command, Harry Diamond Laboratories, Adelphi, MD: June, 1980 (AD-A090449).

Yaghjian, Arthur D. "An Overview of Near-Field Antenna Measurements," IEEE Transactions on Antennas and Propagation, 34: 30-45 (January 1986).

Vita

Captain Thomas D. Moore

He graduated from high school in Cass City, Michigan in 1970. He entered the Air Force in October, 1975 and served as an electronics technician (AFSC 30455) with tours of duty at Wright-Patterson AFB, Ohio and Clark AB, Philippines. He attended the University of Arizona, from which he received the degree of Bachelor of Science in Electrical Engineering (with highest honors) in 1983. Upon graduation, he received a commission through Officer Training School at Lackland AFB, Texas. He then served as a Radar Signal Analysis Engineer at the Foreign Technology Division, Wright-Patterson AFB, Ohio until entering the School of Engineering, Air Force Institute of Technology, in May 1987.

UNCLASSIFIED
SECURITY CLASSIFICATION OF THIS PAGE

REPORT DOCUMENTATION PAGE

Form Approved
OMB No. 0704-0188

1a. REPORT SECURITY CLASSIFICATION UNCLASSIFIED	1b. RESTRICTIVE MARKINGS
2a. SECURITY CLASSIFICATION AUTHORITY	3. DISTRIBUTION/AVAILABILITY OF REPORT Approved for public release; distribution unlimited.
2b. DECLASSIFICATION/DOWNGRADING SCHEDULE	
4. PERFORMING ORGANIZATION REPORT NUMBER(S) AFIT/GE/ENG/ENP/88D-1	5. MONITORING ORGANIZATION REPORT NUMBER(S)
6a. NAME OF PERFORMING ORGANIZATION School of Engineering 6b. OFFICE SYMBOL (If applicable) AFIT/ENG/ENP	7a. NAME OF MONITORING ORGANIZATION
6c. ADDRESS (City, State, and ZIP Code) Air Force Institute of Technology (AU) Wright-Patterson AFB, Ohio 45433-6583	7b. ADDRESS (City, State, and ZIP Code)
8a. NAME OF FUNDING/SPONSORING ORGANIZATION Air Force Electronic Warfare Center 8b. OFFICE SYMBOL (If applicable) AFEWC/ATD/SAX	9. PROCUREMENT INSTRUMENT IDENTIFICATION NUMBER
8c. ADDRESS (City, State, and ZIP Code) Kelly AFB, Texas 78243-5000	10. SOURCE OF FUNDING NUMBERS PROGRAM ELEMENT NO. / PROJECT NO. / TASK NO / WORK UNIT ACCESSION NO.

11. TITLE (Include Security Classification)
THE RESPONSE OF SINGLE ELEMENT HgCdTe AND InSb SOLID STATE INFRARED DETECTORS TO MILLIMETER WAVE ELECTROMAGNETIC ENERGY

12. PERSONAL AUTHOR(S)
Thomas D. Moore, B.S.E.E., Capt, USAF

13a. TYPE OF REPORT	13b. TIME COVERED	14. DATE OF REPORT (Year, Month, Day)	15. PAGE COUNT
MS Thesis	FROM _____ TO _____	1988 December	153

16. SUPPLEMENTARY NOTATION

17. COSATI CODES			18. SUBJECT TERMS (Continue on reverse if necessary and identify by block number)
FIELD	GROUP	SUB-GROUP	Infrared Detectors, Infrared Countermeasures Millimeter Waves, Electromagnetic Interference
17	04	04	

19. ABSTRACT (Continue on reverse if necessary and identify by block number)

Thesis Advisor: David H. Stone, Major, USAF
Assistant Professor of Physics

Approved for release in accordance with AFR 190-1
12 Jan 1989

20. DISTRIBUTION/AVAILABILITY OF ABSTRACT	21. ABSTRACT SECURITY CLASSIFICATION
☒ UNCLASSIFIED/UNLIMITED ☐ SAME AS RPT. ☐ DTIC USERS	UNCLASSIFIED
22a. NAME OF RESPONSIBLE INDIVIDUAL David H. Stone, Major, USAF	22b. TELEPHONE (Include Area Code) 513-255-2012 / 22c. OFFICE SYMBOL AFIT/ENP

DD Form 1473, JUN 86 — Previous editions are obsolete. — SECURITY CLASSIFICATION OF THIS PAGE

UNCLASSIFIED

An experimental determination of the millimeter wave (MMW) response of single element InSb and HgCdTe infrared (IR) detectors is made. The detectors were mounted in standard metal dewars and cooled to 77K. Bias and amplification for the detectors were provided by external preamplifiers. The detectors were irradiated with amplitude modulated (AM) electromagnetic energy in the Ka and E microwave bands. Transmitted MMW power levels were limited to values less than 10 mW. Tests were accomplished in the near-field of standard gain pyramidal horns.

Response measurements were made on a spectrum analyzer by monitoring the level of the MMW AM rate spectral component. The detector MMW responses were measured for linearity, RF, AM rate, and polarization dependence. The effect of simultaneous IR and MMW sources in the detector field-of-view were also examined. Of the detectors tested, only the HgCdTe detector exhibited a MMW response. The measured HgCdTe MMW response was square law in behavior and displayed dependence on the RF, AM rate, and incident MMW polarization. The MMW response was not effected by the presence of IR sources within the detector field-of-view.